Structures and Materials Research
Department of Civil Engineering

Report No. UCSESM 71-7

Non-Linear Analysis of Plates Considering Geometric and Material Effects

by

Pal G. Bergan

This research was sponsored by the Structures Department of the Naval Ship Research and Development Center under Naval Ship Systems Command Subproject SF 013 0301, Task 1968, Contract N00014-69-A-0020-1045, continuation of Contract N00014-67-A-0114-0020.

Structural Engineering Laboratory
University of California
Berkeley, California

April 1971

ABSTRACT

The purpose of this investigation is to study nonlinear behavior of plates considering both geometric and physical nonlinearities.

Large deflections are accounted for using the von Karman strain expressions for plates and initial deformations are considered using the Marguerre shallow shell theory. Establishing the variational principles, the equilibrium and incremental equations for general Rayleigh-Ritz type solution methods are derived.

The finite element method is adopted for the numerical solution of the problem. A doubly curved quadrilateral element including nonlinear geometric effects is derived. Special simplifications are made resulting in a highly efficient technique.

Inelastic material behavior is accounted for using the flow theory of plasticity. In particular, the Prandtl-Reuss flow rule and isotropic hardening are utilized. Inelastic, quadrilateral finite elements allowing for both membrane and flexural behavior are developed. The tangent stiffness approach is adopted forming the incremental stiffnesses by numerical integration over the volume of the elements.

Different general numerical techniques for solving nonlinear structural problems are considered. The problems of convergence and accuracy of iteration methods are also discussed.

A wide range of numerical examples are presented, such as large deflections of different plates, post buckling behavior of plates, snap-through problems and inelastic behavior of various plates.

ACKNOWLEDGMENT

This research was sponsored by the Department of Structural Mechanics, Naval Ship Research and Development Center, under the Naval Ship Systems Command Subproject SF 013 0301, Task 1968, Contract N00014-67-A-0114-0020.

The purpose of this investigation is to study nonlinear behavior of plates considering both geometric and physical nonlinearities.

In addition, the author would like to express his gratitude to the American-Scandinavian Foundation and the Royal Norwegian Research Council for their support during his studies, and to the Computer Center at the University of California, Berkeley, which provided facilities for the computer work.

TABLE OF CONTENTS

1. INTRODUCTION

1.1 GENERAL REMARKS

Today, structural plates constitute important load carrying components of numerous types of structures, such as ships, airplanes, aerospace structures, plate girder bridges and various other constructions. Economy, weight and other functional requirements together with new developments in materials technology have resulted in a drive for increasingly daring design, which indeed represents a great challenge to modern methods of analysis. The demand for a better utilization of the material most often leads to "thinner" structures for which geometric nonlinearlities are of significant importance and also to structures in which nonlinear material behavior occurs. Economy and other considerations call for an ever increasing precision of the method of analysis itself. Further, the whole concept of structural "safety" must be viewed in the light not only of "allowable stress" or "ultimate load", but also considering the entire structural behavior in the non-linear range.

All of this points to the need for accurate and efficient methods of analysis of nonlinear behavior of plates. Such methods should be capable of accounting for both geometric and material non-linearities and have a high degree of precision. Fortunately, modern computers and recent advances in the field of structural mechanics make such computations feasible for plates of general geometry and with general boundary conditions. This will be demonstrated in the course of the present study. Moreover, imperfections in the plate geometry or

deliberately made initial deformations will also be accounted for in the present investigation. Such deformations may have a dramatic influence on the overall behavior of the plate.

1.2 PREVIOUS STUDIES

The complete differential equations for large deflections of plates were formulated by von Karman in 1910 [1]. Three years earlier, an approximate method of analysis had been suggested by Föppl [2]. Timoshenko [3] and Marguerre and Trefftz [4] derived the expressions for the strain energy of plates with large deflections in the nineteen thirties. Since then, a long series of approximate and nearly exact solutions to the nonlinear plate problem has emerged. In 1937, Marquerre [5] presented an approximate solution for postbuckling behavior of simply supported rectangular plates in compression. S. Way [6] studied uniformly loaded clamped plates with large deflections using the Ritz method. In some important papers published in 1942, Levy derived solutions of a theoretically exact nature to large deflections of simply supported [7] and clamped [8] rectangular plates subjected to various loading conditions. Levy's results will be used for comparisons later in this study. Noteworthy are also the works by Wang [9] who used the differential equations and the finite difference technique, and by Coan [10] who studied buckling of plates with initial deformations.

The development of modern electronic computers now makes it possible to use extremely complicated and involved methods of analysis that earlier were completely inconceivable. Since its origin in the middle of the nineteen-fifties [11], the so-called finite element approach for structural problems has been developed with almost

explosive rapidity. This method has proven to provide a very powerful approach to a wide range of linear and nonlinear structural problems. The first attempt of including geometric effects into the method for the purpose of studying buckling, was made by Turner et. al. in 1960 [12]. Later, a long series of papers has extended the method to be applicable to various types of buckling and large deformation problems [13 - 18]. Among the papers dealing specifically with large deformations of plates, the ones by Murray and Wilson [19 - 21] should be noted. They used a triangular element and re-assembled the deformed plate in a global coordinate system. An investigation by Brebbia and Connor [22] was based on von Karman's large deflection strain expressions for plates. The same strain expressions will be used in the present investigation.

Although elastic-plastic behavior of metals has been well understood and documented for a couple of decades, not much theoretical work has so far been done with general elastic-plastic deformations of plates. The reasons for this are obvious; the problem is extremely complicated and closed form solutions cannot be obtained for more general types of plates. However, the extremum principles of plasticity may be used to obtain upper and lower bounds for the true solution [23]. The finite element method has proved to be a powerful method also for solving elastic-plastic problems [24 - 31]. Most of the finite element studies performed so far have dealt with rotationally symmetric shells and with simple plane stress problems. Among previous investigations of elastic-plastic plates in bending, the ones by Marcal et. al. [29] and Armen et. al. [30] deserve mentioning.

1.3 PURPOSE AND SCOPE OF PRESENT INVESTIGATION

This study is concerned with the nonlinear behavior of plates. Flat plates and plates with initial deformations under loads for which second order geometric effects become significant are investigated. Based on the principle of virtual work, the equilibrium and incremental equations are derived using a Lagrangian description. Assuming a Ritz-type of approach, the equilibrium and incremental equations for a plate with initial deformations (shallow shell) are developed utilizing matrix notations.

In Chapter 3, it is shown how the finite element method can be used for solving the nonlinear plate problem. The plate is idealized by general quadrilateral finite elements, considering, of course, both membrane and bending actions. The elements have 5 degrees of freedom at each corner node. Initial deformations of the plate are accounted for using a special 12 parameter interpolation polynomial for the initial deflections, thereby obtaining a doubly curved element. Special simplifications are made for the deflection interpolation polynomials to achieve highly increased efficiency when computing the nonlinear stiffness terms. These terms are obtained numerically using Gaussian quadrature.

The elastic-plastic behavior of plates is dealt with in Chapter 4. The flow theory of plasticity is adopted, utilizing the von Mises yield criterion, the Prandtl-Reuss equation and the isotropic hardening rule. It is shown how this theory can be formulated for the finite element approach. The plastic behavior is accounted for using an incremental tangent stiffness approach. Again, both membrane and bending actions are dealt with. The displacement functions of the

elastic-plastic elements are identical to those of the purely elastic elements. However, numerical integration over the entire volume of the elastic-plastic elements is necessary when computing the incremental stiffnesses due to the variable material properties.

The numerical problems associated with the analysis of nonlinear structures are specifically dealt with in Chapter 5. Different methods for solving the nonlinear equations are discussed, partially from a mathematical point of view, but also in the light of experience gained from dealing with different classes of nonlinear problems. The questions of convergence and accuracy are also discussed, suggesting some new approaches to these problems.

Chapter 6 compares a great variety of different examples. Two different computer programs have been developed, one for studying nonlinear geometric effects and one for dealing with nonlinear material effects. Large deflection behavior of various types of plates is studied, carrying the analysis far into the nonlinear range. Postbuckling behavior of flat and initially deformed plates is also investigated. The study of the "snap-through" behavior of transversally loaded shallow shells is a particularly interesting problem. Several examples in which the plate is loaded above the elastic limit are considered. These examples demonstrate the versatility and efficiency of the elastic-plastic finite elements derived in Chapter 4.

2. BASIC EQUATIONS

2.1 CLASSIFICATION OF THE PROBLEMS

It is a well known fact that during continuously increasing load application, all real structures, sooner or later, start behaving in a nonlinear fashion. The sources of nonlinearities may be classified into two main groups, namely geometric and material nonlinearities. The geometric nonlinearities account for the fact that the shape of the structure itself changes during deformation which in turn results in relative changes of the force pattern. Nonlinear material behavior may be due to nonlinear elastic behavior, plasticity, creep or other material effects. Which of these two main sources of nonlinearities is most important, depends, of course, on the geometry and material properties themselves. In general, the geometric effects are most important for "thin" structures whereas for "thick" structures the latter group of effects is prevailing.

Considering a plate subjected to transversal loading, the midsurface will start stretching during deformation and the plate will act in a hammock-like manner. In this case, a stiffening geometric effect is observed. However, the opposite effect will be observed if large compressive membrane forces are applied at the time of transversal loading.

Geometric effects do frequently result in stability problems. Such cases can sometimes be idealized as linearized eigenvalue problems. However, in the following, a much broader concept which includes interacting membrane-bending behavior will be adopted. This approach makes it possible to study the entire course of deformations.

Nonlinear problems require that extra care must be taken when defining strains and stresses. This in turn leads to very complicated kinematic relations, frequently unfit for practical applications. Luckily, some substantial simplifications may be made in the strain expressions for plates with only insignificant loss of accuracy. Such approximations will be discussed later in this chapter.

2.2 BASICS FOR NONLINEAR ELASTICITY PROBLEMS

2.2.1 Fundamental Concepts

Great progress has been made in the fields of continuum and solid mechanics during the last few decades. This is mainly due to investigators like Green, Truesdell, and others [32 - 35]. A powerful system of mathematical symbols has been developed parallel to the progress in these fields. However, it is inherent to the nature and the complexity of these problems that this mathematical language is rather complicated and that its understanding calls for special studies. Therefore, the theoretical derivations to follow are generally presented in the matrix and simple tensor symbols which are familar to most investigators in the structural field. The use of this notation is possible because the plate is a special type of structure for which several simplifying assumptions may be made.

Some vitally important concepts need to be defined before attacking the plate problem. In this discussion, only Euclidian spaces (E_n) will be considered. The Euclidian is the "real" space in which distances can be observed and measured. A set of base vectors with a corresponding field of scalars is used to locate any point in this linear vectorspace.

A "material body" is used to denote elements (particles) say $\{X\}$, which are isomorphic (1 to 1 correspondence) to points in Euclidean space. A configuration of a body is a one parameter family of deformations of the set $\{X\}$, at time t. Of special importance is the reference configuration. Usually, this is the unloaded, stress-free state of a material body at time $t = 0$.

In large deformation theory one basically deals with motion and deformations of material bodies. A set of configurations as a function of the time parameter t defines the motion of a body. The local measure of deformation, called strain will be dealt with further in the next section.

There are several ways in which motion and deformation can be described. The two classical approaches to the problem are the material description and the spatial description. Both methods are due to Euler although the first method is usually denoted the "Lagrangian description". The material description is based on following the path of single material particles of the body. A special form of material description is the "referential description" based on reference configuration and time (the entire body is considered).

The spatial description is frequently used in mechanics of fluids. Fixed points in space are observed while particles flow through these locations. Displacements are found by integrating velocities.

A further method is "current configuration as reference". This method is used in fluid mechanics and viscoelasticity.

Finally, a method of great importance for large deformation theory is the convected description. In this case the coordinate

system remains fixed in the body and deforms as the body deforms. All particles in the body will therefore have the same coordinates throughout the deformation while the metric tensor of the coordinate system changes continuously.

2.2.2 Definition of Strains and Stresses

Different methods of describing motion were discussed in Section 2.2.1. Further derivations will now be limited to the Lagrangian description only and the reference coordinate system to be used is the rectangular Cartesian one.

Let X_i be the coordinates of an arbitrary point P in the reference system and let x_i denote the location of that material point after deformation (point transformation). Hence,

$$x_i = X_i + u_i \tag{2.1}$$

where u_i are the displacement components. Fig. 2.1 shows an arbitrary infinitesimal line element PQ mapped into $P'Q'$ after deformation. The squared lengths are given by

$$\begin{aligned} ds_o^2 &= dX_k\, dX_k = \delta_{ij}\, dX_i\, dX_j \\ ds^2 &= dx_k\, dx_k = \frac{\partial x_k}{\partial X_i}\,\frac{\partial x_k}{\partial X_j}\, dX_i\, dX_j \end{aligned} \tag{2.2}$$

Since Cartesian coordinate systems will be used, only lower indices are used and summation should be performed on repeated indices. The symbol δ_{ij} is the Kronecker delta. Latin indices range from 1 to 3.

The Lagrangian (or Green) finite strain tensor E_{ij} is now defined by the following relation

$$ds^2 - ds_0^2 = 2 E_{ij} dX_i dX_j \tag{2.3}$$

The strain tensor represents the local measure of deformation. Substituting Eq. (2.2) into Eq. (2.3) and using Eq. (2.1) the following expression is obtained

$$\begin{aligned} E_{ij} &= \frac{1}{2}\left(\frac{\partial x_k}{\partial X_i} \frac{\partial x_k}{\partial X_j} - \delta_{ij} \right) \\ &= \frac{1}{2}\left(\frac{\partial u_j}{\partial X_i} + \frac{\partial u_i}{\partial X_j} + \frac{\partial u_k}{\partial X_i} \frac{\partial u_k}{\partial X_j} \right) \end{aligned} \tag{2.4}$$

Note from the definition Eq. (2.3) that the strain tensor E_{ij} refers back to the reference configuration. It is seen from Eq. (2.4) that E_{ij} is symmetric in i and j. Of course, this strain definition satisfies the fundamental requirement that finite rigid body displacements render E_{ij} equal to zero. For derivation of the Green strain tensor in general curvilinear coordinates, see for instance Fung [36].

The more familiar symbols x, y, z and u, v, w will now be introduced instead of coordinates X_i and displacements u_i. As an example, three of the elements of the strain tensor are now written out fully

$$\begin{aligned} E_{xx} &= \frac{\partial u}{\partial x} + \frac{1}{2}\left(\left(\frac{\partial u}{\partial x}\right)^2 + \left(\frac{\partial v}{\partial x}\right)^2 + \left(\frac{\partial w}{\partial x}\right)^2 \right) \\ E_{yy} &= \frac{\partial v}{\partial y} + \frac{1}{2}\left(\left(\frac{\partial u}{\partial y}\right)^2 + \left(\frac{\partial v}{\partial y}\right)^2 + \left(\frac{\partial w}{\partial y}\right)^2 \right) \\ E_{xy} &= \frac{1}{2}\left(\frac{\partial u}{\partial y} + \frac{\partial v}{\partial x} + \frac{\partial u}{\partial x}\frac{\partial u}{\partial y} + \frac{\partial v}{\partial x}\frac{\partial v}{\partial y} + \frac{\partial w}{\partial x}\frac{\partial w}{\partial y} \right) \end{aligned} \tag{2.5}$$

If the quadratic strain terms are neglected, Eq. (2.5) is reduced to the usual engineering strains.

The definition of the stress vector (traction) and the corresponding stress tensor in Cartesian coordinates is given by

$$T_i = \nu_j \sigma_{ji} \tag{2.6}$$

where T_i are the components of the traction vector, ν_j the components of a outward unit vector of the surface and σ_{ji} is the stress tensor. Extra care has to be exercised when dealing with large deformations. The Eulerian stress tensor, also called Cauchy-stress, for large deformations is defined by

$$dT_i = \nu_j \sigma_{ji} \, dS \tag{2.7}$$

where dS is the surface area of the deformed body.

Since the Lagrangian approach is employed and strains are referred back to the reference configuration, the definition of stresses should also be based on the reference configuration. The (second) Piola-Kirchhoff stress tensor S_{ji} is defined by the following relation

$$\frac{\partial X_i}{\partial x_k} \, dT_k = S_{ji} \, \nu_{oj} \, dS_o \tag{2.8}$$

dS_o and ν_{oj} are taken in the reference configuration and a transformation is performed on dT_k. The definition of the Piola-Kirchhoff stress tensor in Cartesian coordinates is illustrated in Fig. 2.2. It can easily be shown that S_{ji} is a symmetric tensor [36, 37].

2.2.3 Variational Principles - The Principles of Virtual Work and Stationary Potential Energy

The objective of this analysis is to establish the state of static equilibrium of a body subjected to known loads and known boundary

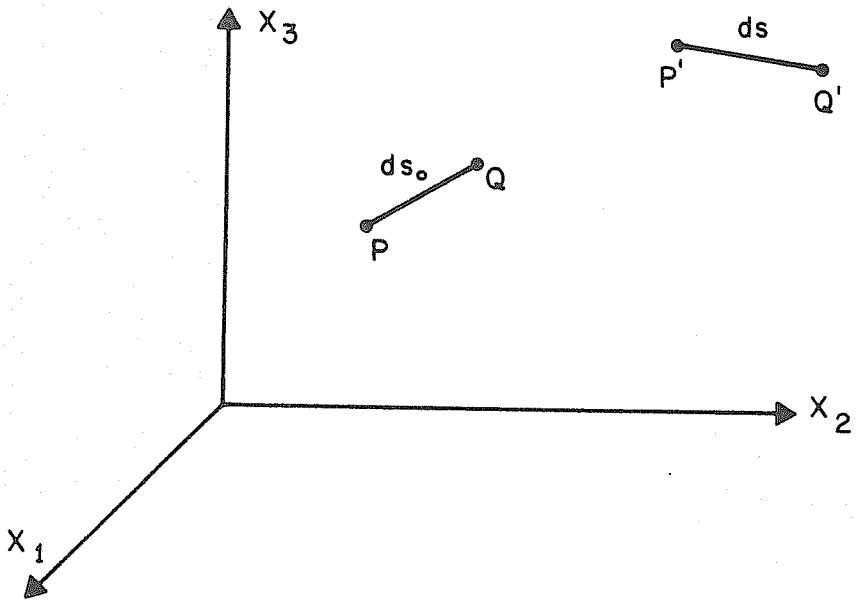

FIG. 2.1 FINITE DISPLACEMENT OF INFINITESIMAL LINE ELEMENT

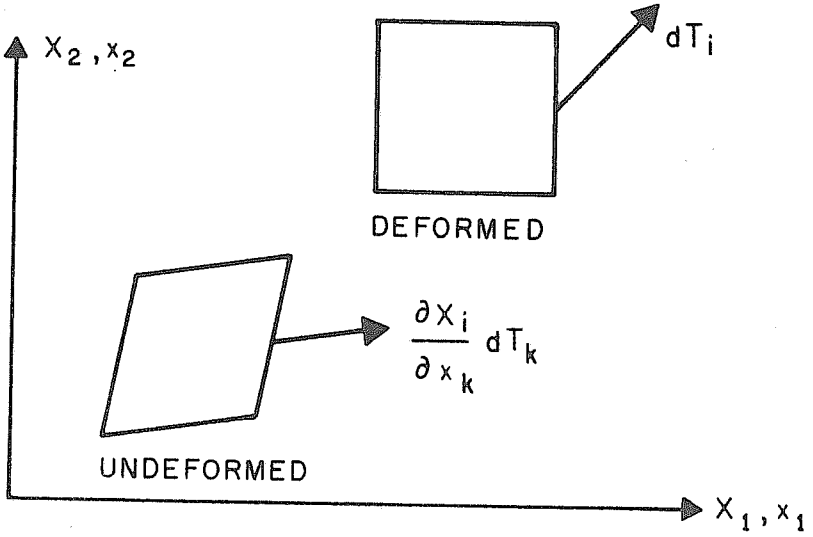

FIG. 2.2 DEFINITION OF THE 2nd PIOLA - KIRCHHOFF STRESS TENSOR

conditions. In such a state, equilibrium of an arbitrary infinitesimal element of the body must also be satisfied. Still using the Lagrangian approach and referring back to the reference configuration, the Cauchy equilibrium equation can be expressed as [34, 36]

$$\frac{\partial}{\partial X_k}\left(\frac{\partial x_i}{\partial X_j} S_{jk}\right) + P_i = 0 \qquad (2.9)$$

where P_i is the body force per unit volume of the reference configuration. An additional term accounting for acceleration may easily be incorporated on the right hand side of the equation if the equation is to be used in dynamic conditions.

The equilibrium equations will now be used for derivation of the principle of virtual work. A general material body B will be considered. The surface S of the body is assumed to consist of two parts, S_1 where the surface traction is prescribed and S_2 where displacements are prescribed. Now, using the equilibrium Equations (2.9), the prescribed conditions on the surface and Gauss' divergence theorem, the virtual work equation can be established [37, 38]

$$\int_V S_{ij}\,\delta E_{ij}\,dV - \int_{S_1} T_i\,\delta u_i\,dS - \int_V P_i\,\delta u_i\,dV = 0 \qquad (2.10)$$

δ is the variational symbol. S_{ij}, E_{ij} and u_i were defined in the previous section. The principle of virtual work as given by Eq. (2.10) is just an equivalent way of stating the equilibrium conditions for the body. However, a variational formulation has many computational advantages. Both the surface integral and the volume integral are taken over the reference configuration. Subscript zero is neglected since it is understood that the Lagrangian approach is used. δu_i is an arbitrary, kinematically admissible, virtual displacement field, that is, u_i must satisfy the rigid boundary conditions on S_2.

Equation (2.10) is valid for large displacements. However, it is not the only form in which the principle of virtual work may be stated. For instance, Reference [37] gives similar equations using Cauchy-stresses. Note that the principle of virtual work is independent of material properties.

Another important variational principle is the principle of complementary virtual work, which is, as indicated by its name, complementary to the principle of virtual work. The complementary virtual work principle is based on variation of stresses and forces instead of strains and displacements. From these two basic principles, several other variational principles may be derived, such as the principle of stationary potential energy, the principle of stationary complementary energy, the Hellinger-Reissner variational principle [39, 40] and the very general Hu-Washizu variational principle [38]. However, for the purpose of this investigation only the principle of stationary potential energy among the derived principles will be discussed further.

The principle of stationary potential energy is based on the existence of a single valued state function called the strain energy function. For the Lagrangian approach employed here, the stress tensor must be given by

$$S_{ij} = \frac{\partial W}{\partial E_{ij}} \tag{2.11}$$

where W is the strain energy function defined per unit volume of the reference body.

Substituting the strain energy function into Eq. (2.10), the principle of stationary potential energy can be formed as

$$\delta \int_V W(u_i)\, dV - \int_{S_1} T_i\, \delta u_i\, dS - \int_V P_i\, \delta u_i\, dV = 0 \qquad (2.12)$$

The first term expresses the variation of the strain energy integrated over the volume of the reference body. Among all admissible displacement functions u_i, the actual ones are those under which the total potential energy becomes stationary. In many cases potential functions may be substituted in Eq. (2.12) instead of surface tractions and volume forces.

Limiting the principle to small displacements only, it can be shown that the stationary state is a minimum potential energy state [36]. However, in large displacement theory the energy does not necessarily attain a minimum for the stationary condition. A broad study of the stability of the stationary configuration was made by Trefftz in 1930 [41].

2.2.4 Incremental Form of the Variational Principle

The purpose of this section is to extend the virtual work principles to a special incremental form. The need for the incremental form will be evident when numerical methods for solving nonlinear equations are beind discussed later.

Cauchy [42] was the first to derive the correct constitutive equations for a body under initial stress. Since then, much work has been done in studying the behavior of elastic bodies under initial stress. Truesdell [43] and Yaghmai [28] have given historical accounts of the development in this field and this history will not be repeated here.

The possible choices that can be made of coordinate systems and ways of referring stresses and strains are indeed numerous. Here, the Lagrangian approach using one global coordinate system will still be used. Figure 2.3 shows the material body at three different stages

during deformation. At the initial (reference) configuration, a material point is located by coordinates X_i ; the same point has coordinates x_i at an arbitrary, deformed configuration 1, and at a later configuration 2, the coordinates are $\bar{x}_i$.

Using Eq. (2.10) the virtual work equation in configuration 1 can be expressed as

$$\int_V S'_{ij}\,\delta E'_{ij}\,dV - \int_{S_1} T_i'\,\delta u_i' dS - \int_V P_i'\,\delta u_i'\,dV = 0 \tag{2.13}$$

Superscript 1 indicates configuration 1. Similarly, for configuration 2

$$\int_V S^2_{ij}\,\delta E^2_{ij}\,dV - \int_{S_1} T_i^2\,\delta u_i^2\,dS - \int_V P_i^2\,\delta u_i^2\,dV = 0 \tag{2.14}$$

Since forces are referred to the reference configuration, one may write

$$\begin{aligned} \Delta T_i &= T_i^2 - T_i^1 \\ \Delta P_i &= P_i^2 - P_i^1 \end{aligned} \tag{2.15}$$

and also

$$\delta u = \delta u^1 = \delta u^2 \tag{2.16}$$

By subtraction of Eq. (2.13) from Eq. (2.14), an incremental form of the variational principle can be established

$$\int_V S^2_{ij}\,\delta E^2_{ij} - S'_{ij}\,\delta E'_{ij}\,dV - \int_{S_1} \Delta T_i\,\delta u_i\,dS - \int_V \Delta P_i\,\delta u_i\,dV = 0 \tag{2.17}$$

However, in this form the equation is not very convenient. Employing the X_i, x_i and $\bar{x}_i$ coordinates and the definition of Eq. (2.4), the strain at configuration 2 can be expressed as

$$E^2_{ij} = \frac{1}{2}\left(\frac{\partial \bar{x}_k}{\partial X_i}\frac{\partial \bar{x}_k}{\partial X_j} - \delta_{ij}\right)$$

$$= \frac{1}{2}\left(\frac{\partial x_k}{\partial X_i}\frac{\partial x_k}{\partial X_j} - \delta_{ij}\right) + \frac{1}{2}\left(\frac{\partial \bar{x}_l}{\partial x_m}\frac{\partial \bar{x}_l}{\partial x_n} - \delta_{mn}\right)\frac{\partial x_m}{\partial X_i}\frac{\partial x_n}{\partial X_j} \qquad (2.18)$$

$$= E'_{ij} + \frac{\partial x_m}{\partial X_i}\frac{\partial x_n}{\partial X_j}\bar{E}_{mn}$$

where $\bar{E}_{ij}$ is the Green strain in configuration 2 referred to configuration 1.

Introducing

$$\xi_{ij} = \frac{\partial x_m}{\partial X_i}\frac{\partial x_n}{\partial X_j}\bar{E}_{mn} \qquad (2.19)$$

the strain at configuration 2 is

$$E^2_{ij} = E^1_{ij} + \xi_{ij} \qquad (2.20)$$

Substitution of Eq. (2.20) into Eq. (2.17) yields

$$\int_V \Delta S_{ij}\,\delta E'_{ij} + S^2_{ij}\,\delta\xi_{ij}\,dV - \int_{S_1} \Delta T_i\,\delta u_i\,dS - \int_V \Delta P_i\,\delta u_i\,dV = 0 \qquad (2.21)$$

where

$$\Delta S_{ij} = S^2_{ij} - S'_{ij} \qquad (2.22)$$

Yaghmai [28] has shown that for hyperelastic materials the first term of Eq. (2.21) can be transformed into the variation of the incremental free energy function. Instead, Equation (2.17) will again be considered here. Assuming an elastic material for which the stress can be found from a strain energy function, Equation (2.21) can be rewritten in a fashion similar to Eq. (2.12)

$$\int_V \delta W(u_i^2) - \delta W(u_i') \, dV - \int_{S_1} \Delta T_i \, \delta u_i \, dS - \int_V \Delta P_i \, \delta u_i \, dV = 0 \qquad (2.23)$$

Now, expanding the strain energy function

$$W(u_i^2) = W(u_i^1) + \delta W(u_i^1) + \text{higher order terms} \qquad (2.24)$$

and taking its variation

$$\begin{aligned} \delta W(u_i^2) &= \delta W(u_i') + \delta^2 W(u_i') + \text{higher order terms} \\ &= \delta W(u_i') + \Delta^2 W(u_i') \end{aligned} \qquad (2.25)$$

Equation (2.23) can finally be written

$$\int_V \delta^2 W(u_i') \, dV - \int_{S_1} \Delta T_i \, \delta u_i \, dS - \int_V \Delta P_i \, \delta u_i = \text{higher order terms} \qquad (2.26)$$

When configuration 2 is close to 1, the higher order terms become small and can be truncated. Hence Eq. (2.26) can be used to find a new configuration when displacements at configuration 1 and the load increments are known.

2.3 PLATE EQUATIONS

2.3.1 Basic Assumptions for Small Displacement Theory

The membrane and bending theories of plates are widely known and extensively described in the literature [44, 45]. However, for clarity and completeness, the basic assumptions will be repeated here briefly.

The motion of the plate will be referred to a right handed rectangular Cartesian coordinate system x, y, z whose axes x and y lie in the midplane of the undeformed plate, see Fig. 2.4. The displacement components of points lying in the midsurface are u_o, v_o

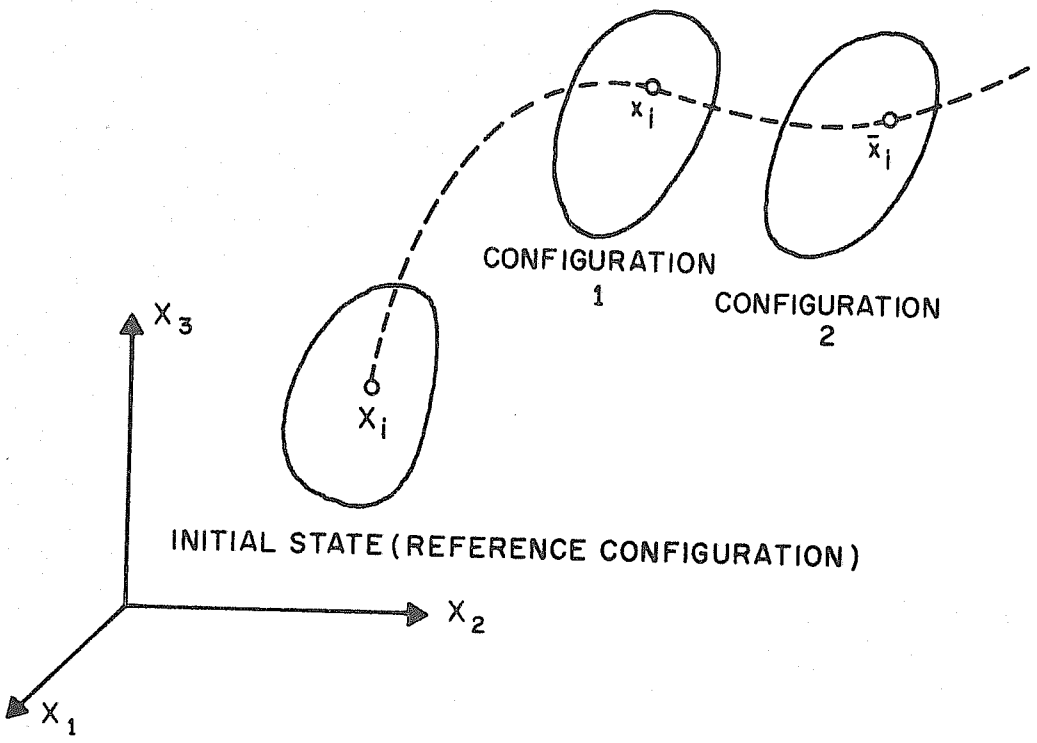

FIG. 2.3 LARGE DISPLACEMENTS OF A BODY

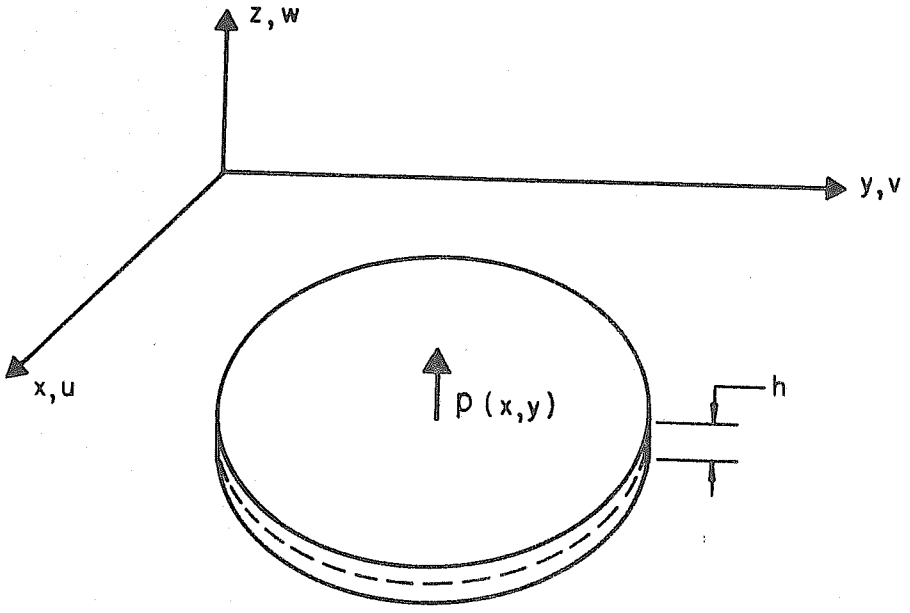

FIG. 2.4 DESCRIPTION OF THE PLATE IN A CARTESIAN COORDINATE SYSTEM

and w_o. To reduce the problem from a 3-dimensional to a 2-dimensional one, certain restrictions must be imposed on the displacement field. The Kirchhoff theory for thin plates will be adopted resulting in the following kinematic assumptions.

a) Normals to the midsurface remain straight and normal after deformation.

b) The strain in the z-direction is negligible in establishing the displacement of a material point.

After introducting these assumptions, only 3 non-zero strain components are left, namely ε_x, ε_y and γ_{xy}; furthermore

$$w = w_o \tag{2.27}$$

Introducing the rotations

$$\theta_x = \frac{\partial w}{\partial y}$$
$$\theta_y = -\frac{\partial w}{\partial x} \tag{2.28}$$

the inplane displacements are found from

$$u = u_o + z\,\theta_y$$
$$v = v_o - z\,\theta_x \tag{2.29}$$

and the corresponding strains are

$$\varepsilon_x = \frac{\partial u}{\partial x} = \frac{\partial u_o}{\partial x} - z\frac{\partial^2 w}{\partial x^2} \tag{2.30}$$

$$\varepsilon_y = \frac{\partial v}{\partial y} = \frac{\partial v_o}{\partial y} - z\frac{\partial^2 w}{\partial y^2} \tag{2.31}$$

$$\gamma_{xy} = \frac{\partial u}{\partial y} + \frac{\partial v}{\partial x} = \frac{\partial u_o}{\partial y} + \frac{\partial v_o}{\partial x} - 2z\frac{\partial^2 w}{\partial x \partial y} \tag{2.32}$$

2.3.2 A Nonlinear Strain - Displacement Relationship for Flat Plates

The strain - displacement Equations (2.5) will now be reconsidered, having applications to plates especially in mind. For almost all practical purposes when dealing with thin plates, the rotational terms $\frac{\partial w}{\partial x}$ and $\frac{\partial w}{\partial y}$ are large compared to the other terms involved in the quadratic part of Eq. (2.5). This justifies retaining only the rotational contributions among the higher order terms, resulting in

$$\begin{aligned} E_{xx} &= \frac{\partial u}{\partial x} + \frac{1}{2}\left(\frac{\partial w}{\partial x}\right)^2 \\ E_{yy} &= \frac{\partial v}{\partial y} + \frac{1}{2}\left(\frac{\partial w}{\partial y}\right)^2 \\ E_{xy} &= \frac{1}{2}\left(\frac{\partial u}{\partial y} + \frac{\partial v}{\partial x} + \frac{\partial w}{\partial x}\frac{\partial w}{\partial y}\right) \end{aligned} \tag{2.33}$$

These equations were first used by von Karman [1] who derived two fundamental partial differential equations for the deflection and the stress function based on Eq. (2.33). By examining these equations it is seen that the primary effect of the stretching of the reference surface is included. Timoshenko [45] has shown how the Equations (2.33) can be derived in a more direct manner by considering the straining of an infinitesimal plate element during a rotation and truncating higher order terms.

Novozhilov [46, 53] has classified the von Karman strain equations as "the case of small strain components and small angles of rotation, the latter considerably exceeding the former". One should note that these equations cannot be classified as "finite strain" expressions. However, as will be demonstrated by a wide range of

examples later, the accuracy of these strain terms is sufficient for almost all practical applications to nonlinear plate problems.

These strain terms will now be applied to the midsurface of the plate. The Kirchhoff assumptions will still be employed as for the linear small deflection theory and integrals formulated according to the variational principles will be evaluated over undeformed volumes.

2.3.3 Strain - Displacement Relations for Initially Deformed Plates

This section will deal with the special strain expressions for plates which are not perfectly plane in the initial configuration but have some initial deflection. Such initial deformations may have important consequences for the overall behavior of the plate and will have to be accounted for using a so-called "shallow shell" theory.

The classical shallow shell theory was suggested by Marguerre in 1938 [47]. He referred the initial deflections of the midplane of the shallow shell to a rectangular global coordinate system, see Fig. 2.5. Letting $\bar{w}$ denote the initial deflection of the plate and w the additional deflection, the Marguerre strain-displacement equations read

$$
\begin{aligned}
E_{xx} &= \frac{\partial u}{\partial x} + \frac{\partial \bar{w}}{\partial x}\frac{\partial w}{\partial x} + \frac{1}{2}\left(\frac{\partial w}{\partial x}\right)^2 \\
E_{yy} &= \frac{\partial v}{\partial y} + \frac{\partial \bar{w}}{\partial y}\frac{\partial w}{\partial y} + \frac{1}{2}\left(\frac{\partial w}{\partial y}\right)^2 \\
2E_{xy} &= \frac{\partial u}{\partial y} + \frac{\partial v}{\partial x} + \frac{\partial \bar{w}}{\partial x}\frac{\partial w}{\partial y} + \frac{\partial \bar{w}}{\partial y}\frac{\partial w}{\partial x} + \frac{\partial w}{\partial x}\frac{\partial w}{\partial y}
\end{aligned}
\qquad (2.34)
$$

As was demonstrated by Marguerre, these equations can be derived by considering the straining during rotation of an infinitesimal

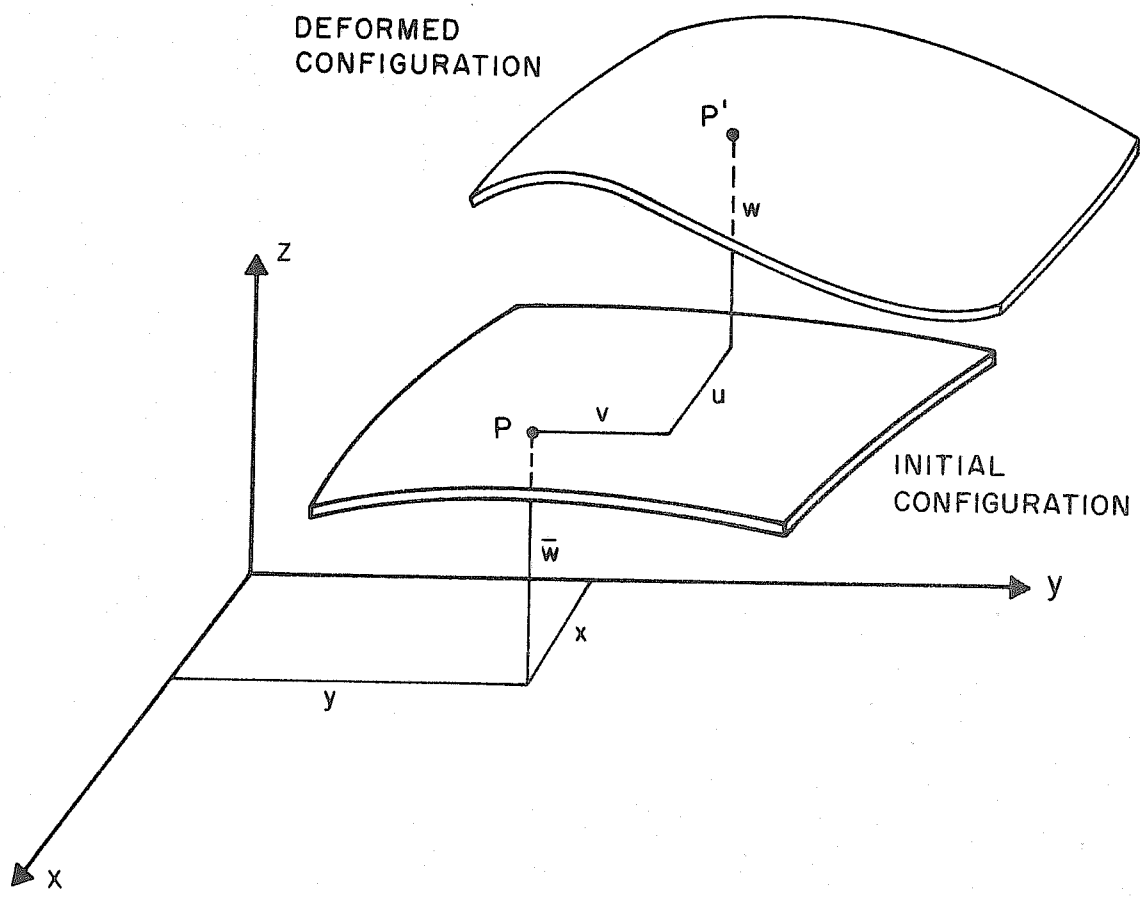

FIG. 2.5 INITIALLY DEFORMED PLATE

plate element and truncating higher order terms. However, it is of interest to note that the same equations can be obtained using the Green strain tensor Eq. (2.4). This will now briefly be demonstrated. Introducing

$$u_i^* = \bar{u}_i + u_i \tag{2.35}$$

where $\bar{u}_i$ represents the initial deformation. The "effective" strain will be defined as

$$\begin{aligned} E_{ij}^e &= E_{ij}^* - \bar{E}_{ij} \\ &= \frac{1}{2}\left(\frac{\partial u_j^*}{\partial x_i} + \frac{\partial u_i^*}{\partial x_j} + \frac{\partial u_k^*}{\partial x_i}\frac{\partial u_k^*}{\partial x_j} - \frac{\partial \bar{u}_j}{\partial x_i} - \frac{\partial \bar{u}_i}{\partial x_j} - \frac{\partial \bar{u}_k}{\partial x_i}\frac{\partial \bar{u}_k}{\partial x_j}\right) \\ &= \frac{1}{2}\left(\frac{\partial u_j}{\partial x_i} + \frac{\partial u_i}{\partial x_j} + \frac{\partial \bar{u}_k}{\partial x_i}\frac{\partial u_k}{\partial x_j} + \frac{\partial \bar{u}_k}{\partial x_j}\frac{\partial u_k}{\partial x_i} + \frac{\partial u_k}{\partial x_i}\frac{\partial u_k}{\partial x_j}\right) \end{aligned} \tag{2.36}$$

Imposing $\bar{u} = \bar{v} = 0$ and neglecting quadratic terms of the derivatives of u and v, one is left with exactly the equations of Marguerre (2.34). However, the derivation demonstrated here is believed to be more consistent with the previous use of the Green strain tensor and the von Karman type of simplification of those expressions.

Flügge and Conrad [48] reformulated the Marguerre equations defining the displacements in a curved coordinate system lying in the midplane of the shallow shell. It turns out that their expressions can be obtained from a more general derivation using curvilinear coordinates given by Green and Zerna [32]. However, the original approach defining the displacements in a global Cortesian coordinate system as given by Marguerre proves to be more suited for the numerical methods to be applied later.

The range of validity of the Marguerre shallow shell theory has been studied by several investigators such as E. Reissner [49], Vlasov [50], and Flügge and Conrad [48]. Reissner stated in reference [49] that shallow shell theory is more than sufficiently accurate as long as $\frac{\partial \bar{w}}{\partial x}$ and $\frac{\partial \bar{w}}{\partial y}$ are less than 1/8.

2.3.4 Calculation of the Strain Energy for the Plate

The strain-displacement Equations (2.33) and (2.34) correspond to the strain of an infitesimal element lying parallel to the surface of the plate during deformation. Adopting the Kirchhoff assumptions also for initially deformed plates and using matrix notation, the strains at a distance ζ from midsurface can be expressed in general as

$$\{\varepsilon\} = \{\varepsilon_o\} + \zeta \{\varkappa\} \tag{2.37}$$

where the strains at the midsurface are

$$\{\varepsilon_o\} = \begin{Bmatrix} E_{xx} \\ E_{yy} \\ 2E_{xy} \end{Bmatrix} \tag{2.38}$$

and the curvatures

$$\{\varkappa\} = - \begin{Bmatrix} \frac{\partial^2 w}{\partial x^2} \\ \frac{\partial^2 w}{\partial y^2} \\ 2\frac{\partial^2 w}{\partial x \partial y} \end{Bmatrix} \tag{2.39}$$

The ζ-axis is perpendicular to the midsurface.

A corresponding set of stresses are defined by

$$\{\sigma\} = \begin{Bmatrix} \sigma_x \\ \sigma_y \\ \tau_{xy} \end{Bmatrix} = [D]\{\varepsilon\} \tag{2.40}$$

where [D] is the constitutive relation for generalized plane stress. For isotropic Hookean materials [D] is, of course,

$$[D] = [E] = \frac{E}{1-\nu^2}\begin{bmatrix} 1 & \nu & 0 \\ \nu & 1 & 0 \\ 0 & 0 & \frac{1-\nu}{2} \end{bmatrix} \tag{2.41}$$

where E is Youngs modulus and ν is Poissons ratio. Expressing the strain energy function directly in terms of the strains, as shown in Reference [36], for instance the total strain energy is obtained by integrating over the entire body

$$\begin{aligned} U &= \int_V W(\varepsilon)\,dV = \frac{1}{2}\int_V \{\varepsilon\}^T [D]\{\varepsilon\}\,dV \\ &= \frac{1}{2}\int_A \int_{-\frac{h}{2}}^{\frac{h}{2}} \left\{\begin{array}{c} \varepsilon_o \\ \hline \zeta\kappa \end{array}\right\}^T \left[\begin{array}{c|c} D & 0 \\ \hline 0 & D \end{array}\right] \left\{\begin{array}{c} \varepsilon_o \\ \hline \zeta\kappa \end{array}\right\} d\zeta\,dA \\ &= \frac{1}{2}\int_A \left\{\begin{array}{c} \varepsilon_o \\ \hline \kappa \end{array}\right\} \left[\begin{array}{c|c} D_{11} & D_{12} \\ \hline D_{21} & D_{22} \end{array}\right] \left\{\begin{array}{c} \varepsilon_o \\ \hline \kappa \end{array}\right\} dA \end{aligned} \tag{2.42}$$

where

$$[D_{11}] = \int_{-\frac{h}{2}}^{\frac{h}{2}} [D]\,d\zeta \tag{2.43}$$

$$[D_{12}] = [D_{21}]^T = \int_{-\frac{h}{2}}^{\frac{h}{2}} \zeta\,[D]\,d\zeta \tag{2.44}$$

and

$$[D_{22}] = \int_{-\frac{h}{2}}^{\frac{h}{2}} \zeta^2 [D] \, d\zeta \tag{2.45}$$

dA is taken at the undeformed midsurface and h is the thickness. When the material properties are symmetric about the midplane, $[D_{12}]$ and $[D_{21}]$ become identical to zero.

Finally, the total strain energy Eq. (2.42) will be divided into three separate terms as follows:

$$\begin{aligned} U &= U_m + U_b + U_{mb} \\ &= \frac{1}{2}\int_A \{\varepsilon_o\}^T [D_{11}] \{\varepsilon_o\} \, dA + \frac{1}{2}\int_A \{\varkappa\}^T [D_{22}] \{\varkappa\} \, dA \\ &+ \int_A \{\varepsilon_o\}^T [D_{12}] \{\varkappa\} \, dA \end{aligned} \tag{2.46}$$

where U_m is the membrane contribution, U_b stands for the bending contribution and U_{mb} is the combined membrane-bending term which vanishes for homogeneous Hookean materials.

2.4 MATRIX FORMULATION OF THE PLATE PROBLEM

2.4.1 The Ritz Method

The variational principle as stated in Eq. (2.12) can be used for derivation of the differential equation of equilibrium (Euler equation) and the natural boundary conditions. In fact, the variational formulation and the differential equations are equivalent ways of stating the same physical requirements. However, the differential equation with arbitrary boundary conditions generally cannot be solved using analytic functions. Therefore some numerical method has to be applied to find an approximate solution to the problem.

The Ritz-method has extensively been used for solution of structural problems. This method, which was proposed by Ritz in 1908, deals with solution of the differential equation

$$L\,u = f \tag{2.47}$$

where L is a positive definite, linear operator defined in domain D_L, u is the field function sought in D_L, and f is a known function that has a finite norm. The Ritz method is throughly discussed in Reference [51] and [52], and will not be described in detail here. The method basically consists of using a sequence of linearly independent functions seq (u_n) that is complete in energy; then by minimizing a functional $F(u_n)$, it can be shown that seq (u_n) is a minimizing sequence that converges to the exact solution in energy. For elasticity problems, the functional F corresponds to the potential energy of the structure; and the minimal functional theorem [51] on which the Ritz procedure is based, corresponds to the principle of minimum potential energy in the theory of elasticity. A basic theorem necessary for the proof of convergence of the Ritz-method is that when the operator L is positive definite, Eq. (2.47) cannot have more than one solution. This corresponds to the Kirchhoff uniqueness theorem in linear elasticity.

However, the main objective of this study is to solve a class of nonlinear elasticity problems for which the differential operator generally does not satisfy either linearity or positive definiteness. Consequently, uniqueness of the solution cannot be proved, which in turn implies that convergence of the Ritz method generally can not be proved. On the other hand, Ritz-type solution techniques like the finite element method have been used successfully for solving nonlinear

structural problems. But it is also known that using these methods, convergence to the exact solution is hard to obtain in some cases and that a wide range of numerical difficulties may be encountered. At this stage, therefore, it will only be stated that experience has shown that Ritz-type solution methods can in most cases be used for solving nonlinear problems. No doubt, much work is left to be done in studying in a rigorous mathematical manner the application of Ritz-type methods to problems for which L is not linear and positive definite.

2.4.2 Matrix Formulation of the Strain Expressions

The strain expressions will now be rewritten in a matrix form that is more suitable for numerical calculations. The strains at the middle surface as given by Equations (2.38) and (2.34) consist of three separate contributions:

$$\{\varepsilon_o\} = \{\varepsilon_o\}_1 + \{\varepsilon_o\}_2 + \{\varepsilon_o\}_3$$

$$= \begin{Bmatrix} \frac{\partial u_o}{\partial x} \\ \frac{\partial v_o}{\partial y} \\ \frac{\partial u_o}{\partial y} + \frac{\partial v_o}{\partial x} \end{Bmatrix} + \begin{Bmatrix} \frac{\partial \bar{w}}{\partial x}\frac{\partial w}{\partial x} \\ \frac{\partial \bar{w}}{\partial y}\frac{\partial w}{\partial y} \\ \frac{\partial \bar{w}}{\partial x}\frac{\partial w}{\partial y} + \frac{\partial \bar{w}}{\partial y}\frac{\partial w}{\partial x} \end{Bmatrix} + \begin{Bmatrix} \frac{1}{2}\left(\frac{\partial w}{\partial x}\right)^2 \\ \frac{1}{2}\left(\frac{\partial w}{\partial y}\right)^2 \\ \frac{\partial w}{\partial x}\frac{\partial w}{\partial y} \end{Bmatrix} \qquad (2.48)$$

The first two terms are both linear, the second of these is due to the shallow shell effect. The last term is the nonlinear von Karman strain contribution.

The Ritz method requires a set of field functions with a corresponding set of coefficients to be chosen. The inplane and out of plane variables will now be separated, so that

$$\begin{Bmatrix} u_o \\ v_o \end{Bmatrix} = [\Phi_v]\{v_i\} \tag{2.49}$$

and

$$w = \langle \varphi_w \rangle \{w_i\} \tag{2.50}$$

where $[\Phi_v]$ and $\langle \varphi_w \rangle$ are the field functions satisfying the displacement boundary conditions and $\{v_i\}$ and $\{w_i\}$ are the corresponding coefficients.

For later use, let the following two linear differential operators be defined

$$[\Delta_1] = \begin{bmatrix} \frac{\partial}{\partial x} & 0 \\ 0 & \frac{\partial}{\partial y} \\ \frac{\partial}{\partial y} & \frac{\partial}{\partial x} \end{bmatrix} \tag{2.51}$$

and

$$\{\Delta_2\} = \begin{Bmatrix} \frac{\partial}{\partial x} \\ \frac{\partial}{\partial y} \end{Bmatrix} \tag{2.52}$$

The first strain contribution in Eq. (2.48) then becomes

$$\{\varepsilon_o\}_1 = [\Delta_1][\Phi_v]\{v_i\} = [B_v]\{v_i\} \tag{2.53}$$

where $[B_V]$ contains the first derivatives of the field functions.

The shallow shell contribution of Eq. (2.48) can be expressed as a product of two matrices

$$\{\varepsilon_o\}_2 = \begin{bmatrix} \frac{\partial \bar{w}}{\partial x} & 0 \\ 0 & \frac{\partial \bar{w}}{\partial y} \\ \frac{\partial \bar{w}}{\partial y} & \frac{\partial \bar{w}}{\partial x} \end{bmatrix} \begin{Bmatrix} \frac{\partial w}{\partial x} \\ \frac{\partial w}{\partial y} \end{Bmatrix} = [\bar{M}]\{M\} \tag{2.54}$$

Using the differential operator defined in Eq. (2.52), $\{M\}$ becomes

$$\{M\} = \{\Delta_2\} \langle \varphi_w \rangle \{w_i\} = [B_{w2}]\{w_i\} \tag{2.55}$$

It is assumed that the initial deflection of the plate can be expressed in a manner similar to Eq. (2.50)

$$\bar{w} = \langle \bar{\varphi}_w \rangle \{\bar{w}_i\} \tag{2.56}$$

where $\{\bar{w}_i\}$ is a set of known coefficients, not necessarily of the same dimension as $\{w_i\}$. Arranging the two vectors in corner matrices

$$[\bar{W}_i] = \left[\begin{array}{c|c} \bar{w}_i & 0 \\ \hline 0 & \bar{w}_i \end{array}\right] \tag{2.57}$$

and

$$[\bar{\Phi}_w] = \left[\begin{array}{c|c} \bar{\varphi}_w & 0 \\ \hline 0 & \bar{\varphi}_w \end{array}\right] \tag{2.58}$$

the matrix $[\bar{M}]$ in Eq. (2.54) can finally be expressed as

$$[\bar{M}] = [A_1][\bar{\Phi}_w][\bar{W}_i] = [\bar{B}_{w1}][\bar{W}_i] \tag{2.59}$$

The shallow shell strains in Eq. (2.48) therefore become

$$\{\varepsilon_o\}_2 = [\bar{B}_{w1}][\bar{W}_i][B_{w2}]\{w_i\} \tag{2.60}$$

The remaining term in Eq. (2.48) is the nonlinear one. Expanding it in a manner similar to Eq. (2.54)

$$\{\varepsilon_o\}_3 = \frac{1}{2}\begin{bmatrix} \frac{\partial w}{\partial x} & 0 \\ 0 & \frac{\partial w}{\partial y} \\ \frac{\partial w}{\partial y} & \frac{\partial w}{\partial x} \end{bmatrix} \begin{Bmatrix} \frac{\partial w}{\partial x} \\ \frac{\partial w}{\partial y} \end{Bmatrix} \tag{2.61}$$

and defining two new corner matrices

$$[W_i] = \left[\begin{array}{c|c} w_i & 0 \\ \hline 0 & w_i \end{array}\right] \tag{2.62}$$

and

$$[\bar{\Phi}_w] = \left[\begin{array}{c|c} \varphi_w & 0 \\ \hline 0 & \varphi_w \end{array}\right] \tag{2.63}$$

the nonlinear strain term becomes

$$\begin{aligned} \{\varepsilon_o\}_3 &= \frac{1}{2}[\Delta_1][\bar{\Phi}_w][W_i]\{\Delta_2\}\langle\varphi_w\rangle\{w_i\} \\ &= \frac{1}{2}[B_{w1}][W_i][B_{w2}]\{w_i\} \end{aligned} \tag{2.64}$$

The Equations (2.55), (2.61) and (2.64) now constitute the total strain expression Eq. (2.48).

To obtain the curvatures of Eq. (2.39) the following second order operator is introduced

$$\{\Delta_3\} = -\begin{Bmatrix} \frac{\partial^2}{\partial x^2} \\ \frac{\partial^2}{\partial y^2} \\ 2\frac{\partial^2}{\partial x \partial y} \end{Bmatrix} \tag{2.65}$$

The curvatures are now found from

$$\{\kappa\} = \{\Delta_3\} \langle \varphi_w \rangle \{w_i\} = [B_{w3}]\{w_i\} \tag{2.66}$$

and the strains at any point are easily obtained using Eq. (2.37).

2.4.3 The Total Strain Energy Expression

The strain energy of the body was expressed as a sum of three terms in Eq. (2.46). The strain expressions derived in the proceding section are now to be used for rewriting the energy expression Eq. (2.46). By substitution of Eq. (2.48), the membrane energy is seen to be made up by 6 separate terms

$$\begin{aligned} U_m &= \frac{1}{2}\int_A \{\varepsilon_o\}^T [D_{11}] \{\varepsilon_o\}\, dA \\ &= \frac{1}{2}\int_A \{\varepsilon_o\}_1^T [D_{11}] \{\varepsilon_o\}_1\, dA + \frac{1}{2}\int_A \{\varepsilon_o\}_2^T [D_{11}] \{\varepsilon_o\}_2\, dA \\ &+ \frac{1}{2}\int_A \{\varepsilon_o\}_3^T [D_{11}] \{\varepsilon_o\}_3\, dA + \int_A \{\varepsilon_o\}_1^T [D_{11}] \{\varepsilon_o\}_2\, dA \\ &+ \int_A \{\varepsilon_o\}_2^T [D_{11}] \{\varepsilon_o\}_3\, dA + \int_A \{\varepsilon_o\}_3^T [D_{11}] \{\varepsilon_o\}_1\, dA \\ &= U_{m1} + U_{m2} + U_{m3} + U_{m4} + U_{m5} + U_{m6} \end{aligned} \tag{2.67}$$

The strain expressions given in the Equations (2.53), (2.60) and (2.64) can now be inserted in Eq. (2.67) and the membrane strain energy terms can be stated as

$$
\begin{aligned}
U_{m1} &= \frac{1}{2}\{v_i\}^T [k_v] \{v_i\} \\
U_{m2} &= \frac{1}{2}\{w_i\}^T \int_A [B_{w2}]^T [\bar{W}_i]^T [\bar{P}] [\bar{W}_i] [B_{w2}] dA \{w_i\} \\
U_{m3} &= \frac{1}{8}\{w_i\}^T \int_A [B_{w2}]^T [W_i]^T [P] [W_i] [B_{w2}] dA \{w_i\} \\
U_{m4} &= \{v_i\}^T \int_A [P_1] [\bar{W}_i] [B_{w2}] dA \{w_i\} \\
U_{m5} &= \frac{1}{2}\{w_i\}^T \int_A [B_{w2}]^T [\bar{W}_i]^T [P_2] [W_i] [B_{w2}] dA \{w_i\} \\
U_{m6} &= \frac{1}{2}\{w_i\}^T \int_A [B_{w2}]^T [W_i]^T [P_3] dA \{v_i\}
\end{aligned}
\tag{2.68}
$$

where the following symbols have been introduced

$$
\begin{aligned}
[k_v] &= \int_A [B_v]^T [D_{11}] [B_v] dA \\
[P] &= [B_{w1}]^T [D_{11}] [B_{w1}] \\
[\bar{P}] &= [\bar{B}_{w1}]^T [D_{11}] [\bar{B}_{w1}] \\
[P_1] &= [B_v]^T [D_{11}] [\bar{B}_{w1}] \\
[P_2] &= [\bar{B}_{w1}]^T [D_{11}] [B_{w1}] \\
[P_3] &= [B_{w1}]^T [D_{11}] [B_v]
\end{aligned}
\tag{2.69}
$$

A closer look at these energy terms is worth while. In linear elasticity, the strain energy is known to be a quadratic function of the displacements (strains). It is seen that U_{m1}, U_{m2} and U_{m4} are such terms, the last two of which are due to the shallow shell effect. $[k_v]$ is easily recognized as the linear membrane coefficient (stiffness) matrix. The other terms are higher order contributions of nonlinear elasticity. U_{m3} is a quartic function of the displacements. Nevertheless, this term is not negligible; it accounts for the stretching of the plate when it deflects during zero inplane displacements.

Some simplifications of the terms (2.69) can be obtained when the initial deflection $\bar{w}$ is chosen to be represented by the same field function as w. ($<\phi_w> \equiv <\bar{\phi}_w>$) In that case the following identities hold true

$$[P] \equiv [\bar{P}] \equiv [P_2] \tag{2.70}$$

and

$$[P_1] \equiv [P_3]^T \tag{2.71}$$

The next energy term of Eq. (2.46) to be evaluated is the bending contribution. Substituting the curvature as given by Eq. (2.66), it becomes

$$\begin{aligned} U_b &= \frac{1}{2}\{\omega_i\}^T \int_A [B_{w3}]^T [D_{22}] [B_{w3}]\, dA\, \{\omega_i\} \\ &= \frac{1}{2}\{\omega_i\}^T [k_w] \{\omega_i\} \end{aligned} \tag{2.72}$$

where the linear bending stiffness is

$$[k_w] = \int_A [B_{w3}]^T [D_{22}] [B_{w3}] \, dA \tag{2.73}$$

The remaining term in Eq. (2.46) is the membrane - bending coupling term. By substitution of Eq. (2.48) and Eq. (2.66) into Eq. (2.46) and then after using Eqs. (2.53), (2.60) and (2.64), the following expression for U_{mb} is obtained

$$\begin{aligned} U_{mb} &= \int_A [\{\varepsilon_o\}_1 + \{\varepsilon_o\}_2 + \{\varepsilon_o\}_3]^T [D_{12}] \{\kappa\} \, dA \\ &= U_{mb1} + U_{mb2} + U_{mb3} \end{aligned} \tag{2.74}$$

where

$$\begin{aligned} U_{mb1} &= \{v_i\}^T [\hat{k}_{vw}] \{w_i\} \\ U_{mb2} &= \{w_i\}^T \int_A [B_{w2}]^T [\bar{W}_i]^T [P_4] \, dA \, \{w_i\} \\ U_{mb3} &= \frac{1}{2} \{w_i\}^T \int_A [B_{w2}]^T [W_i]^T [P_5] \, dA \, \{w_i\} \end{aligned} \tag{2.75}$$

and

$$\begin{aligned} [\hat{k}_{vw}] &= \int_A [B_v]^T [D_{12}] [B_{w3}] \, dA \\ [P_4] &= [\bar{B}_{w1}]^T [D_{12}] [B_{w3}] \\ [P_5] &= [B_{w1}]^T [D_{12}] [B_{w3}] \end{aligned} \tag{2.76}$$

When

$$\langle \varphi_w \rangle \equiv \langle \bar{\varphi}_w \rangle \tag{2.77}$$

the following identity holds

$$[P_4] \equiv [P_5] \tag{2.78}$$

2.4.4 The Equilibrium Equations

The variational principle was stated in Section 2.2.3. According to Eq. (2.12), the first variation of the total strain energy is needed for establishing the equilibrium equations. First, considering the membrane strain energy as expressed in Eq. (2.63) and remembering that the only quantities to be varied are the displacement coefficients $\{v_i\}$ and $\{w_i\}$, the following equations are obtained.

$$
\begin{aligned}
\delta U_{m1} &= \delta\{v_i\}^T [k_v] \{v_i\} \\
\delta U_{m2} &= \delta\{w_i\}^T \int_A [B_{w2}]^T [\bar{W}_i]^T [\bar{P}] [\bar{W}_i] [B_{w2}] dA \{w_i\} \\
\delta U_{m3} &= \tfrac{1}{2} \delta\{w_i\}^T \int_A [B_{w2}]^T [W_i]^T [P] [W_i] [B_{w2}] dA \{w_i\} \\
\delta U_{m4} &= \delta\{v_i\}^T \int_A [P_1] [\bar{W}_i] [B_{w2}] dA \{w_i\} \\
&\quad + \delta\{w_i\}^T \int_A [B_{w2}]^T [\bar{W}_i]^T [P_1]^T dA \{v_i\} \qquad (2.79) \\
\delta U_{m5} &= \tfrac{1}{2} \delta\{w_i\}^T \int_A [B_{w2}]^T [\bar{W}_i]^T [P_2] [W_i] [B_{w2}] dA \{w_i\} \\
&\quad + \delta\{w_i\}^T \int_A [B_{w2}]^T [W_i]^T [P_2]^T [\bar{W}_i] [B_{w2}] dA \{w_i\} \\
\delta U_{m6} &= \delta\{w_i\}^T \int_A [B_{w2}]^T [W_i]^T [P_3] dA \{v_i\} \\
&\quad + \tfrac{1}{2} \delta\{v_i\}^T \int_A [P_3]^T [W_i] [B_{w2}] dA \{w_i\}
\end{aligned}
$$

Note that transposition of energy terms can be performed unrestrictedly here since they are scalar quantities. The variations $\delta\{w_i\}$ and $\delta\{W_i\}$ can also be interchanged since they represent the same quantities.

The variation of the bending strain Eq. (2.72) goes in a similar manner

$$\begin{aligned} \delta U_b &= \delta \{w_i\}^T \int_A [B_{w3}]^T [D_{22}] [B_{w3}] dA \{w_i\} \\ &= \delta \{w_i\}^T [k_{ww}] \{w_i\} \end{aligned} \tag{2.80}$$

and finally the first variation of the combined membrane-bending energy Eq. (2.75) becomes

$$\begin{aligned} \delta U_{mb1} &= \delta \{v_i\}^T [k_{vw}] \{w_i\} + \delta \{w_i\}^T [k_{vw}]^T \{v_i\} \\ \delta U_{mb2} &= \delta \{w_i\}^T \int_A [B_{w2}]^T [\bar{W}_i]^T [P_4] dA \{w_i\} \\ &\quad + \delta \{w_i\}^T \int_A [P_4]^T [\bar{W}_i] [B_{w2}] dA \{w_i\} \\ \delta U_{mb3} &= \delta \{w_i\}^T \int_A [B_{w2}]^T [W_i]^T [P_5] dA \{w_i\} \\ &\quad + \frac{1}{2} \delta \{w_i\}^T \int_A [P_5]^T [W_i] [B_{w2}] dA \{w_i\} \end{aligned} \tag{2.81}$$

The virtual work Equation (2.12) includes two terms accounting for work done by surface tractions and body forces. Since the plate is a special form of geometry degenerated to two dimensions, the work done by these forces can be expressed by work done by forces defined at the midsurface. Making use of field functions as was done for the displacements (2.49), (2.50), the midsurface loads can be written

$$\{P_v\} = \begin{Bmatrix} P_x \\ P_y \end{Bmatrix} = [\bar{\Phi}_{pv}] \{P_{vi}\} \tag{2.82}$$

and

$$P_{w} = \langle \varphi_{pw} \rangle \{P_{wi}\} \tag{2.83}$$

The field functions are assumed to be of a very general form, capable of expressing concentrated forces and boundary loads. $\{P_{vi}\}$ and $\{P_{wi}\}$ are the known load coefficients. Again, using Eqs. (2.49) and (2.50), the virtual work done by these forces is

$$\begin{aligned} \delta V_p = {} & \delta\{v_i\}^T \int_A [\bar{\Phi}_v]^T [\bar{\Phi}_{pv}]\, dA \; \{P_{vi}\} \\ & + \delta\{w_i\}^T \int_A \langle \varphi_{w} \rangle^T \langle \varphi_{pw} \rangle\, dA \; \{P_{wi}\} \end{aligned} \tag{2.84}$$

Let two generalized force vectors be defined

$$\{P_{vi}\} = \int_A [\bar{\Phi}_v]^T [\bar{\Phi}_{pv}]\, dA \; \{P_{vi}\} \tag{2.85}$$

and

$$\{P_{wi}\} = \int_A \langle \varphi_{w} \rangle^T \langle \varphi_{pw} \rangle\, dA \; \{P_{wi}\} \tag{2.86}$$

Eliminating the virtual displacement vectors, the virtual work Equation (2.12) for the domain in which the field functions are defined may be stated as

$$[k]\{r_i\} = \{P_i\} \tag{2.87}$$

or

$$\left[\begin{array}{c|c} k_{vv} & k_{vw} \\ \hline k_{wv} & k_{ww} \end{array}\right] \left\{\begin{array}{c} v_i \\ \hline w_i \end{array}\right\} = \left\{\begin{array}{c} P_{vi} \\ \hline P_{wi} \end{array}\right\} \tag{2.88}$$

This equation expresses the state of equilibrium for the system, and it is valid for the entire plate or a subdomain of the plate (as in finite element method). The submatrices of the coefficient matrix are obtained directly from the Equations (2.79), (2.80), and (2.81)

$$[k_{uu}] = [k_u] \tag{2.89}$$

$$[k_{uw}] = \int_A [P_1][\bar{W}_i][B_{w2}]dA + \frac{1}{2}\int_A [P_3]^T[W_i][B_{w2}]dA + [\hat{k}_{uw}] \tag{2.90}$$

$$[k_{wu}] = \int_A [B_{w2}]^T[\bar{W}_i]^T[P_1]^T dA + \int_A [B_{w2}]^T[W_i]^T[P_3]dA + [\hat{k}_{uw}]^T \tag{2.91}$$

$$\begin{aligned}[k_{ww}] = & \int_A [B_{w2}]^T[\bar{W}_i]^T[\bar{P}][\bar{W}_i][B_{w2}]\,dA \\ & + \frac{1}{2}\int_A [B_{w2}]^T[W_i]^T[P][W_i][B_{w2}]\,dA \\ & + \frac{1}{2}\int_A [B_{w2}]^T[\bar{W}_i]^T[P_2][W_i][B_{w2}]dA \\ & + \int_A [B_{w2}]^T[W_i]^T[P_2][\bar{W}_i][B_{w2}]dA \\ & + [k_w] + \int_A [B_{w2}]^T[\bar{W}_i]^T[P_4]\,dA \\ & + \int_A [P_4]^T[\bar{W}_i][B_{w2}]\,dA + \int_A [B_{w2}]^T[W_i]^T[P_5]\,dA \\ & + \frac{1}{2}\int_A [P_6]^T[W_i][B_{w2}]\,dA \end{aligned} \tag{2.92}$$

The equilibrium Equation (2.88) is nonlinear since the coefficient matrix is a function of the displacements. Further, it is not symmetric, in general

$$[k_{vw}] \neq [k_{wv}]^T$$
$$[k_{ww}] \neq [k_{ww}]^T \qquad (2.93)$$

This last fact may, at first glance, seem rather disappointing. However, it is without significant importance since the numerical solution methods to be applied do not depend on inversion of $[k]$. As will be seen in the next section, the incremental form of the variational principle leads to a symmetric coefficient matrix, a fact which is of great importance.

A noteworthy fact is also that many of the terms become zero when there is no initial deflection or when the constitutive equation is constant through the thickness.

2.4.5 The Incremental Equations

The incremental form of the variational principle was given in Eq. (2.26). It is assumed that this principle is to be applied to two consecutive configurations that are close to each other. The higher order terms mentioned in Eq. (2.26) will therefore be neglected.

The second variation of the total strain energy is obtained by taking the variation of the Eqs. (2.79), (2.80) and (2.81) in the previous section. Equation (2.79) results in

$$\delta^2 U_{m1} = \delta\{v_i\}^T [k_v] \delta\{v_i\}$$

$$\delta^2 U_{m2} = \delta\{w_i\}^T \int_A [B_{w2}]^T [\bar{W}_i]^T [\bar{P}] [\bar{W}_i] [B_{w2}] dA \, \delta\{w_i\}$$

$$\delta^2 U_{m3} = \frac{3}{2} \delta\{w_i\}^T \int_A [B_{w2}]^T [W_i]^T [P] [W_i] [B_{w2}] dA \, \delta\{w_i\}$$

$$\delta^2 U_{m4} = \delta\{v_i\}^T \int_A [P_1][\bar{W}_i][B_{w2}]\, dA\ \delta\{w_i\} + \delta\{w_i\}^T \int_A [B_{w2}]^T [\bar{W}_i]^T [P_1]^T dA\ \delta\{v_i\}$$

$$\delta^2 U_{m5} = \delta\{w_i\}^T \int_A [B_{w2}]^T [\bar{W}_i]^T [P_2][W_i][B_{w2}] dA\ \delta\{w_i\} + 2\,\delta\{w_i\}^T \int_A [B_{w2}]^T [W_i]^T [P_2]^T [\bar{W}_i][B_{w2}] dA\ \delta\{w_i\} \quad (2.94)$$

$$\delta^2 U_{m6} = \delta\{w_i\}^T \int_A [B_{w2}]^T [W_i]^T [P_3]\, dA\ \delta\{v_i\} + \delta\{v_i\}^T \int_A [P_3]^T [W_i][B_{w2}]\, dA\ \delta\{w_i\}$$

Second variation terms of the displacements have been neglected here. Since the energy is a scalar quantity, $\delta^2 U_{m5}$ can be rewritten as

$$\delta^2 U_{m5} = \frac{3}{2}\,\delta\{w_i\}^T \int_A [B_{w2}]^T [\bar{W}_i]^T [P_2][W_i][B_{w2}]\, dA\,\delta\{w_i\} + \frac{3}{2}\,\delta\{w_i\}^T \int_A [B_{w2}]^T [W_i]^T [P_2]^T [\bar{W}_i][B_{w2}] dA\,\delta\{w_i\} \quad (2.95)$$

The second variation contribution from the bending energy is obtained from Eq. (2.80)

$$\delta^2 U_b = \delta\{w_i\}^T [k_{ww}]\ \delta\{w_i\} \quad (2.96)$$

Finally, using Eq. (2.81)

$$\delta^2 U_{mb1} = \delta\{v_i\}^T [\hat{k}_{vw}]\ \delta\{w_i\} + \delta\{w_i\}^T [\hat{k}_{vw}]^T \delta\{v_i\}$$

$$\delta^2 U_{mb2} = \delta\{w_i\}^T \int_A [B_{w2}]^T [\bar{W}_i]^T [P_4]\ \delta A\ \delta\{w_i\}$$

$$+ \quad \delta\{\omega_i\}^T \int_A [P_4]^T [\bar{W}_i][B_{\omega 2}]\, dA\, \delta\{\omega_i\}$$

$$\delta^2 U_{m63} = \frac{3}{2}\delta\{\omega_i\}^T \int_A [B_{\omega 2}]^T [W_i]^T [P_5]\, dA\, \delta\{\omega_i\} \qquad (2.97)$$

$$+ \quad \frac{3}{2}\delta\{\omega_i\}^T \int_A [P_5]^T [W_i]\, [B_{\omega 2}]\, dA\, \delta\{\omega_i\}$$

Reconsidering the incremental Equation (2.26), the object is to apply it in going from one configuration to another nearby configuration, as shown in Fig. 2.3. The second variation $\delta^2 U$ will be replaced by $\Delta^2 U$ which is a function of the finite displacement parameters $\{\Delta v_i\}$ and $\{\Delta \omega_i\}$. Again, crossing out the premultiplying displacement vectors, the following incremental equation remains

$$[k_I]\{\Delta r_i\} = \{\Delta P_i\} \qquad (2.98)$$

or

$$\left[\begin{array}{c|c} k_{Ivv} & k_{Ivw} \\ \hline k_{Iwv} & k_{Iww} \end{array}\right] \left\{\begin{array}{c} \Delta v_i \\ \hline \Delta \omega_i \end{array}\right\} = \left\{\begin{array}{c} \Delta P_{vi} \\ \hline \Delta P_{wi} \end{array}\right\} \qquad (2.99)$$

Here, Δ denotes the difference between configuration 2 and 1. This equation has a form similar to the equilibrium Equation (2.88) but deals with increments. $[k_I]$ is therefore denoted the incremental coefficient matrix.

The submatrices of the incremental coefficient matrix are now easily obtained from the Equations (2.94) to (2.97).

$$[k_{I_{vv}}] = [k_v] \tag{2.100}$$

$$[k_{I_{vw}}] = \int_A [P_1][\bar{W}_i][B_{w2}]dA + \int_A [P_3]^T[W_i][B_{w2}]dA + [\hat{k}_{vw}] \tag{2.101}$$

$$[k_{I_{wv}}] = \int_A [B_{w2}]^T[\bar{W}_i][P_1]^T dA + \int_A [B_{w2}]^T[W_i]^T[P_3]dA + [\hat{k}_{vw}]^T \tag{2.102}$$

$$\begin{aligned}[k_{I_{ww}}] = & \int_A [B_{w2}]^T[\bar{W}_i]^T[\bar{P}][\bar{W}_i][B_{w2}]dA \\ & + \frac{3}{2}\int_A [B_{w2}]^T[W_i]^T[P][W_i][B_{w2}]dA \\ & + \frac{3}{2}\int_A [B_{w2}]^T[\bar{W}_i]^T[P_2][W_i][B_{w2}]dA \\ & + \frac{3}{2}\int_A [B_{w2}]^T[W_i]^T[P_2]^T[\bar{W}_i][B_{w2}]dA \\ & + [k_w] + \int_A [B_{w2}]^T[\bar{W}_i]^T[P_4]dA \\ & + \int_A [P_4]^T[\bar{W}_i][B_{w2}]dA + \frac{3}{2}\int_A [B_{w2}]^T[W_i]^T[P_5]dA \\ & + \frac{3}{2}\int_A [P_5]^T[W_i][B_{w2}]dA\end{aligned} \tag{2.103}$$

It is seen that the incremental coefficient matrix is symmetric, which is of great importance for the numerical applications. Again, one should note that many terms cancel for special cases. For instance, only two terms remain for $[k_{iww}]$ when considering a plate without initial deformations which is made of an elastic homogeneous material.

2.4.6 Effect of Temperature

A frequently occurring problem in structural mechanics is that of determining the effect of heating or cooling on the structure. The strain energy contribution resulting from temperature changes of a thermo-isotropic plate is as follows, using Helmholtz's free energy function [36, 54, 55]:

$$U_T = -\int_A \left(\left(\frac{\partial u_o}{\partial x} + \frac{\partial v_o}{\partial y} \right) N_T + \left(\frac{\partial^2 w}{\partial x^2} + \frac{\partial^2 w}{\partial y^2} \right) M_T \right) dA \qquad (2.104)$$

$\frac{\partial u_o}{\partial x}$ and $\frac{\partial v_o}{\partial y}$ are strains at the midsurface. Assuming a Hookean material, the two thermal functions are

$$N_T = \frac{E}{1-\nu} \int_{\frac{h}{2}}^{\frac{h}{2}} \alpha T \, d\zeta$$

$$M_T = -\frac{E}{1-\nu} \int_{-\frac{h}{2}}^{\frac{h}{2}} \alpha T \zeta \, d\zeta \qquad (2.105)$$

Here T is the temperature change from the stress free initial state and α is known as the coefficient of thermal expansion. N_T and M_T are frequently termed the temperature force and temperature moment, respectively.

Let it be assumed that thermal forces can be expressed by field functions as

$$N_T = \langle \varphi_{T1} \rangle \{N_{Ti}\}$$

$$M_T = \langle \varphi_{T2} \rangle \{M_{Ti}\} \qquad (2.106)$$

where $\{N_{Ti}\}$ and $\{M_{Ti}\}$ are known coefficients. Using the operator defined in Eq. (2.52) and Eq. (2.49), the sum of the strains at the mid-surface becomes

$$\frac{\partial u_o}{\partial x} + \frac{\partial v_o}{\partial y} = \{\Delta_2\}^T [\Phi_v] \{v_i\} = \langle B_{Tv} \rangle \{v_i\} \tag{2.107}$$

Introducing a new differential operator

$$\Delta_4 = \frac{\partial^2}{\partial x^2} + \frac{\partial^2}{\partial y^2} \tag{2.108}$$

and using Equation (2.50), the sum of the curvatures is

$$\frac{\partial^2 w}{\partial x^2} + \frac{\partial^2 w}{\partial y^2} = \Delta_4 \langle \varphi_w \rangle \{w_i\} = \langle B_{Tw} \rangle \{w_i\} \tag{2.109}$$

Substitution of Eqs. (2.106), (2.107) and (2.109) into the thermal energy expression Eq. (2.104) yields

$$\begin{aligned} U_T = &- \{v_i\}^T \int_A \langle B_{Tv} \rangle^T \langle \varphi_{T1} \rangle \, dA \, \{N_{Ti}\} \\ &- \{w_i\}^T \int_A \langle B_{Tw} \rangle^T \langle \varphi_{T2} \rangle \, dA \, \{M_{Ti}\} \end{aligned} \tag{2.110}$$

This energy expression will now be inserted into the variational equation. Taking the first variation leads to

$$\begin{aligned} \delta U_T = &- \delta \{v_i\}^T \int_A \langle B_{Tv} \rangle^T \langle \varphi_{T1} \rangle \, dA \, \{N_{Ti}\} \\ &- \delta \{w_i\}^T \int_A \langle B_{Tv} \rangle^T \langle \varphi_{T2} \rangle \, dA \, \{M_{Ti}\} \end{aligned} \tag{2.111}$$

This equation shows that the temperature field gives contributions to the load vector. These forces correspond to the forces necessary to

restrain the plate against deformation when it is subjected to a temperature change, T. The stresses originating from restraining the element are known as initial stresses and the corresponding load vector is termed initial loads. Transferring the initial loads to the right hand side of the equilibrium equation as in (2.84) results in a sign change, thus

$$\{P_{vi}\}_{temp} = \int_A \langle B_{Tv} \rangle^T \langle \varphi_{T1} \rangle \, dA \, \{N_{Ti}\} \tag{2.112}$$

and

$$\{P_{wi}\}_{temp} = \int_A \langle B_{Tw} \rangle^T \langle \varphi_{T2} \rangle \, dA \, \{M_{Ti}\} \tag{2.113}$$

The temperature field can also be changed stepwise using increments of the coefficients $\{N_{Ti}\}$ and $\{M_{Ti}\}$ combined with the incremental form of the variational principle.

3. THE FINITE ELEMENT METHOD

3.1 FINITE ELEMENT FORMULATION

3.1.1 Choice of Method

The derivations of the previous chapter can be adopted for any Ritz-type solution technique. Three specific methods will now be suggested for solving the nonlinear plate problem, as follows:

1) The traditional Ritz method
2) The finite element method
3) Energy formulation of the finite difference method

The Ritz method could be applied directly to the equilibrium and incremental equations using some appropriate field function expansion, for instance Fourier series, defined over the entire domain of the plate. The main disadvantage associated with this method is its lack of generality. That is, it is very difficult to account for arbitrary shape and boundary conditions of the plate. In addition, this solution method frequently turns out to be numerically ill-conditioned and unstable.

The second method is a further development of the Ritz-technique. The finite element method is based on expansion of field functions in subdomains called elements instead of over the entire domain. Certain continuity conditions are required to be satisfied between each subdomain. This method has proved to be very powerful, and is capable of dealing with complicated shapes and boundary conditions. It is also well suited for automatic computations. For

linear problems, the method results in a symmetric banded system of linear equations that is well conditioned. The finite element approach will be discussed more in detail in the following.

The third method that could be applied is an energy formulation of the finite difference method. Usually, the finite difference method is used to satisfy, at discrete points, the differential equations of equilibrium of the problem [56, 57]. However, investigations in which the difference technique has been applied directly to associated functional have been reported by Greenspan [58, 59]. This approach has been effectively utilized for structural problems by Almroth, Bushnell [60] and others. It is believed that the finite difference method could be successfully applied to the equations derived in the preceding chapter. The difference operators defined in the Equations (2.51), (2.52) and (2.65) would then have to operate directly on displacements at discrete nodal points. The equilibrium and incremental equations would be essentially the same, only with substitution of discrete difference operators instead of B-matrices. Nevertheless, the finite difference approach will also suffer from some of the same shortcomings as method 1; in particular, it is complicated to apply this method to non-rectangular domains. It may be note that some work is presently beind done toward applying the finite difference method to completely irregular meshes [61].

On the basis of the preceding considerations, it was concluded that the finite element approach would be the best method here; it is well suited for computer programming and easily applicable to complicated geometry and boundary conditions. But it also is

possible that the finite difference technique is equally efficient for plates with rectangular boundaries; this question is left to be decided by later investigators.

3.1.2 A Brief Description of the Finite Element Method

It was stated in the previous section that a special form of the Ritz technique, called the finite element method, will be used for solving the nonlinear plate problem. The basic idea of this method is that the total domain is divided into subdomains, in each of which the field variables are expressed as polynomial expansions. Certain continuity conditions must be satisfied between each subdomain in the assumed expansions. The finite element method was originally proposed for solving a limited class of structural problem, namely the case of plane stress elasticity [11]. Since that classical paper, the method has successfully been extended to all kinds of two and three-dimensional structural continua. Moreover, the method has been applied effectively to a wide range of physical field problems, such as heat conduction, electro-magnetism, seepage problems and many others. Several textbooks dealing with theory and applications of this method have been published [62, 63, 64]. The method has been dealt with in a more rigorous mathematical sense in the References [65, 66, 67].

Considering the method applied to structural problems in a more practical physical manner, the structure can be said to be idealized as an assemblage of small inter-connected "pieces" (finite elements). Each element is connected to adjacent elements at joints called nodal points, through which continuity of certain displacement parameters is maintained (nodal degrees of freedom). The total number of degrees of freedom for one element is the same as the number of

functions assumed to represent the displacements within the element. A set of nodal point forces corresponding to the nodal degrees of freedom is also defined. A stiffness relationship between the nodal forces and displacements is then established using the virtual work principle for each element.

Even for the solution of a specific type of problem, many different types of finite elements may be considered, depending on the particular form of the displacement functions, choice of nodal degrees of freedom and the general geometry of the elements. The choice of the displacement polynominals is a rather crucial one. Based on mathematical analysis and experience, certain requirements should be satisfied by these function to obtain convergence and good results. One such requirement is that of "completeness" which essentially states that the field functions must be capable of expressing rigid body displacements without resulting in "self-straining" and also capable of expressing so-called "constant straining modes" of the element. Another basic requirement deals with inter-element continuity of the displacement polynomials. In theory, the polynomials should satisfy inter-element continuity of class C^{n-1} when differentials of order n enter the energy expression. However, there are many examples of elements that violate one or more of these requirements and still do converge to the right solution.

3.1.3 Element Idealization of the Plate Problem

The equilibrium equations and incremental equations of Chapter 2 will now be applied to single elements, thus establishing the element stiffness relations. Then by assembling all elements (which

corresponds to integration over the total plate) the total structural response of the plate will be obtained. The assemblage procedure is further discussed in Section 3.6.1.

The nodal point degrees of freedom will be separated into two groups, namely those associated with inplane displacements $\{v_i\}$ and those associated with transverse displacement $\{w_i\}$. Correspondingly according to Equations (2.49) and (2.50), two sets of displacement functions must be prescribed. These functions will from now on be denoted "interpolation functions" since they are expressed directly in terms of the nodal degrees of freedom.

The two sets of interpolation polynomials that will be chosen for membrane and bending actions have both previously been reported in the literature. They have both proved to give very good and reliable results for linear analysis. Since not all plates are rectangular, general quadrilateral elements will be utilized in this investigation.

3.2 THE PLATE BENDING ELEMENT

The plate bending element that will be used here is one which was developed over a period of several years. Clough and Tocher reported in 1965 a conforming(*) triangular bending element with only 9 degrees of freedom [68]. This element uses 3 subdomains, each having separate displacement expansions. By prescribing certain continuity conditions between the subregions, the conforming element is obtained. It can be shown [15] that a conforming triangular element with only 3 degrees of freedom per corner node cannot be obtained using a single cubic expansion.

(*) Conforming means here that slope and displacement continuity between elements is satisfied.

This element was further developed by Felippa [15] who used natural (triangular) coordinates instead of Cartesian ones. He also extended the element to include a prescribed number of midside rotations, thus making it possible to form a conforming quadrilateral element called Q19 from 4 subtriangles with 11 degrees of freedom each called LCCT11(**). 7 internal degrees of freedom of the Q19 element can be eliminated by so-called static condensation, thus leaving 4 corner nodes with only 3 degrees of freedom each. The derivation of the Q19 element was later simplified by Clough and Felippa [69], and also extended to include transversal shear deformation. This element which satisfies both completeness and conformity seems to be the most efficient quadrilateral bending element yet developed.

Only the main steps of the derivation of the Q19 element will be described here since the details can be found in Reference [69]. Fig. 3.1 shows how the quadrilateral element is assembled from 4 LCCT11 triangles. Node 5 is chosen to be the centroid of the quadrilateral. A LCCT12 triangle with 12 degrees of freedom is shown in more detail in Fig. 3.2. The triangle shown is divided into 3 subdomains, each having separate interpolation polynomial expansions expressed by natural coordinates of the entire triangle. For subtriangle l the deflection is given by

$$w^{(l)} = \langle \varphi_w^{(l)} \rangle \{ w_i^{(l)} \} \tag{3.1}$$

(**) LCCT stands for "Linear Curvature Compatible Triangle", the eleven indicates 11 degrees of freedom.

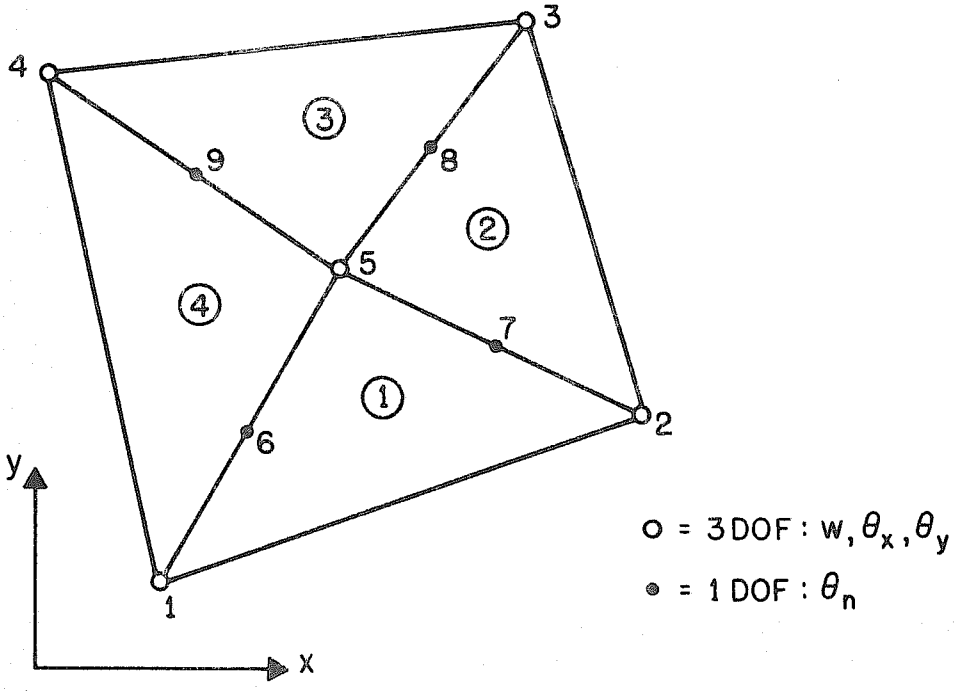

FIG. 3.1 THE Q19 QUADRILATERAL

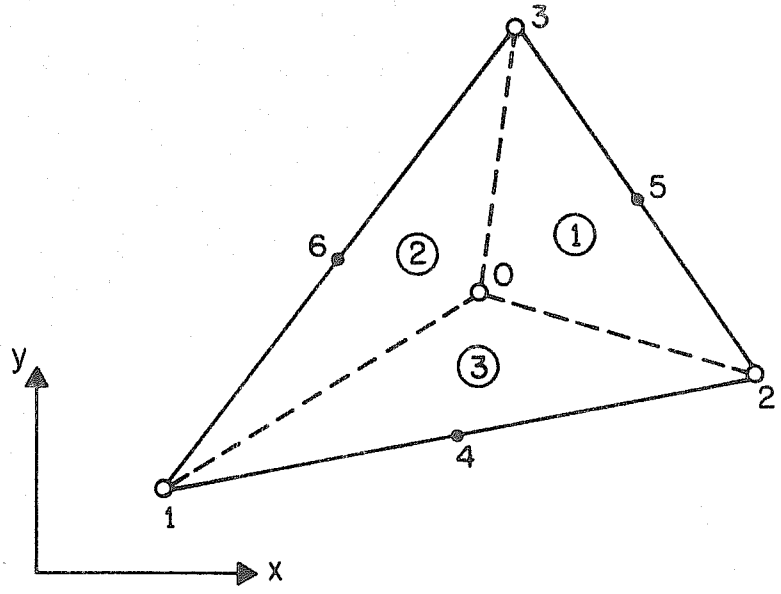

FIG. 3.2 THE LCCT12 ELEMENT

where for instance the nodal displacement vector for subtriangle 3 is

$$\{\omega_i^{(3)}\}^T = \langle \omega_1, \theta_{x1}, \theta_{y1}, \omega_2, \theta_{x2}, \theta_{y2}, \omega_0, \theta_{x0}, \theta_{y0}, \theta_4 \rangle \qquad (3.2)$$

By matching the deflections and rotations at the centroid 0 for all 3 subtriangles and enforcing continuity of slopes between these subtriangles, the internal degrees of freedom can be eliminated. This is a very extensive and tedious algebraic operation [69], but the result turns out to be quite simple. The resulting compatible interpolation polynomials for subtriangle number 3 are given in Appendix A.

The 12 degrees of freedom LCCT12 triangle can easily be reduced to LCCT11 triangle by prescribing a kinematic constraint such that the midside rotation on one of the sides is set equal to the arithmetic average of the corresponding slopes at the adjacent corner nodal points. This results in a slight modification of the interpolation polynomials in Appendix A. The linear stiffness matrix of the LCCT11 element is obtained using Eq. (2.73) and performing the integration utilizing natural coordinates over each of the subtriangles. The stiffness matrix of the Q19 element is obtained simply by assembling the 4 LCCT11 stiffness matrices.

3.3 THE MEMBRANE ELEMENT

A general quadrilateral membrane element is needed to match the plate bending element. Use of so-called "refined" elements utilizing polynomials of higher order will be avoided because stiffness evaluations of such elements will be extremely time consuming when including the nonlinear geometric effects. Therefore an element with only 2 degrees of freedom at each corner node has been chosen for this study.

Such elements can easily be built up using 2 or 4 triangles followed by a static condensation of internal nodes, [15, 70]. However, a simpler formulation may be obtained using natural coordinates and Hermitian interpolation expansion over the entire quadrilateral. Such an element is the Zienkiewicz-Irons quadrilateral described in Reference [62]. An improvement of this element may be obtained by including an internal nodal point with 2 degrees of freedom as shown in Figure 3.3. The interpolation polynomials for this element are given in Appendix B. The derivation of the linear membrane stiffness $[k_v]$ as defined in Eq. (2.69) is demonstrated in Reference [62]. 2 by 2 or 3 by 3 Gaussian quadrature is used for the numerical computation of the stiffness.

As has been pointed out in Reference [71], the performance of the element when used for plates with discretized eccentric stiffeners can be substantially improved by including additional midside nodes with each having one tangential degree of freedom. This makes it possible for the element to pick up high stress gradients near the stiffeners. Such additional nodes are not desired for plates without stiffeners due to the increased band width of the system of equations. The flexibility of the element can also be considerably increased by using a mixed energy formulation including the shear stress as an additional parameter [70]. This idea was originally proposed by Doherty et. al. in [72], then based on a more practical physical observation. This approach is particularly useful for improving the inplane bending mode response of the element, but it is not expected to be of great importance for large plates with combined bending membrane type of action. Besides, this mixed energy element is not invariant, its stiffness depends on the

orientation of the local Cartesian coordinate system in which the stiffness relation is formed. Therefore, the expansions given in Appendix B will be used here. An invariant quadrilateral element with improved bending mode action and with only 8 remaining degrees of freedom has been suggested by Wilson [73].

3.4 NONLINEAR GEOMETRIC EFFECTS

3.4.1 The Concepts of Secant and Incremental Stiffness

As mentioned in the Introduction, the finite element method has been extended to be applied to a wide range of nonlinear problems during the last decade. Some authors, particularly during the first period of development, took a rather physical approach to the problem by including nonlinear corrections to the linear solution. Such an approach will frequently lead to incorrect solutions due to the omission of significant terms, although it might work well for the linearized buckling problem. A more proper and safe way to proceed is to start with a correct energy or variational principle from which a set of nonlinear equation may be deduced and solved numerically. This latter approach was adopted in Chapter 2.

Figure 3.4 shows a typical load-deflection curve for a nonlinear structural problem, which for simplicity in this discussion has only 1 degree of freedom. The various slopes on the figure represent different stiffnesses defined for point P of the curve

K_L is the linear stiffness originating from linear small displacement theory

K_S is the secant stiffness relating forces directly to displacements

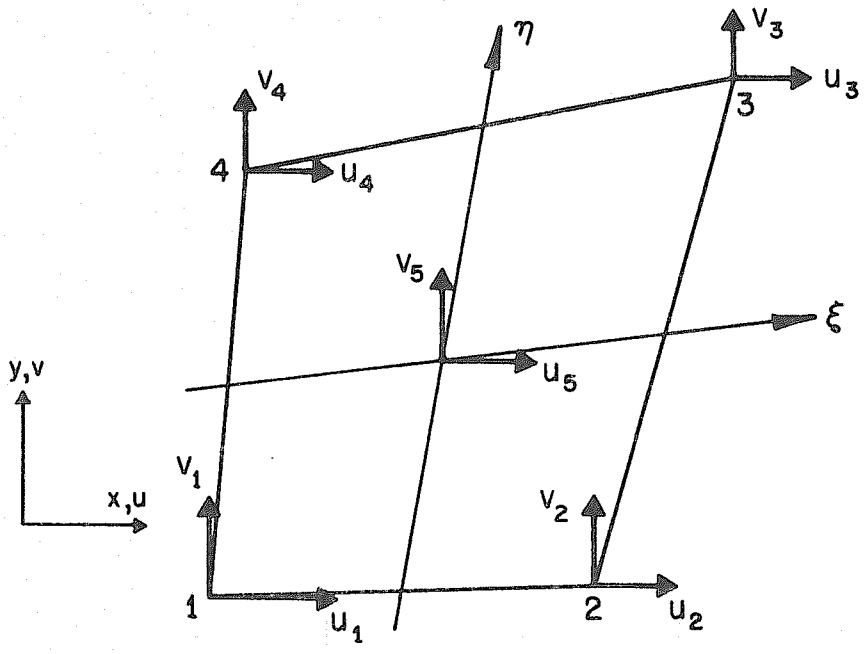

FIG. 3.3 THE PLANE STRESS ELEMENT

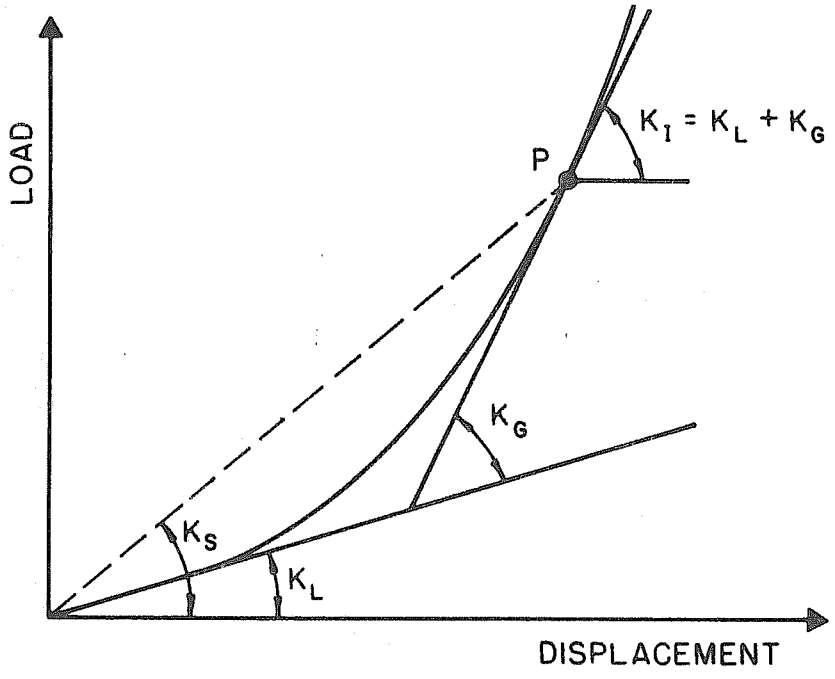

FIG. 3.4 CLASSIFICATION OF STIFFNESS CONTRIBUTIONS

K_I is the incremental stiffness which relates the incremental forces to the incremental displacements. K_I is also called the tangent stiffness by many authors.

K_G is the geometric stiffness accounting for the additional stiffness due to changed geometry.

From Figure 3.4 it is seen that

$$K_I = K_G + K_L \tag{3.3}$$

Some authors like to call the geometric stiffness contribution "initial stress matrix". Such an expression is inadequate since a complete derivation reveals that there are indeed stiffness terms that cannot be classified as initial stress terms. The "initial stress" designation fits better for the special case of a linearized eigenvalue formulation for buckling which can be stated as

$$[\,[K_L - \lambda[K_G]\,]\,\{r\} = \{0\} \tag{3.4}$$

where $[K_G]$ can be expressed in terms of membrane stresses and λ represents the eigenvalue which actually is a load multiplier.

In Appendix C it is shown that the nonlinear coupling term between the inplane and the transverse displacements of Eq. (2.90) can be rewritten in a form that is like the traditional "initial stress" stiffness for plates [14]. However, the form used in Eq. (2.90) is far more convenient for the present computational purposes.

Marcal suggested in Reference [74] that the incremental stiffness be separated into 3 contributions, namely a small displacement linear stiffness, an initial stress matrix and an initial strain

or initial displacement matrix. Such a classification gives a more complete picture of the situation. However, in connection which the derivations used here, it seems more logical to classify all nonlinear terms only as "geometric" since they indeed are due to the change of geometry after load application. Besides, all stiffness contributions have here been expressed directly in terms of displacements for computational convenience and efficiency.

The numerical solution of the nonlinear equations is extensively discussed in Chapter 5.

3.4.2 The Calculation of Nonlinear Stiffness Terms

The numerical evaluation of the nonlinear stiffness terms given by Equations (2.90) through (2.92) and (2.101) through (2.103) can be carried out in a straight-forward manner. It is seen from the stiffness expressions that some value of the nodal point displacements $\{w_i\}$ must be used when the calculation is performed. As will be discussed later in Chapter 5, the solution of nonlinear problems involves repeated recalculation of nonlinear stiffness terms, often a substantial number of times. Consequently, it is of vital importance that the nonlinear terms be calculated in a very efficient manner.

The interpolation functions for the deflections (Eq. (A.3) of Appendix A) yield very good results for the linear bending of plates, but they are rather complicated. This indicates that the formulation time of nonlinear stiffness terms might be rather high when performed in a straight forward manner. However, a crucial observation is that the nonlinear stiffnesses are functions only of the first derivatives of the deflections, not of the second derivatives which is the case for the linear bending stiffness. This suggests that simplified

interpolation polynomials can be employed when calculating the nonlinear terms, still yielding good results. Indeed, the numerical results of Chapter 6 do verify this hypothesis. A similar conclusion for linearized buckling was reached by Clough and Felippa [69].

Several simple interpolation polynomials with only deflectional and rotational degrees of freedom at the four corner nodes are available for rectangular and parallelogram elements. Such functions are the Hermitian polynomials [75] and the ones suggested by Melosh [76] and Argyris [77]. These polynomials do not satisfy both conformity and constant curvature nodes; only expansions of the type described in Section 3.2 do that. However, the results obtained by using the different polynomials mentioned above for the nonlinear geometric stiffness terms turn out to be very close to each other. The Hermitian polynomial interpolation was perferred here since it satisfies inter-element slope continuity, and it is the slopes that are essential for computation of the nonlinear stiffness terms. Its lack of a so-called "constant twist mode" is not important in this connection. This interpolation polynomial is given explicitly in Appendix D.

The nonlinear stiffness contributions of Sections 2.4.4 and 2.4.5 are now obtained using a 2 by 2 or a 3 by 3 Gaussian quadrature scheme. Although not tested here, the Hermitian interpolation polynomials could also be used for general quadrilateral elements if expressed in a natural coordinate system like that of Fig. 3.3. The Jacobian matrix would then enter the stiffness evaluation and a transformation to the rectangular global coordinates would have to be performed for the rotational degrees of freedom.

3.5 PLATES WITH INITIAL DEFORMATIONS

The initial shape of the plate surface was defined in Eq. (2.56) by a set of field functions and a corresponding set of arbitrary coefficients. It will now be assumed that the coefficients are real initial deflection quantities at the nodal points of a finite element and that $<\bar{\phi}_W>$ represents the corresponding interpolation polynomials. There are several computational advantages connected with using the same interpolation polynomials for the initial shape as used for calculating the nonlinear effect of the additional displacements. $<\bar{\phi}_W>$ is therefore chosen to be defined by Eq. (D.3) (Appendix D) and the corresponding nodal point vector is

$$\{\bar{w}_i\}^T \quad < \bar{w}_1, \bar{\theta}_{x1}, \bar{\theta}_{y1}, \bar{w}_2, \bar{\theta}_{x2}, \bar{\theta}_{y2}, \bar{w}_3, \bar{\theta}_{x3}, \bar{\theta}_{y3}, \bar{w}_4, \bar{\theta}_{x4}, \bar{\theta}_{y4} > \quad (3.5)$$

where the subscript numbers indicate nodal point number. The $[\bar{B}_{W1}]$ matrix defined in Eq. (2.59) thereby becomes identical to $[B_{W1}]$ of Eq. (2.64) and consequently the identities Eqs. (2.70), (2.71) and (2.78) also hold true. It is demonstrated in Sections 2.4.4 and 2.4.5 that the initial displacements results in both linear and nonlinear stiffness contributions. The numerical evaluation of these terms is similar to what was described in the preceeding section.

The element defined by Eq. (3.5) and Eq. (D.3) is a doubly curved quadrilateral element. It is well known that for such an element it is difficult to satisfy both the requirement of rigid body modes and constant straining modes as described in Section 3.1.2. The translational rigid body modes however, are seen to be included directly since the displacements are described in a global Cartesian

coordinate system and the interpolation polynomials of all three displacement components contain a constant term. However, the rotational modes are harder to satisfy. Fig. 3.5 shows a shallow shell element rotated about the y-axis. The displacements caused by such a rotation are

$$u = (\cos\theta - 1)\, x - (\sin\theta)\, \bar{w}\,(x, y) \tag{3.6}$$

$$w = (\sin\theta)\, x + (\cos\theta - 1)\, \bar{w}\,(x, y) \tag{3.7}$$

It is seen that Eq. (3.6) can be satisfied identically only as long as u is a polynomial of at least the same degree as $\bar{w}$. Since u is of lower degree than $\bar{w}$ here, Eq. (3.6) will not be identically satisfied. However, as long as the linear terms dominate $\bar{w}$ and the curvature (quadratic) terms are relatively small this equation is satisfied with sufficient accuracy. Further, it is also seen that Eq. (3.7) is satisfied identically as long as w is at least of the same order as $\bar{w}$, which is the case here. Moreover, the rigid body rotation mode about the z-axis is also included since u and v are of higher order than the bilinear expansion which is required to represent this specific rigid body motion. The constant straining modes are also satisfied within the range of validity of the shallow shell strain Equations (2.48).

According to the variational principle, the energy should be integrated over the volume of the undeformed body, that is, integration should be performed over the initial volume of the shallow shell itself. However, for convenience the integration will be performed over the projection of the shell onto the x-y plane. Thence

$$dV = d\zeta\, dA' = d\zeta\, \frac{dA}{\cos\alpha} \tag{3.8}$$

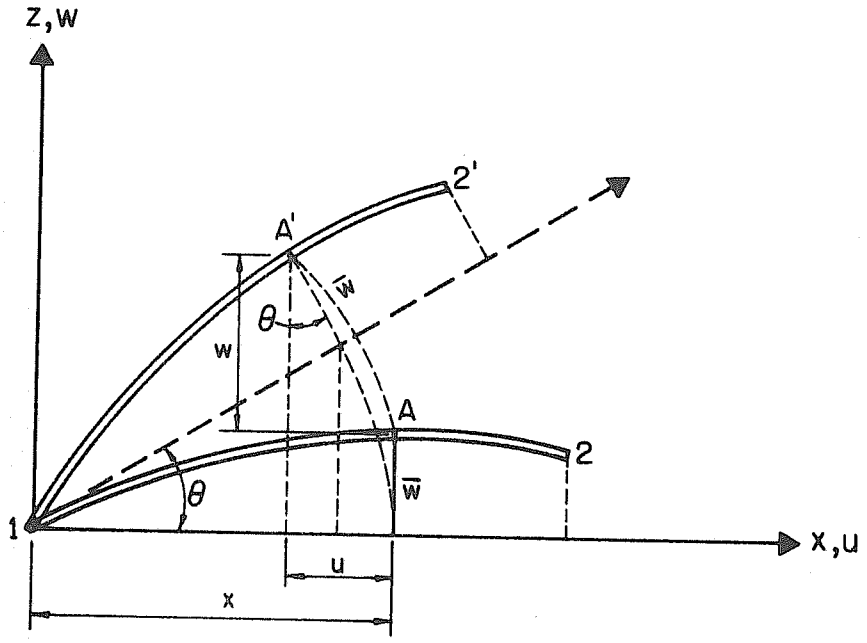

FIG. 3.5 RIGID BODY ROTATION OF CURVED ELEMENT

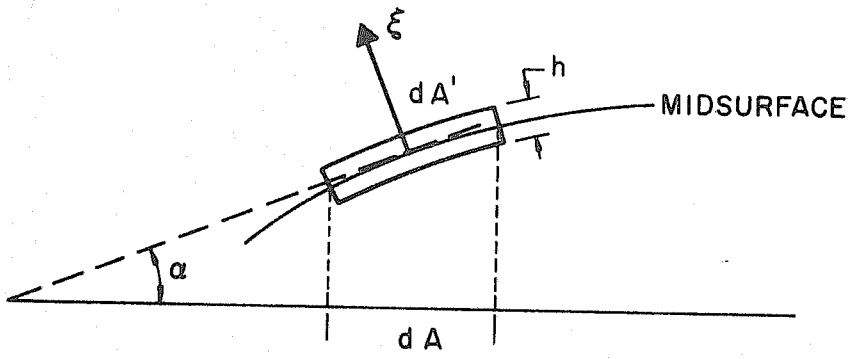

FIG. 3.6 PROJECTION OF INFINITESIMAL AREA ELEMENT

where dA is the projection of dA' onto the x-y plane as shown in Fig. 3.6 and α is the angle between the tangential plane of the shell and the x-y plane. A correctional term accounting for the curvature could be included but is without significance here. In most practical cases, $\cos\alpha$ can be approximated by 1.

3.6 ASSEMBLAGE PROCEDURE AND STRESS COMPUTATION

3.6.1 Assemblage Procedure

The variational principle has been applied to a subdomain of the total body for deriving the element stiffness terms. The principle, of course, also is valid for the entire body. This implies integration over the entire domain which in fact just corresponds to arranging and adding together element stiffness terms. This procedure can easily be carried out in a computer and is known as the "direct stiffness method". Capital K's are here used to denote the system stiffness matrices. Thus, corresponding to the element equilibrium expansion Eq. (2.87), the equilibrium equation of the total system becomes

$$[K] \{r\} = \{R\} \tag{3.9}$$

in which $[K]$ is a function of the nodal point displacements $\{r\}$ of the assembled system. The incremental equation of the total system reads

$$[K_I] \{\Delta r\} = \{\Delta R\} \tag{3.10}$$

which corresponds to Eq. (2.98) for a single element. The system incremental stiffness matrix is banded and symmetric, but not always

positive definite for nonlinear problems. Kinematic constraints are introduced into the stiffness matrix after the assemblage procedure is completed.

Calculation of nodal point loads is performed elementwise according to Equations (2.85) and (2.86). A load matrix consistent with the complete displacement expansion for the plate bending element is not computed since experience shows that lumped corner loads yield equally good results.

3.6.2 Stress Computation

After the displacements of a stationary state have been found using some numerical technique the corresponding stresses can be easily obtained. The midplane strains and the curvatures were defined in Eqs. (2.48) and (2.66) respectively. Thus the membrane stresses and the moments are found at any location by premultiplying these vectors by the corresponding constitutive matrices Eqs. (2.41) and (2.45). Membrane stresses and moments are not continuous between adjacent elements, but good stress estimates are obtained by taking the arithmetic average of the stress value of adjoining elements at such points.

4. THE ELASTIC-PLASTIC PROBLEM

4.1 SOLUTION OF ELASTIC-PLASTIC PROBLEMS USING THE FINITE ELEMENT METHOD

An ultimate strength analysis of a structure usually requires the nonlinear behavior of the structure material to be taken into consideration. In the present discussion, attention will be confined to metallic materials exhibiting an elastic-plastic type of behavior. The analysis will further be limited to inviscid materials under isothermal conditions, and subjected to quasistatic loading. Before approaching the problem numerically, two major decisions must be made. The first is the selection of a mathematical model (plasticity theory) by which the macroscopic behavior of the material is described. The second important decision is related to the numerical technique itself, and concerns the incorporation of the elastic-plastic effects into the numerical equations of the discretized system.

The two major plasticity theories that will be considered here are the deformation theory and the flow theory. Comparative discussions may also be found in the classical book by Hill [78] and a very comprehensive review paper by Naghdi [79]. The deformation theory, which was suggested by Hencky in 1924 [80], assumes a unique relation between total stresses and total strains. The plastic strain components are given by a proportionality factor (which is only a function of the prevailing equivalent stress) times the corresponding deviatoric stress components. Because of its mathematical simplicity, the deformation theory is indeed attractive both for analytical and numerical approaches.

However, many experiments clearly contradict the Hencky theory, particularily for repeated loading and unloading [78]. Real materials exhibit a "memory" of previous plastic deformations, while the deformation theory does not account for such effects.

For the sake of mathematical consistency and physical appropriateness the flow theory will be adopted here. The basic equation of this theory is that of Prandtl [81] and Reuss [82] assuming the increment of plastic strains to be proportional to the corresponding deviatoric stress components. The plastic deformations are "memorized" by integrating the equivalent plastic strain increment over the previous load history, thereby accounting for hardening effects. The concept of the Bauschinger effect can be incorporated using a kinematic hardening model as suggested by Prager [83]. The flow theory can be classified as a nonconservative and "nonholonomic" type of theory. A result of this definition is that the true loadpath must be followed during load application. A pure incremental method must therefore be used for solving problems of this type. It is of interest to note that the deformation theory and the flow theory coincide when the strain path is a straight line [78].

The second important decision that must be made is the selection of a method for incorporating the elastic-plastic material behavior into the finite element analysis. Two approaches are readily available; they are the so-called "initial strain" method and the "tangent stiffness" method. The method of initial strains is based on the same principle that was used for incorporation of thermal strains in Section 2.4.6. The plastic strains are accounted for by introduction of a set of equivalent body forces. The analogy between

plastic strains and body forces was first suggested by Ilyushin in 1943 [84]. Later, this approach has been developed and used in the finite element approach by Padlog et. al. [24], Argyris et. at. [25], and many others. The main advantage of this method is that the system stiffness matrix remains independent of the plastic deformations, the effects of which appear only in nodal forces. However, since the plastic increments are not known in advance, an iteration has to be carried out at each load level.

The tangent stiffness method, on the other hand, requires that a new stiffness matrix be formulated (or the previous one be updated) for every loadstep. This method also has been widely used for finite element analysis of elastic-plastic problems [85, 15, 26] and it will be further discussed in the next sections. Comparative studies between the two methods have been reported by Khojasteh-Bakht [27] and Marcal [31, 86]. Although the initial strain method seemingly is the simpler of the two, it is less reliable and breaks down for elastic-perfectly plastic materials, which truly is an important special case. Furthermore, when plasticity is combined with large displacements, the incremental stiffness has to be recalculated anyway during load incrementation. For these reasons, the tangent stiffness method was chosen to be used here.

4.2 THE GOVERNING EQUATIONS OF THE FLOW THEORY

4.2.1 Basic Principles and Assumptions

The basic equations of the flow theory needed for deriving the incremental stiffness relation will briefly be discussed in the

following, Details and proofs will not be pursued since more complete derivations may be found in the references by Hill [78], Naghdi [79], and Koiter [87].

Stresses and strains will be referred to a rectangular Cartesian coordinate system, and the strains are assumed to be infinitesimal. In spite of the small strain assumption this plasticity theory can be used in connection with the large displacement theory for plates based on the von Karman strain expressions. As will be recalled from Section 2.3.2, the strains of the von Karman theory are infinitesimal, it is only the rotations that are finite quantities.

Some attempts at deriving a large deformation theory of plasticity have been made, notably by Green and Naghdi [88] and by Yaghmai [28] who applied the theory to rotational symmetric shells. However, this theory is questionable since it is assumed that the elastic and plastic strains may be additively decomposed. Some recent papers by Lee and Liu [89, 90] and by Tseng [91] do not make use of the addition of elastic and plastic strains. Anyway, the large deformation theory of plasticity is extremely complicated, and it seems that no theory which satisfies the laws of both thermodynamics and continuum mechanics is available for general practical use at the present time.

The derivation of the plasticity theory will be based on three major assumptions. The first is that elastic and plastic strains may be added

$$\varepsilon_{ij} = \varepsilon^{E}_{ij} + \varepsilon^{P}_{ij} \tag{4.1}$$

where superscripts E and P denote elastic and plastic respectively. This assumption is perfectly sound for infinitesimal strains. The elastic strains are related to the total stresses by Hookes law:

$$\sigma_{ij} = E_{ijkl}\,\varepsilon^{E}_{kl} = \lambda\,\delta_{ij}\,\delta_{kl} + \mu\,(\delta_{ik}\,\delta_{jl} + \delta_{jk}\,\delta_{il}) \qquad (4.2)$$

where λ and μ are Lame's constants:

$$\lambda = \frac{E\nu}{(1+\nu)(1-2\nu)} \qquad \text{and} \qquad \mu = \frac{E}{2(1+\nu)} \qquad (4.3)$$

The plastic part of the deformation is postulated to be incompressible

$$\varepsilon^{P}_{ii} = 0 \qquad (4.4)$$

Experimental results confirm this assumption.

The second major assumption is that there exists a socalled loading function f in 9-dimensional stress space. This function is such that the state of the material is given by the value of this function

$$\begin{aligned} f &< 0 \quad \text{elastic state} \quad (d\varepsilon^{E} = 0,\ d\varepsilon^{P} = 0) \\ f &= 0 \quad d\sigma_{ij} \text{ can cause } d\varepsilon^{P}_{ij} \neq 0 \\ f &> 0 \quad \text{inadmissible state} \end{aligned} \qquad (4.5)$$

The special value $f = 0$ at time t constitutes the yield condition at that time. Further load incrementation can only cause f to change, it is impossible to get outside $f = 0$. As it turns out that f is a function of σ_{ij} and ε^{P}_{ij}, (see the next section) three different loading conditions from a plastic state result from Eq. (4.5)

$$\frac{\partial f}{\partial \sigma_{ij}} \dot{\sigma}_{ij} < 0 \quad , \quad f = 0 \quad \text{(during unloading)}$$

$$\frac{\partial f}{\partial \sigma_{ij}} \dot{\sigma}_{ij} = 0 \quad , \quad f = 0 \quad \text{(during neutral loading)} \qquad (4.6)$$

$$\frac{\partial f}{\partial \sigma_{ij}} \dot{\sigma}_{ij} > 0 \quad , \quad f = 0 \quad \text{(during loading)}$$

The dot denotes time differentiation.

The third basic assumption to be made is that the material is stable as defined by Drucker [92]. Drucker's quasi-thermodynamic law may be stated as follows [79]: "Consider an element initially in some state of stress to which by an external agency an additional set of stresses is slowly applied and slowly removed. Then, during the application of the added stresses and in a cycle of application and removal of the added stresses, the work done by an external agency is non-negative". This postulate has three important implications, namely "convexity", "consistency" and "normality". Convexity means that the initial yield surface and all subsequent loading surfaces are convex. Consistency implies that if a stress point moves inside the yield surface, then $\varepsilon^P_{ij} = 0$. The third result, normality, means that at a regular point of the loading surface $f = 0$, the vector $d\varepsilon^P_{ij}$ (in stress space) is in the direction of the outward normal to the yield surface, so that

$$d\varepsilon^P_{ij} = d\lambda \frac{\partial f}{\partial \sigma_{ij}} \qquad \text{or} \qquad \dot{\varepsilon}^P = \dot{\lambda} \frac{\partial f}{\partial \sigma_{ij}} \qquad (4.7)$$

$d\lambda$ is a non-negative scalar. This important result constitutes a flow rule, i.e. determines the direction of the incremental plastic strains. When the material obeys the von Mises yield criterion, this equation is

equivalent to the Prandtl-Reuss equation. By virtue of Eq. (4.7), the loading function plays the role of a plastic potential.

4.2.2 The Yield Criterion and the Hardening Rule

The explicit form of the loading function will not be studied. f can in general be written as a function of the state of stress, plastic strains and a hardening parameter $\varkappa$

$$f = f(\sigma_{ij}, \varepsilon^p_{ij}, \varkappa) \tag{4.8}$$

The hardening parameter is again a function of σ_{ij} and ε^p_{ij}, therefore without loss of generality

$$f = f(\sigma_{ij}, \varepsilon^p_{ij}) \tag{4.9}$$

f remains zero when going from one plastic state to another (consistency), hence

$$df = \frac{\partial f}{\partial \sigma_{ij}} d\sigma_{ij} + \frac{\partial f}{\partial \varepsilon^p_{ij}} d\varepsilon^p_{ij} = 0 \tag{4.10}$$

Substitution of Eq. (4.10) into Eq. (4.7) yields

$$d\lambda = - \frac{\frac{\partial f}{\partial \sigma_{ij}} d\sigma_{ij}}{\frac{\partial f}{\partial \varepsilon^p_{mn}} \frac{\partial f}{\partial \sigma_{mn}}} \tag{4.11}$$

for a hardening material.

Evaluation of Eq. (4.11) requires an explicit expression for f at f = 0. It will be assumed that the material is initially isotropic. Both the Tresca and the von Mises yield criteria satisfy isotropy, however, most experimental evidence for metals is in favor of the latter criterion. The von Mises criterion for initial yielding may be written

$$J_2 - k_o^2 = 0 \tag{4.12}$$

J_2 is the second deviatoric stress invariant defined by

$$J_2 = \frac{1}{2} s_{ij} s_{ij} \tag{4.13}$$

in which the deviatoric stresses are defined by

$$s_{ij} = \sigma_{ij} - \frac{1}{3} \delta_{ij} \sigma_{kk} \tag{4.14}$$

k_o denotes the initial yield stress in pure shear. In many cases it is more convenient to use the initial yield stress in pure tension T_o instead, which is related to k_o by

$$T_o^2 = 3k_o^2 \tag{4.15}$$

For convenience, the symbol for equivalent stress $\bar{\sigma}$ is introduced

$$\bar{\sigma} = \sqrt{3 J_2} = \sqrt{\frac{3}{2} s_{ij} s_{ij}} \tag{4.16}$$

The initial loading function and yield criterion now reads

$$f_o = \bar{\sigma} - T_o = \bar{\sigma} - k\sqrt{3} = 0 \tag{4.17}$$

Further, it is assumed that the material exhibits an isotropic hardening behavior. This implied a uniform expansion of the initial yield surface, as shown in Fig. 4.1. One way of measuring the amount of hardening that has taken place is to consider the plastic work carried out

$$W^P = \int_0^{\varepsilon_{ij}^P} \sigma_{ij}\, d\varepsilon_{ij}^P \tag{4.18}$$

or here also

$$W^P = \int_0^{\bar{\varepsilon}^P} \bar{\sigma}\, d\bar{\varepsilon}^P \tag{4.19}$$

where it can be shown that the equivalent plastic strain is given by

$$d\bar{\varepsilon}^P = \sqrt{\frac{2}{3}}\left(d\varepsilon_{ij}^P\, d\varepsilon_{ij}^P\right)^{1/2} \tag{4.20}$$

The yield stress in uniaxial tension is then

$$\bar{T} = G\,(W^P) \tag{4.21}$$

On the other hand, the plastic strain hypothesis assumes that

$$\bar{T} = H(\bar{\varepsilon}^P) \tag{4.22}$$

where

$$\bar{\varepsilon}^p = \int_0^{\bar{\varepsilon}^p} d\bar{\varepsilon}^p \tag{4.23}$$

For the von Mises yield criterion (and Tresca when there is no yielding at corners), Eqs. (4.21) and (4.22) are quivalent [93]. After initial yielding has occurred, the von Mises yield criterion now becomes

$$f = \bar{\sigma} - H\ (\bar{\varepsilon}^p) = 0 \tag{4.24}$$

Figure 4.2 shows a typical curve obtained from uniaxial tension testing. As will be seen later, $H' = \frac{\partial H}{\partial \bar{\varepsilon}^p}$ is of special interest and is easily obtainable from the curve in Fig. 4.2

$$d\bar{\sigma} = E_T\, d\bar{\varepsilon} = E_T \left(\frac{d\bar{\sigma}}{E} + d\bar{\varepsilon}^p \right)$$

hence

$$\frac{1}{H'} = \frac{1}{\frac{\partial \bar{\sigma}}{\partial \bar{\varepsilon}^p}} = \frac{1}{E_T} - \frac{1}{E} \tag{4.25}$$

E_T being the tangent modulus which can be obtained from a simple tension test.

One apparent weakness of the isotropic hardening hypothesis is that it does not account for the Bauschinger effect. One attempt of including this was made by Prager [83] who suggested kinematic hardening in which the yield surface is translated without rotation. Other theories attempt to account for corners of the yield surface [94] since

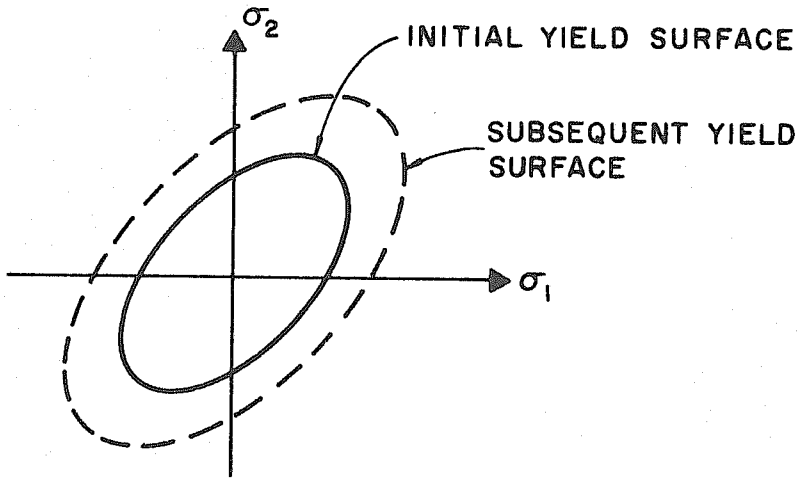

FIG. 4.1 ISOTROPIC HARDENING

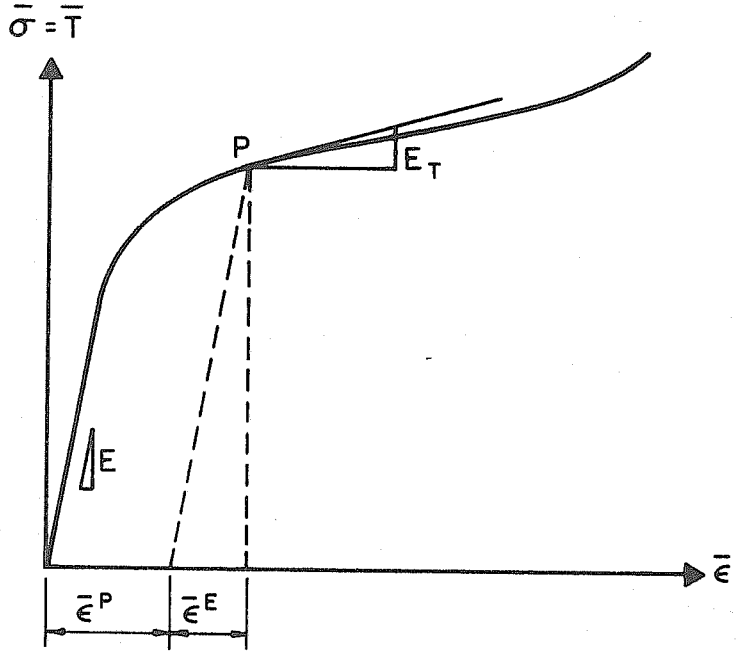

FIG. 4.2 EXPERIMENTAL STRESS-STRAIN CURVE

such corners have been observed experimentally [95]. Because cyclic loading is not of particular interest here, the isotropic hardening approach is considered adequate and is adopted in the following derivations.

4.2.3 Derivation of the Incremental Stress-Strain Relationship

The scaling factor $d\lambda$ for a hardening material was given by Eq. (4.11) and will now be considered again. The partial derivatives of the loading function Eq. (4.24) are needed for this purpose. Use of Eqs. (4.16) and (4.14) yields

$$\frac{\partial f}{\partial \sigma_{ij}} = \frac{\partial \bar{\sigma}}{\partial \sigma_{ij}} = \sqrt{\frac{3}{2}} \frac{\partial}{\partial \sigma_{ij}} \left[(\sigma_{mn} - \tfrac{1}{3}\delta_{mn}\sigma_{kk})(\sigma_{mn} - \tfrac{1}{3}\delta_{mn}\sigma_{kk}) \right]^{1/2} = \frac{3}{2} \frac{s_{ij}}{\bar{\sigma}} \tag{4.26}$$

Differentiation with respect to the plastic strains using Eqs. (4.19) and (4.18) gives

$$\frac{\partial f}{\partial \varepsilon^p_{ij}} = - \frac{\partial H(\bar{\varepsilon}^p)}{\partial \varepsilon^p_{ij}} = - \frac{\partial H}{\partial \bar{\varepsilon}^p} \frac{\partial \bar{\varepsilon}^p}{\partial W^p} \frac{\partial W^p}{\partial \varepsilon^p_{ij}} = - H' \frac{1}{\bar{\sigma}} \sigma_{ij} \tag{4.27}$$

in which H' is obtained from Eq. (4.25). Now, substitution of Eqs. (4.26) and (4.27) into (4.11) yields

$$d\lambda = \frac{3}{2} \frac{s_{ij}\, ds_{ij}}{H' \bar{\sigma}} = \frac{d\bar{\sigma}}{H'} \tag{4.28}$$

and using Eq. (4.7)

$$d\varepsilon^p_{ij} = d\lambda \frac{\partial f}{\partial \sigma_{ij}} = \frac{3}{2} \frac{s_{ij}\, d\bar{\sigma}}{H' \bar{\sigma}} \tag{4.29}$$

Equation (4.29) gives the plastic strain increments in terms of the state of stress and the stress increments. This equation represents the Prandtl-Reuss equation for a isotropic hardening material obeying the von Mises yield criterion. However, using the displacement formulation of the finite element method, the objective is to express the plastic strains by the total displacement (strain $d\varepsilon_{ij}$) increment. This can be obtained by substituting Hookes law Eq. (4.2) and Eq. (4.1) into $d\lambda$ Eq. (4.11):

$$d\lambda \left(\frac{\partial f}{\partial \varepsilon^P_{mn}} \frac{\partial f}{\partial \sigma_{mn}} \right) = - \frac{\partial f}{\partial \sigma_{ij}} E_{ijkl} \left(d\varepsilon_{kl} - d\lambda \frac{\partial f}{\partial \sigma_{kl}} \right)$$

which yields

$$d\lambda = \frac{3\mu \, s_{kl} \, d\varepsilon_{kl}}{\sigma \, (H' + 3\mu)} \tag{4.30}$$

The relation

$$E_{ijkl} \, s_{kl} = 2\mu \, s_{ij} \tag{4.31}$$

has been used here, μ being Lambe's constant of Eq. (4.3)

Then, substituting Eq. (4.30) into Eq. (4.7) and utilizing Eq. (4.31), the desired result is obtained

$$d\varepsilon^P_{ij} = d\lambda \frac{\partial f}{\partial \sigma_{ij}} = A_{ijkl} \, d\varepsilon_{kl} \tag{4.32}$$

in which

$$A_{ijkl} = \frac{9\mu \, s_{ij} \, s_{kl}}{2\sigma^2 (H' + 3\mu)} \tag{4.33}$$

The incremental stress-strain relationship is now easily obtained

$$d\sigma_{ij} = E_{ijkl}\,(d\varepsilon_{kl} - d\varepsilon^{p}_{kl}) = C_{ijkl}\,d\varepsilon_{kl} \tag{4.34}$$

where

$$C_{ijkl} = E_{ijkl} - \frac{9\mu^2 s_{ij} s_{kl}}{\bar{\sigma}^2 (H' + 3\mu)} \tag{4.35}$$

This incremental relation is valid between two consecutive plastic states. According to Eq. (4.6) when

$$\bar{\sigma} < H = \bar{T} \tag{4.36}$$

or

$$\bar{\sigma} = \bar{T} \quad \text{and} \quad S_{ij}\,d\varepsilon_{ij} < 0 \tag{4.37}$$

the last term of Eq. (4.35) should be neglected and only Hookes law remains. Note also the symmetry properties of C_{ijkl}.

The incremental stress-strain relation could also be obtained by direct inversion of the strain-stress relationship obtainable from Eq. (4.29). However, this operation is more time consuming and Eq. (4.29) is not defined for a non-hardening material ($H' = 0$). By taking the limit, it is seen that Eq. (4.35), on the other hand, is still valid for $H' = 0$. The uniqueness and existence of this inversion has been discussed by Koiter [87].

A more general incremental stress-strain relation was previously obtained by Hill [78]*. This form of the flow equation has

---

* Eq. 25, page 69 in Hill's book

been adopted by several investigators using the finite element method [27, 28, 29, 96]. Here it was chosen to show the derivation for the preselected yield criterion and hardening rule. The more general expression given by Hill can easily be adopted for kinematic hardening as demonstrated in [27] by using

$$f = \frac{1}{2}(s_{ij} - \alpha_{ij})(s_{ij} - \alpha_{ij}) - k^2 \tag{4.38}$$

in which α_{ij} represents the translation of the yield locus.

4.2.4 Plane Stress.

The special case will be considered in which

$$\sigma_{i3} = d\sigma_{i3} = 0 \qquad i = 1, 2, 3 \tag{4.39}$$

and the incremental total strain components

$$d\varepsilon_{13} = d\varepsilon_{23} = 0 \tag{4.40}$$

as is generally done for thin plate theory. The only nonvanishing terms of the incremental constitutive relation therefore become

$$\begin{Bmatrix} d\sigma_{11} \\ d\sigma_{22} \\ d\sigma_{12} \\ d\sigma_{33} \end{Bmatrix} = \begin{bmatrix} C_{1111} & C_{1122} & C_{1112} & C_{1133} \\ C_{2211} & C_{2222} & C_{2212} & C_{2233} \\ C_{1211} & C_{1222} & C_{1212} & C_{1233} \\ C_{3111} & C_{3322} & C_{3312} & C_{3333} \end{bmatrix} \begin{Bmatrix} d\varepsilon_{11} \\ d\varepsilon_{22} \\ 2d\varepsilon_{12} \\ d\varepsilon_{33} \end{Bmatrix} \tag{4.41}$$

or

$$d\sigma_{\alpha\beta} = C_{\alpha\beta\gamma\delta}\, d\varepsilon_{\gamma\delta} + C_{\alpha\beta 33}\, d\varepsilon_{33} \tag{4.42}$$

and

$$d\sigma_{33} = C_{33\gamma\delta}\, d\varepsilon_{\gamma\delta} + C_{3333}\, d\varepsilon_{33} = 0 \tag{4.43}$$

which yields a contracted relation

$$d\sigma_{\alpha\beta} = \left(C_{\alpha\beta\gamma\delta} - C_{\alpha\beta 33}\,\frac{C_{33\gamma\delta}}{C_{3333}}\right) d\varepsilon_{\gamma\delta} = D_{\alpha\beta\gamma\delta}\, d\varepsilon_{\gamma\delta} \tag{4.44}$$

Greek indices span 1 and 2 only.

The contraction Eq. (4.44) of the 4 by 4 matrix in Eq. (4.41) can also be stated as

$$D_{ij} = C_{ij} - \frac{C_{i4}\, C_{j4}}{C_{44}} \qquad \begin{matrix} j = 1, 2, 3 \\ i = 1, 2, 3 \end{matrix} \tag{4.45}$$

where indices i and j of C now refer to the matrix defined in Eq. (4.41) [D] is also symmetric. Numerically, it is faster to use Eq. (4.45) directly rather than to obtain and use an explicit expression for each element of [D] as suggested by Yamada [97].

Now using matrix symbols, the stress-strain relation becomes

$$\{d\sigma\} = [D]\,\{d\varepsilon\} = [E]\,\{d\varepsilon^{E}\} \tag{4.46}$$

where [E] is Hookes law for plane stress given by Eq. (2.46). Solution of Equation (4.46) with respect to the plastic strain increment yields

$$\{d\varepsilon^P\} = [A] \{d\varepsilon\} \tag{4.47}$$

where

$$[A] = [I] - [F] [D] \tag{4.48}$$

[F] being the inverse of [E]. [A] is generally not symmetric. As will be discussed later, the membrane and the bending stiffnesses of Eqs. (2.43) to (2.45) are obtained by substituting Eq. (4.45) into the equations just mentioned and employing numerical integration through the thickness.

Special simplified equations for rotationally symmetric plane stress was given by Popov et. al. in Reference [98]

4.3 VARIATIONAL FORMULATION OF THE ELASTIC-PLASTIC PROBLEM

Special caution must be exercised when formulating a variational principle for an elastic-plastic material. Whenever the flow theory of plasticity is used, the variational principle must deal with stress rates and strain rates since there is no unique solution for a given set of total loads. The current configuration depends on the previous load history. Further discussions may be found in the References [23], [78] and [87]. As demonstrated by Prager and Hodge [78] two basic extremum principles dealing with admissible stress and strain fields can be derived and used for establishing upper and lower bounds for limit load problems.

In Chapter 2, the virtual work principle including its incremental form was derived. This principle is based on the equilibrium equations only, and is therefore applicable for any material including elastic-plastic types. When there exists a strain

energy function which is uniquely defined by the displacement field (Eq. (2.11)), the virtual work principle can be transferred into the principle of stationary potential energy and its incremental form as shown in Sections 2.2.3 and 2.2.4. In flow theory plasticity, however, no strain energy function exists which is uniquely defined by current displacements. Such a function would depend on previous load and deformation history.

It should be recalled that the incremental form of the variational principle in the Lagrangian description of Section 2.2.4 was later simplified due to special assumptions for plates with moderately large deflections. These simplifications lead to the result that only the rotations become finite quantities, not the deformation part of the strains. This justifies using the small strain plasticity theory previously derived in this chapter. Moreover, the derivations of Section 2.4.5 account for all geometric nonlinear contributions to the incremental equations. Again, Eq. (4.34) constitutes a linear incremental stress-strain expression, dependent on previous load history.

In brief, the nonlinear strain expressions of von Karman can also be used for inelastic materials since the strain itself is infinitesimal, only rotations are finite. The incremental form of the variational principle is also applicable since it arises from the virtual work principle applied to two consequitive equilibrium configurations between which the constitutive equations throughout the body can be assumed to be known. The material nonlinearities thus can be accounted for by substituting Eq. (4.45) into Eqs. (2.43), (2.44) and (2.45) and into the matrix equations of Section 2.4.5.

4.4 FINITE ELEMENTS FOR THE ELASTIC-PLASTIC ANALYSIS

4.4.1 The Plate Bending Element

The derivation of the Q19 plate bending element was discussed in Section 3.2. The same interpolation polynomials as used in the Q19 element will be utilized for the elastic-plastic element. However, after initial yielding has occurred in some part of the element, the material properties will no longer be uniform throughout the element. Two basic approaches can be used for handling this problem. The material properties can be expressed by a special interpolation polynomial, and an explicit strain energy integration then carried out for the stiffness. This method was used by Felippa [16] for elastic-plastic plane stress elements, but it turns out that such an approach is rather complicated for the Q19 element. Instead, the integration here will be carried out numerically, using a "natural" set of integration locations defined by the centroids $A^{(i)}$, $B^{(i)}$ and $C^{(i)}$ of the 12 subtriangles, see Fig. 4.3. The numerical error committed by using such an integration scheme is very small. For instance, this integration scheme was tested for a square elastic plate subjected to uniform transversal load, the plate being divided into a 4 by 4 element mesh. For this case the midpoint deflection increased only 0.4 percent by using numerical instead of exact integration, the result for the numerical integration being closer to the true solution.

The numerical computation of the element stiffness requires evaluation of the curvatures at the centroids of the subtriangle elements. For instance, the location of the centroid of subtriangle

3 of Fig. 3.2 expressed by natural coordinates is (4/9, 4/9, 1/9). Using the interpolation polynomial of Appendix A the incremental curvature at the centroid subtriangle is given by

$$\{\Delta \chi_c^{(j)}\} = [B_{wc}^{(j)}] \{\Delta w_i\} \tag{4.49}$$

where $[B_{wc}^{(j)}]$ is obtained by differentiation of $\langle \varphi_w \rangle$ in Eq. (3.1) at the centroid and $\{\chi\}$ is defined in Eq. (2.39). Since the strains are assumed to vary linearly through the thickness also for the elastic-plastic solution, the element incremental stiffness for one LCCT11 triangle is

$$[k_w] = \frac{A}{3} \sum_{j=1}^{3} [B_{wc}^{(j)}]^T [D_{22}^{(j)}] [B_{wc}^{(j)}] \tag{4.50}$$

where, as in Eq. (2.43)

$$[D_{22}^{(j)}] = \int_{-\frac{h}{2}}^{\frac{h}{2}} \zeta^2 [D^{(j)}(\zeta)] \, d\zeta \tag{4.51}$$

and A is the area of the triangle. The constitutive equation for plane stress $[D(\zeta)]$ was given in Section 4.2.4.

Computation of the curvature-displacement relations $[B_{wc}^{(j)}]$ need be carried out only once and stored for later use during load application. The integration of Eq. (4.51) has to be carried out at each load level because the material properties change as the state of stress is altered. 9 to 11 point Gaussian quadrature through the thickness yields excellent results. For pure bending, only half of these points need to be considered because of symmetry about the

mid-plane . Integration is always carried out starting with the stress state of the integration point closest to the surface. If this point is elastic, the integration of Eq. (4.51) need not be performed since the entire cross-section is elastic (provided that there is no unloading). As will be demonstrated by examples later, this approach turns out to be very efficient.

4.4.2 The Membrane Element

The membrane element has previously been discussed in Section 3.3 and Appendix B, moreover, further details may be found in Reference [62]. The numerical integration scheme for the elastic element was a 2 by 2 or a 3 by 3 Gaussian quadrature. However, to match the elastic-plastic bending element of the preceeding section, the stiffness integration for the elastic-plastic membrane element will be based on the same 12 integration locations chosen for the Q19 element.

The interpolation polynomials for the membrane element was given in a ξ- η system in Appendix B, whereas the integration points of the Q19 element was described in natural triangular coordinate systems. Noting that the mid-point of the Q19 element is the same as the origin of the ξ-η system, the following relation between the two natural coordinate systems is valid for triangle 1 (Fig. 4.3)

$$\xi = -\zeta_1^{(1)} + \zeta_2^{(1)}$$
$$\eta = -\zeta_1^{(1)} - \zeta_2^{(1)} \qquad (4.52)$$

The three centroid points of the subtriangles of triangle 1 therefore have the following coordinates in the ξ-η system

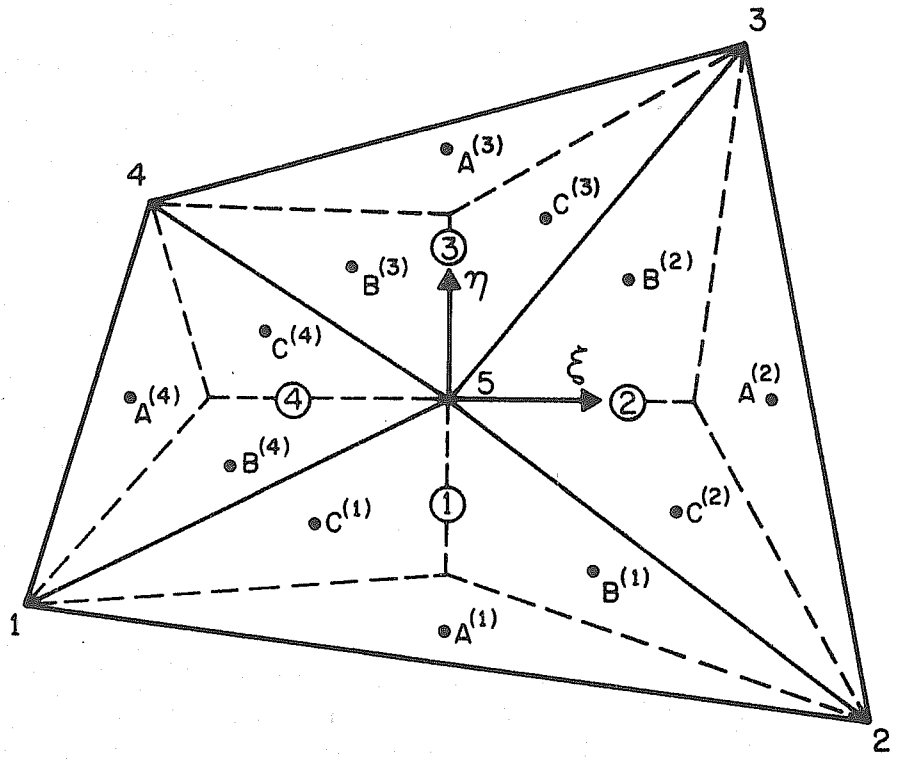

FIG. 4.3 INTEGRATION POINTS FOR ELASTIC-PLASTIC PLATE BENDING ELEMENT

$$
\begin{aligned}
A^{(1)} \quad & (4/9,\ 4/9,\ 1/9) \rightarrow (0,\ -8/9) \quad (\text{in } \xi\text{-}\eta \text{ system}) \\
B^{(1)} \quad & (1/9,\ 4/9,\ 4/9) \rightarrow (1/3,\ -5/9) \\
C^{(1)} \quad & (4/9,\ 1/9,\ 4/9) \rightarrow (-1/3,\ -5/9)
\end{aligned}
\tag{4.53}
$$

Similarily, for triangle 2

$$
\begin{aligned}
A^{(2)} \quad & (4/9,\ 4/9,\ 1/9) \rightarrow (8/9,\ 0) \\
B^{(2)} \quad & (1/9,\ 4/9,\ 4/9) \rightarrow (5/9,\ 1/3) \\
C^{(2)} \quad & (4/9,\ 1/9,\ 4/9) \rightarrow (5/9,\ -1/3)
\end{aligned}
\tag{4.54}
$$

The results for triangle 3 and 4 are the same as for 1 and 2 respectively, only with sign change for ξ and η.

The numerical computation of the incremental stiffness now follows the usual pattern by establishing the strain-displacement relationship for all integration points

$$
\{\Delta \varepsilon^{(m)}\} = [B_{vc}^{(m)}]\{\Delta v^{(m)}\} \qquad m = 1, \cdots\cdots 12 \tag{4.55}
$$

The Jacobian matrix must also be considered at all 12 locations for computation of $[B_{vc}^{(m)}]$. The incremental stiffness is now

$$
[k_v] = \sum_{m=1}^{12} A^{(m)} [B_{vc}^{(m)}]^T [D_{11}^{(m)}][B_{vc}^{(m)}] \tag{4.56}
$$

where, as in Eq. (2.41)

$$
[D_{11}^{(m)}] = \int_{-\frac{h}{2}}^{\frac{h}{2}} [D^{(m)}(\zeta)]d\zeta \tag{4.57}
$$

The area of the surrounding subtriangle $A^{(m)}$ is associated with each integration point. For pure membrane stress only one integration point through the thickness is needed for the numerical computation of Eq. (4.57).

Again $[B_{vc}^{(m)}]$ has to be calculated only once for each integration point, while the constitutive relation and the stiffness matrix has to be recomputed for each load increment.

4.4.3 Combined Bending and Membrane Action

When the plate is in a state of combined bending and membrane action, the material properties will no longer remain symmetric about the midplane after initial yielding has occurred. Consequently, integration has to be carried out through the entire plate thickness to compute the stiffness properties of Eqs. (4.51) and (4.57). Moreover, the coupling stiffness of Eq. (2.76) will no longer cancel out. This incremental stiffness can also be obtained by numerical integration using the 12 centroid points.

$$[\hat{k}_{vw}] = \sum_{m=1}^{12} A^{(m)} [B_{vc}^{(m)}]^T [D_{12}^{(m)}(\zeta)] [B_{wc}^{(m)}] \tag{4.58}$$

where

$$[D_{12}^{(m)}] = \int_{-\frac{h}{2}}^{\frac{h}{2}} \zeta [D^{(m)}(\zeta)] \, d\zeta \tag{4.59}$$

The same Gaussian integration points through the thickness could be used for numerical computation of $[D_{12}^{(m)}]$ as used in Eqs. (4.51) and (4.57). However, it is believed that the trapezoidal integration rule in this case might be more efficient for some extreme states of yielding. This integration should be performed simultaneously for all three D-matrices, considering the total stress-state resulting from combined membrane and bending action.

5. NUMERICAL METHODS

5.1 NUMERICAL TECHNIQUES FOR SOLVING THE NONLINEAR EQUATIONS

5.1.1 Review of Methods

The numerous numerical solution techniques that can be used for solving nonlinear structural problems can roughly be divided into the following four main groups

1. Energy minimization
2. Direct interation methods
3. Incremental methods
4. Combined methods

The first group covers methods that employ some nonlinear programming scheme for a direct search of the extremum values of the potential energy expression. One of the most efficient minimization techniques available today is the Fletcher-Powell method [99] that employs a very fast approximation to the inverse gradient (inverse Jacobian matrix). This nonlinear programming method reportedly has also been applied with some success for structural problems [100, 101, 102]. However, the energy minimization approach is not reliable when used for problems in which structural instability occurs, due to the existence of local minima. It is also doubtful whether this method offers any time saving compared to the other methods described in the following; therefore it will not be considered further in this work.

The second group comprises methods that utilize some direct interation technique applied to the equilibrium equations. Physically these methods are equivalent to those of group 1, although the problem is formulated differently. The lowest order interation method available

is functional iteration [103] which implies successive substitutions of the displacement vector into the inverted equilibrium equation. The method is illustrated for a one degree of freedom system in Fig. 5.1a. Although this method has been used by some authors, it converges only when special conditions are fulfilled and should generally be avoided. The same warning applied to the "chord" method of Fig. 5.1b where a Newton type iteration is performed maintaining a constant preselected gradient such as the initial linear stiffness of the system.

A higher order iteration scheme is Newton-Raphson interation which utilizes the gradient of the stiffness relation, see Fig. 5.1c. This method has proved to be both efficient and reliable and will be described in greater detail in Section 5.1.3. Quasi-Newton methods based on based on approximations to the gradient can also be used; in fact they are highly recommendable in most cases in which they do not impede convergence. The method of false position and Aitkens δ^2 process [103] have also been used by some investigators.

The third group comprises methods treating the incremental form of the equilibrium equations as a first order differential equation which is solved as an initial value problem by applying load increments. Numerous numerical methods capable of solving this problem has been described in the literature [103, 104, 105]. Such methods have been characterized as single step or multistep, implicit or explicit, and they are based on quadrature, series expansions or finite differences. The most important features of the various methods from a numerical point of view are their stability (related to round-off errors) and truncation errors (resulting from omission of higher order terms). For practical applications, their efficiency or time consumption per step is

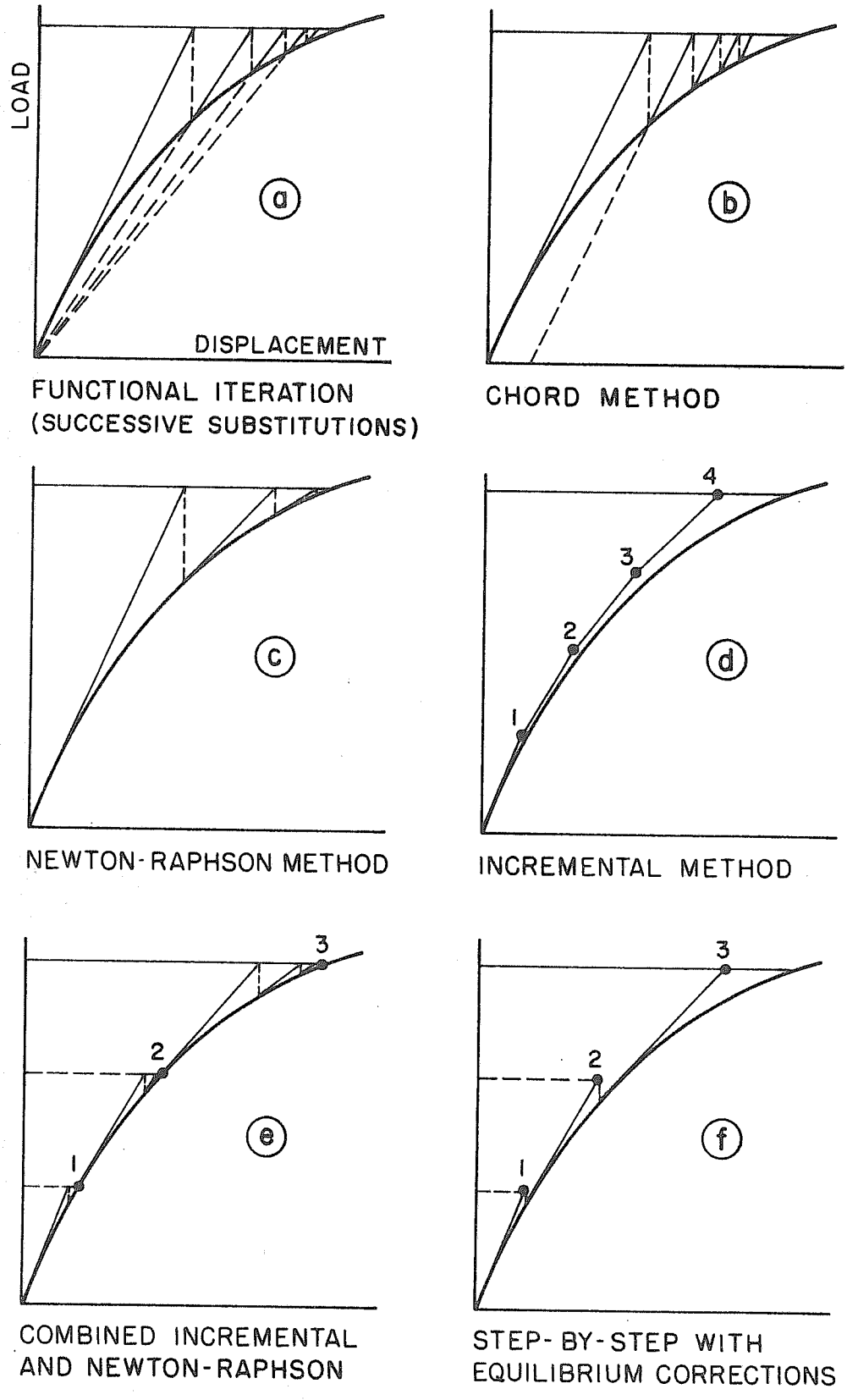

FIG. 5.1 VARIOUS SOLUTION METHODS

also highly critical quantity. The simplest incremental scheme is the Euler-Cauchy method (simple step-by-step) shown in Fig. 5.1d. This method will be discussed more in detail in the next section.

The fourth group of methods comprises those procedures which in some way are combinations of group 2 and 3. A noteworthy method of this category is a step-by-step procedure combined with Newton iteration at certain load intervals, see Fig. 5.1e. A somewhat similar method uses residual force (equilibrium) corrections combined with load incrementation. This method is shown in Fig. 5.1f.

Many different factors are involved when choosing a numerical solution method. The main objective is usually to find a method which comprises high precision and reliability at low cost. However, before the choice can be made it is necessary to define precisely the purpose of the analysis: is it to find the entire load-deformation curve, one point on the curve or several sections of it? Also of importance for the choice of method is whether the system to be analysed is structurally stable or not and whether it is conservative or nonconservative. Therefore, one method generally cannot be said to be "better" than another, and a computer program should ideally include optional methods. In this study it has been decided to incorporate in the computer program both simple step-by-step and Newton-type iteration, or combinations of both. This gives the desired flexibility allowing for solving different classes of problems efficiently.

5.1.2 The Step-by-step Method

The incremental stiffness was derived in Chapter 2 using the incremental form of the variational principle. Equation (2.98) can be written in continuous form as a set of first order differential equations

$$\frac{d\{\tilde{r}\}}{d\{R\}} = [K_I(\tilde{r})]^{-1} \tag{5.1}$$

where $\{\tilde{r}\}$ is used to denote the exact solution. The simplest numerical solution scheme is the Euler-Cauchy method which can be written as

$$\{\Delta r^{(n+1)}\} = [K_I^{(n)}(r)]^{-1}\{\Delta R^{(n+1)}\} \tag{5.2}$$

where

$$\{\Delta r^{(n+1)}\} = \{r^{(n+1)}\} - \{r^{(n)}\} \tag{5.3}$$

$$\{\Delta R^{(n+1)}\} = \{R^{(n+1)}\} - \{R^{(n)}\} \tag{5.4}$$

and (n) denotes the loadstep number. Of course, only triangularization is performed on $[K_I]$ during the computation rather than the formal inversion denoted in Eq. (5.2).

For practical ranges of load increments for quasistatic problems the roundoff errors are negligible compared to the truncation errors associated with a solution technique such as Eq. (5.2). It can easily be shown that the total associated truncation error for one step is proportional to the square of the load increment multiplied by the second derivative of the load-displacement relationship computed at some point within the range of the loadstep. This gives a good indication of how the size of the loadstep should be chosen: the steps should be small where the curvature of the load-displacement curve is high.

Since there are usually many variables involved, a simplified measure of curvature could be used. A displacement component that characterizes the nonlinearity of the problem should preferably be selected. Having chosen this variable, a parabolic fit through 3 consecutive points of the load-displacement curve for this variable gives a good indication of the truncation error associated with the next linearized loadstep. Fig. 5.2 shows how the truncation error due to linearization can be computed as the distance between the parabola Q(R) and the tangent T(R). Given an "allowable" truncation error τ for the chosen displacement component, the corresponding load increment is obtained by solving for ΔR

$$\Delta R = \sqrt{\tau \frac{(R_1 - R_2)(R_2 - R_3)(R_3 - R_1)}{r_1(R_2 - R_3) + r_2(R_3 - R_1) + r_3(R_1 - R_2)}} \tag{5.5}$$

This formula is identical to the one obtained by direct use of the expression for the truncation error

$$\tau = \frac{(\Delta R)^2}{2} \frac{d^2 Q(R)}{dR^2} \tag{5.6}$$

where the second derivative of the parabola is a constant.

When more general functions are used for the fit, the second differential of the load-displacement curve should be taken at some point in the new interval.

Practical computer applications of Eq. (5.4) show its ability to decrease the loadsteps when the structural behavior changes more rapidly. Having concentrated the results in these regions also makes it more easy to reproduce results for intermediate load levels. Moreover, when this load criterion is used in combination with iteration at each

load level the number of iteration cycles needed to obtain convergence seems to be relatively constant during load application. However, the explicit measure of the truncation error τ by Eq. (5.3) does not prove to be very accurate. This is because the interpolating parabola has a constant curvature and consequently introduces considerable inertia into the formula for the truncation error (5.6) For instance, when the true curvature of the load-displacement curve decreases with increasing load intensity, Eq. (5.5) will result in too small a load increment for the desired truncation error, and visa versa when the curvature increases with increasing load intensity. Being aware of these facts, Eq. (5.5) is still a useful formula for determining of the load increment automatically.

A somewhat simpler method that has proven to be quite useful consists of increasing or decreasing the steplength by a constant factor α. So if the system is known to have an increasingly changing load-displacement curve, the step-length is decreased by using a multiplication factor less than one in magnitude. Conversely an α value larger than one is used for systems that become increasingly linear for higher loads. Given the maximum load-level R_{max}, the load increment factor α and the desired number of steps N, the first load-step is found from

$$\Delta R^{(1)} = \frac{R_{max}}{\sum_{n=1}^{N} \alpha^{n-1}} \tag{5.7}$$

and in general

$$\Delta R^{(n)} = \alpha^{n-1} R^{(1)} \tag{5.8}$$

An even more obvious method that can be used to improve computational efficiency is to give all load-levels as input.

"Snap-through" problems require special caution. These problems have local maximum points after which the slope of the load-deflection curve becomes negative. A further continuation along the deflection path requires a decrease of the external loading. Such an extremum point can be detected either by computation of the sign of the determinant of the incremental stiffness or the sign of the increment of external work. However, in practical loading cases, the decreasing curve will not be followed; instead, a "snap" to another stable configuration will occur. By means of the formulation that is chosen here, it is possible to "jump" directly from an extremum point to a new stable configuration when load incrementation is combined with iteration. No errors are accumulated in the snap-through since the stresses and strains are expressed directly in global coordinates. An example of this is given in Section 6.2.5.

A "chord stiffness" method based on computing the incremental stiffness using the extrapolated displacements at some point (usually midpoint) of each new load increment, in general yields more accurate results than the Euler-Cauchy method [106]. However, this "chord stiffness" method is not too well suited when the incremental method is combined with equilibrium corrections or iterations.

5.1.3 Newton-Raphson Iteration

Using a direct iteration scheme like the Newton-Raphson method, the numerical solution of the equilibrium Equations (2.98) can be written symbolically as

$$[K_{T(j)}]\{\Delta r_{(j+1)}\} = \{\Delta R_{(j)}\} \tag{5.9}$$

in which the unbalanced forces are

$$\{\Delta R_{(j)}\} = \{R\} - [K_{(j)}]\{r_{(j)}\} \tag{5.10}$$

and the new improved displacement vector is found from

$$\{r_{(j+1)}\} = \{r_{(j)}\} + \{\Delta r_{j+1}\} \tag{5.11}$$

Subscript j denotes the iteration cycle. The unbalanced forces (often termed "out-of-balance" forces) are found as the residue of the equilibrium Eq. (5.10)

The incremental stiffness of Eq. (5.9) is usually termed the "Jacobian matrix" by numerical analysts. The expression "incremental stiffness" will be retained here, however, because of the direct physical meaning of the matrix. It can be proved that convergence of the Newton iteration method depends on the closeness of the start vector $\{ r_{(o)} \}$ to the true solution, as well as on various properties of the Jacobian matrix at the initial state and on a bound on the second derivative of the function (equilibrium expression) for all vectors within some distance from the initial vector. Further details and proof of the theorem can be found in Reference [103].

Each iteration cycle involves three major computational efforts:

(i) Computation of the functional stiffness of Eq. (5.10)

(ii) Computation of the incremental stiffness of Eq. (5.9)

(iii) Triangularization of $[K_I]$ of Eq. (5.9)

It becomes evident by comparing the equations of Section 2.4.4 with the equations of Section 2.4.5 that the computation of the incremental stiffness terms does not involve much additional work when the functional stiffness is computed. In fact the only additional cost is in assemblage and introduction of boundary conditions into the total matrix $[K_I]$. However, for each new incremental stiffness a triangularization is required. This suggests that an approximation to the Jacobian matrix might be kept constant during the iteration procedure thereby saving the operations of (ii) and (iii). It turns out that this technique saves a substantial amount of computer time (on the order of 25% per cycle for small systems) and is highly recommendable for many cases. However this simplification has consequences both regarding the existence of convergence and the rate of convergence. In particular when the convergence is of oscillatory type, this quasi-Newton method may not be reliable. Therefore the simplified method is not recommendable when the initial vector is far from the true solution or in many stability problems. On the other hand, the simplified iteration technique converges equally as fast as true Newton iteration for some cases. In the present work, an option of computing a new tangent stiffness only for the second iteration cycle and keeping it constant during the rest of the itertion procedure was used for many applications.

It was noted above that iteration convergence is dependent on the closeness of the initial vector. A combination of incrementation and iteration as shown in Fig. 5.1e is therefore advisable in many cases, to avoid moving too far from the true load path. This is particularly true when a simplified iteration scheme is used. The equations for the combined solution method are obtained just by combining Equations (5.2), (5.3), (5.4) and Equations (5.9),(5.10),(5.11).

One should also note that a simplified two-dimensional diagram, showing the load level and one displacement component, may very often give a highly distorted picture of what really happens in N - dimensional space. For a system with only one free variable, the slope of the load-displacement curve at a point outside the path always corresponds to the slope at some point on the true path. This is not so far the general multidimensional case. For a discretized system with several degrees of freedom, the true path corresponds to a specific displacement vector function of the given loading. The incremental stiffness for some point on the path is a function of all elements of the associated displacement vector. Any other displacement vector that does not correspond to a point on the true path yields a "slope" (really a hypersurface) that is different from any "slope" at the true path. For some cases, even a small perturbation of the displacement vector has a tremendous influence on the incremental stiffness. For instance, this is a serious problem in the analysis of very thin plates for which the membrane stiffness is high compared with the bending stiffness. Only a small perturbation in the inplane displacement components in the non-linear range gives a significant change of the stiffness associated with the transverse displacements. For such cases, the rate of convergence is usually very slow, particularly when the Jacobian matrix is kept constant during the iteration

Similar difficulties are known to be encountered when applying various nonlinear programming techniques to optimization problems. Following a "narrow valley" towards an extremum point may results in "zig-zag"-ing and slow convergence. A special approach that

has proved to be useful for special cases of slow convergence of plate problems will be discussed next.

5.1.4 A Special Method for Slowly Converging Systems

As was mentioned in the preceeding section, special geometries of the structure may result in slow convergence of the Newton-Raphson method. A method based on the principle of "extrapolating errors to zero" has proven to be useful in such cases. This approach which resembles the method of "double false position" can be used directly in connection with slowly converging Newton-Raphson iteration. Fig. 5.3 shows how the out-of-balance force associated with one arbitrary displacement component is used for finding a new displacement value for which this force presumably is zero. The following formula is easily derived by consideration of the figure

$$\Delta r_{(j+1)} = \Delta r^{*}_{(j+1)} \frac{\Delta R_{(j)}}{\Delta R_{(j)} - \Delta R^{*}_{(j+1)}} \tag{5.12}$$

The values marked with an asterisk represent intermediate values that are improved by using Eq. (5.12). This equation should be used for all displacement components. The extrapolation method itself is generally not stable and should be used only as a "single shot" adjustment in connection with a stable type of iteration.

A cantilever beam divided into 10 quadrilateral elements and subjected to a concentrated end moment is used to demonstrate the method. The thickness/length ratio is chosen to be 1/100, thereby creating a system with slow convergence due to the small bending stiffness compared to the membrane stiffness. The total load is applied in only four increments, the first and third of which are intoduced without

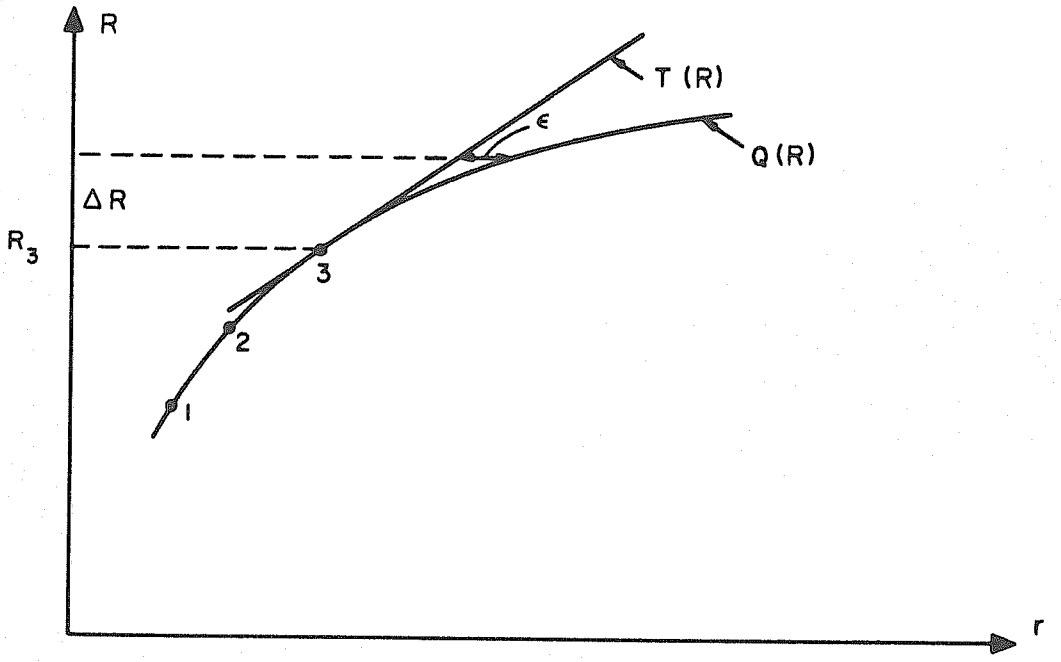

FIG. 5.2 PREDICTION OF TRUNCATION ERROR BY INTERPOLATION POLYNOMIAL

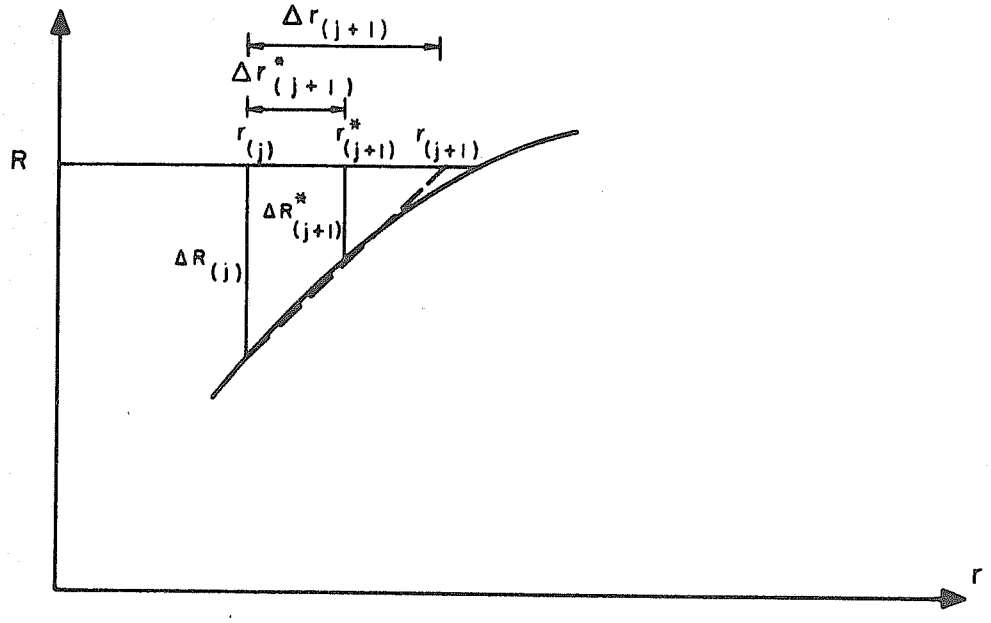

FIG. 5.3 METHOD FOR FINDING IMPROVED DISPLACEMENT VALUES

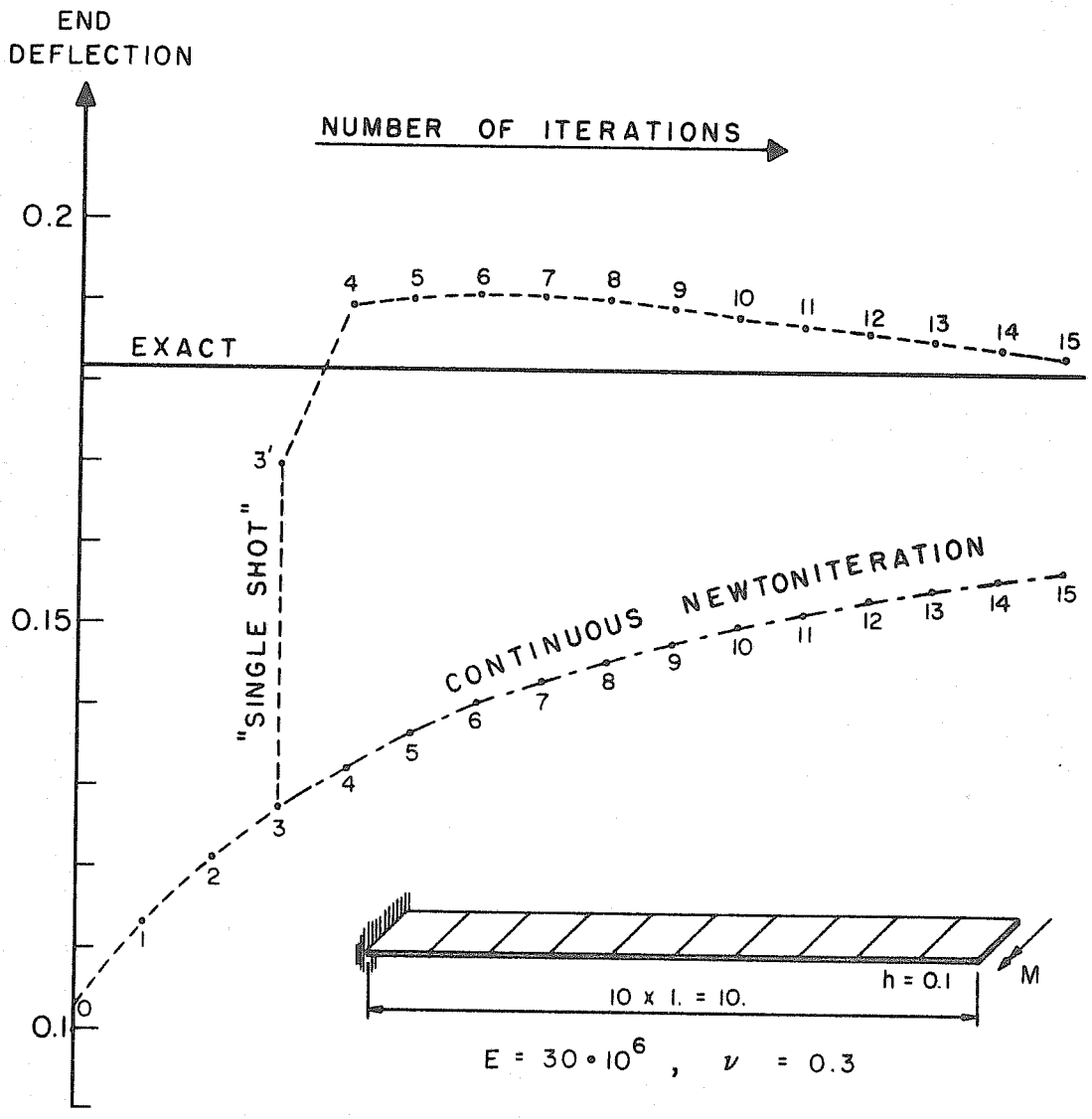

FIG. 5.4 CONVERGENCE OF THIN CANTILEVER BEAM

iteration thereby creating a strongly unbalanced system. Fig. 5.4 reveals the slow convergence of the Newton-Raphson method at the last load increment. The figure also demonstrates the improved results when a "single shot" is used at the third iteration cycle. It should be noted that this example converges easily using regular iteration when the plate thickness is increased to a more realistic value. The method described may also be used in connection with simplified Newton iteration, of course.

5.2 CONVERGENCE AND ACCURACY

When an iteration technique is used for solving the nonlinear equations, a convergence criterion capable of determining when the procedure has converged to the desired degree of accuracy is needed. Use of a fixed number of iteration cycles will not work satisfactorily since some systems converge rapidly and others very slowly; even the same structure may completely change character during load application.

Some investigators have compared the unbalanced forces with the applied external loading to determine when convergence has occurred. However, inplane forces, transversal forces and moments may all be of different order. For instance, if the only external loading lies in the plane of the plate, how can it be determined in an automatic manner whether the transversal out-of-balance forces are sufficiently small? A more correct approach would be to compare the unbalanced forces with the characteristic stiffness properties of the structure. This again corresponds to studying displacement properties, so why not work directly with displacements?

According to the convergence criterion proposed here, an error vector is defined as follows

$$\{\varepsilon_{(j)}\} = \left\langle \frac{\Delta r_1}{r_{1,ref}} , \frac{\Delta r_2}{r_{2,ref}} , \ldots\ldots \frac{\Delta r_N}{r_{N,ref}} \right\rangle^T_{(j)} \qquad (5.13)$$

where Δr_1, Δr_2, ... etc are the changes of the displacement components during cycle j, and N is the total number of nonzero components. Every component is scaled by a reference quantity to obtain a non-dimensional measure. These reference quantities are generally not chosen to be equal to the corresponding total components because if r_k is a number close to zero, the ratio $\Delta r_k/r_k$ could be a large number even after "convergence" has occurred. Therefore, the change of transversal displacements are scaled by the largest of the transversal components, the changes in rotations are scaled by the largest rotation and similarily with the inplane displacements.

It is well known that vector norms are used in numerical analysis for measuring the "size" of vectors. Three alternative norms are now suggested to measure the "size" of the error vector:

(i) Modified absolute norm

$$\|\varepsilon\|_1 = \frac{1}{N} \sum_{k=1}^{N} \left| \frac{\Delta r_k}{r_{k,ref}} \right| \qquad (5.14)$$

(ii) Modified Euclidian (spectral) norm

$$\|\varepsilon\|_2 = \sqrt{\frac{1}{N} \sum_{k=1}^{N} \left| \frac{\Delta r_k}{r_{k,ref}} \right|} \qquad (5.15)$$

(iii) Maximum (uniform) norm

$$\|\varepsilon\|_\infty = \max_k \left| \frac{\Delta r_k}{r_{k,ref}} \right| \qquad (5.16)$$

The two first norms are modified by dividing by N to get quantities that are independent of the total number of displacement components. (i) and (ii) still satisfy the requirements for true norms. These definitions yield convergence criteria that have a direct physical significance. Error bounds on the displacement vector indicate the accuracy both of total displacements and of stresses.

The use of the error norms is illustrated here by two examples. Fig. 5.5 shows the convergence of the different norms for a shallow shell subjected to transversal loading and for a plane plate subjected to inplane loading right after the bifurcation buckling load. It is worth noting that the convergence stabilizes to a linear relationship in the semi-logarithmic diagram. The same result was found for a wide range of other examples, although in a few cases with extremely slow convergence, some "zig-zag"-ing was observed. Note also that the three different norms follow each other in a parallel manner. Therefore it can be concluded that it is of minor importance what specific norm is being used. The maximum norm is, however, probably the safest measure of convergence since it gives a specific error bound on all displacement components; the other norms yield more of an average error bound. The practical range of $\|\varepsilon\|$ is approximately from 10^{-2} to 10^{-4}

$\{ \varepsilon_{(j)} \}$ as defined by Eq. (5.13) really represents the change of the displacement vector during iteration cycle j and is not the true "error" itself. As is illustrated by Fig. 5.6, two cases with the same $\|\varepsilon\|$ (represented by the slope of the curves) may have quite different total errors. A case when the convergence is extremely slow might thus incorrectly be believed to be close to the true solution. However, a bound on the total error E_{ij}, at cycle j is obtained from

$$E_{(j)} = \int_{n=j}^{\infty} \|\varepsilon\| \, dn \tag{5.17}$$

where n denotes the iteration cycle. Since it turns out that the convergence is linear in a semilogarithmic scale, $\|\varepsilon\|$ can be approximated by

$$\|\varepsilon\| \simeq e^{\alpha-\beta j} \qquad \text{or} \qquad \log\|\varepsilon\| \simeq \alpha - \beta j \tag{5.18}$$

The constants α and β can be obtained using a couple of points of the $\|\varepsilon\| - j$ diagram or by using a "best" linear fit. β represents a logarithmic "rate of convergence" and is identified by the slopes of Fig. 5.5. Substituting Eq. (5.18) into Eq. (5.17) and carrying out the integration yields

$$E_{(j)} \leq \frac{1}{\beta} e^{\alpha-\beta j} \tag{5.19}$$

Fig. 5.7 shows the maximum norm and the integrated maximum norm of Eq. (5.17) for one case of fast and one case of slow convergence. At cycle j, $E_{(j)}$ represents the integral (sum) of $\|\varepsilon\|$ at all consecutive cycles. As demonstrated by Fig. 5.7, $E_{(j)}$ is larger than $\|\varepsilon\|$ in case of slow convergence whereas it is smaller when convergence is fast.

The integrated error norms E yield more correct estimates of the error than the $\|\varepsilon\|$ - norms, although when the convergence is oscillatory about the equilibrium configuration, the E- norms result in over-estimates of the total error. Usually, the convergence is uniform. The linearity of the logarithmic convergence (Eq. 5.16) makes it possible during iteration to estimate how many more cycles are necessary to satisfy a given convergence criterion.

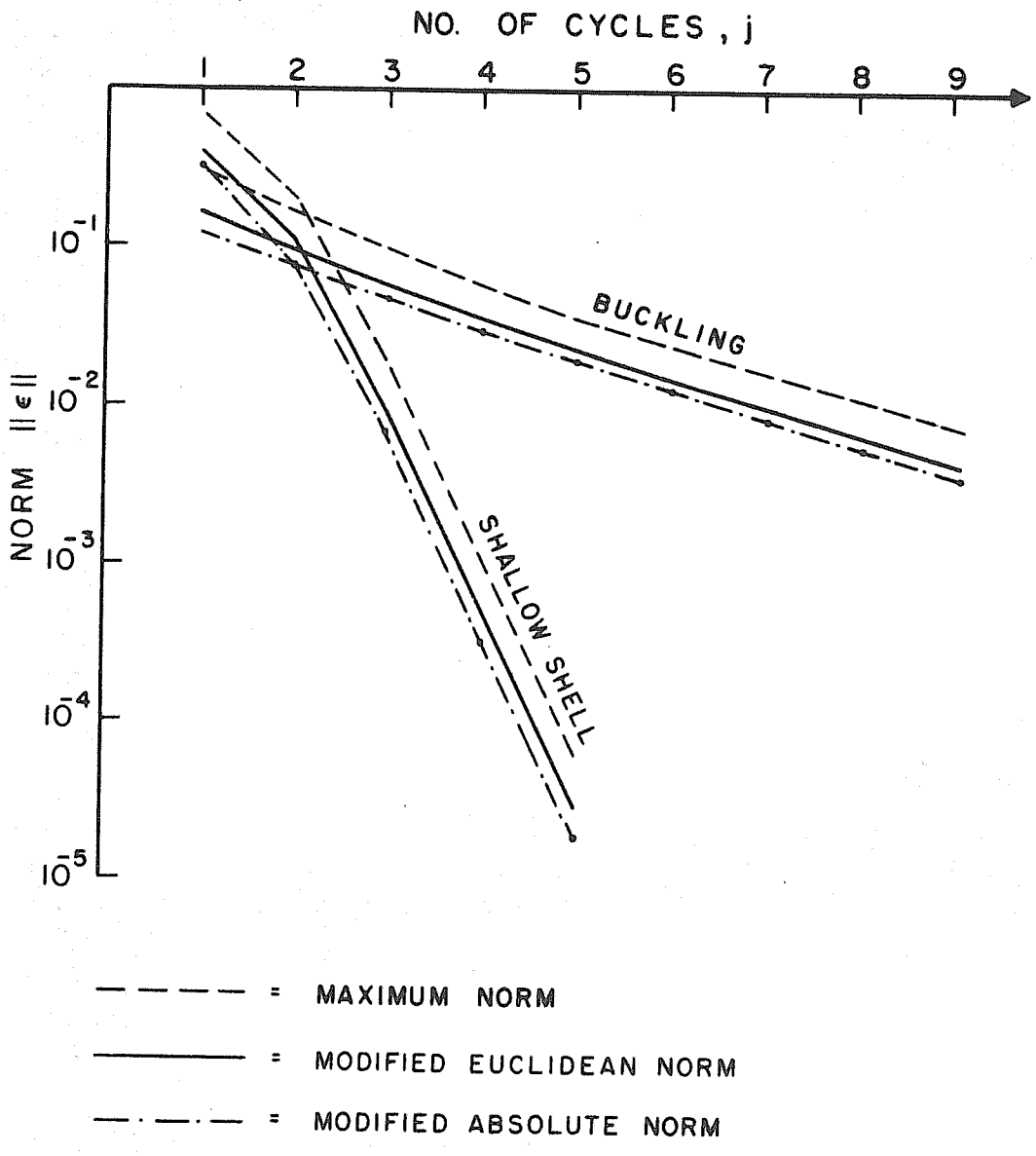

FIG. 5.5 COMPARISON OF CONVERGENCE CRITERIA

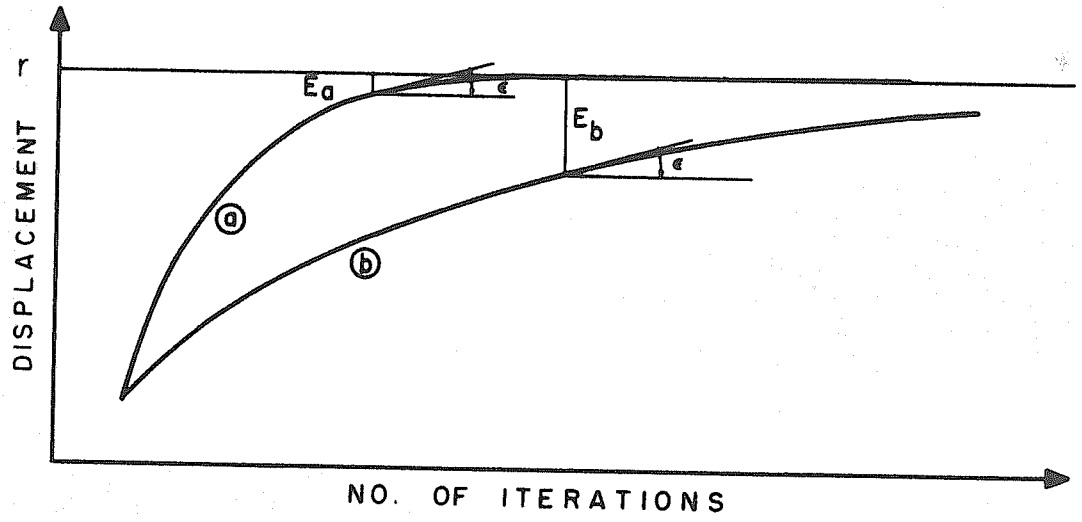

FIG. 5.6 SLOW AND FAST CONVERGENCE

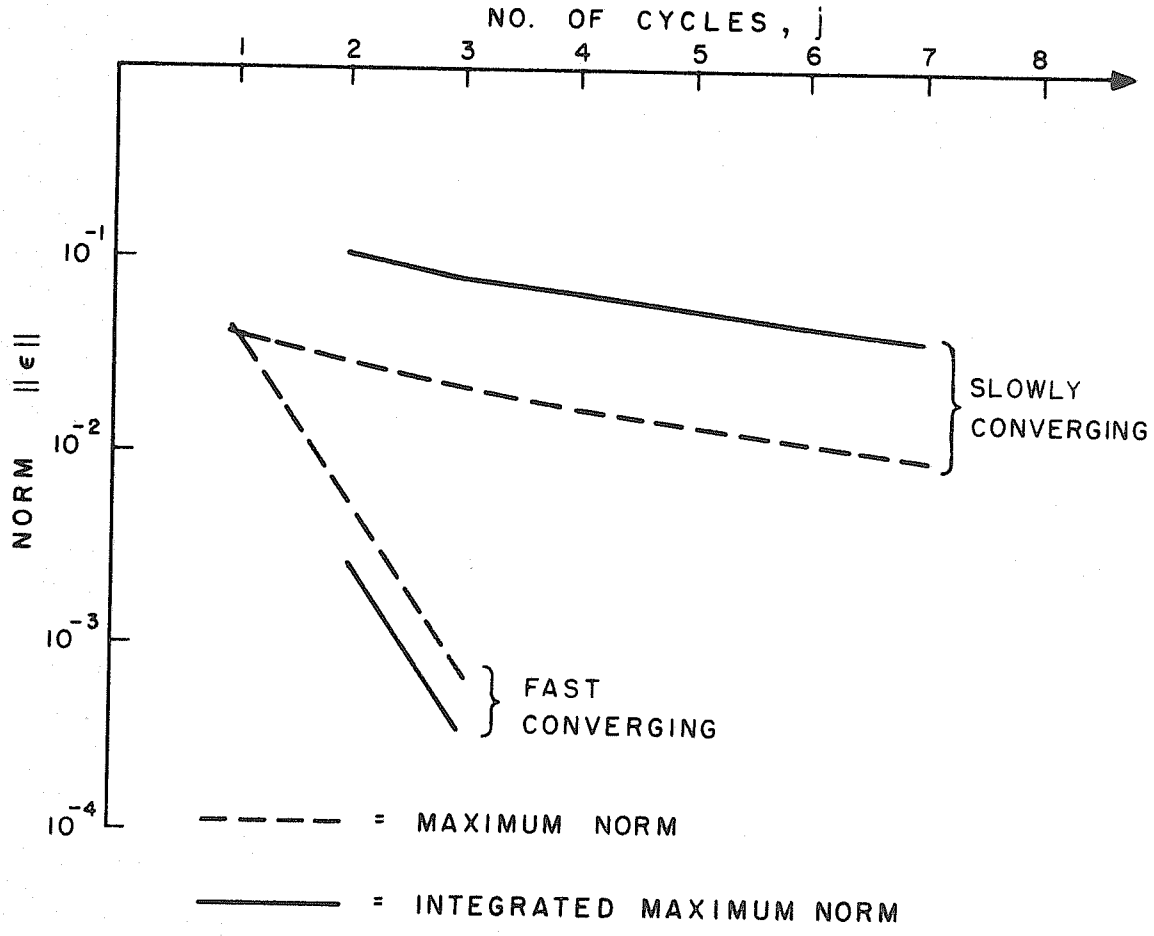

FIG. 5.7 INTEGRATED ERROR NORM

It is also necessary to impose a maximum number of iteration cycles for computer pruposes since there is always a limit on how many cycles can be afforded. Moreover, in the case of buckling, the load-displacement curve is very flat near the buckling load and an exact displacement value (which is hard to obtain) is not needed. Finally, it will be repeated that even the $\|\varepsilon\|$ criteria as defined in Eqs. (5.14), (5.15) and (5.16) are useful and dependable measures of convergence and a bit simpler to use than the integrated norms.

6. COMPUTER STUDIES

6.1 COMPUTER PROGRAMS

In accordance with the previously derived theory, two separate computer programs were developed:

Program A, which handles plate and shallow shell problems accounting for nonlinear geometric effects, and

Program B, which deals with elastic-plastic behavior of plates. The main operations and capabilities of the two programs will be outlined briefly here.

Program A. This program is based on the nonlinear theory for flat and initially deformed plates developed in Chapter 2, combined with the specific finite element approach described in Chapter 3. The linear stiffnesses of all elements are computed once only and stored for later use during load application. Additional nonlinear terms are reformulated when desired, using the simplified interpolation polynomials of Section 3.4.2 and Gaussian quadrature. The derivatives of the interpolation polynomials at the integration points are computed only once. They are efficiently multiplied by nodal point displacements when formulating nonlinear stiffness terms. The incremental stiffnesses and the out of balance forces are thus directly obtained without first having to compute the state of stress within the element.

Having these operations available, a long series of numerical methods are made available in the program to govern the solution procedure. Load increments can be applied in equal steps, using a "load increment factor", automatic load incrementation or by specifying load levels in the input, see Section 5.1.2. Iteration can be performed

as a pure Newton-iteration process or using a simplified approach in which the tangent stiffness is recomputed only for the second iteration cycle. The special method of Section 5.1.4 is also available. Combinations of incremental and iteration methods are allowed for, performing an iteration for every specified number of load increments.

For each load increment, the membrane stresses and the moments are computed at all nodal points. These stress values are taken to be the arithmetic averages between corner values of the adjacent elements. Principal stresses and moments are also computed at all nodal points.

Program B. This program is based on the flow theory of plasticity and the finite element approach to elastic-plastic plate problems, as described in Chapter 4. Program B does not consider geometric nonlinearities. The element stiffnesses for pure bending, pure membrane or a combination of these two states are formulated according to Sections 4.4.1, 4.4.2 and 4.4.3. Only the tangent modulus method is considered. Integration of the stiffness relationships are performed through the thickness as previously described. The external load is automatically scaled so that initial yielding is obtained at the integration point having the highest equivalent stress. Constant load increments being a given ratio of the initial yield load are succeedingly applied to the structure. The computational procedure is terminated when a prescribed number of load steps have been executed or when the equivalent strain at some point exceeds a prescribed maximum value. The experimental curve for the equivalent stress versus the equivalent strain is identified in the input by a set of discretized values. Linear interpolation is performed for intermediate points.

When a new load increment has been applied and the nodal point displacement increments have been evaluated, the corresponding strain increments at all integration points are easily obtained from the interpolation polynomials. Using Eq. (4.47), these strain increments can be separated into an elastic and a plastic part, the elastic strain increment yielding the corresponding stress increment and the new total stresses. If the new state of stress lies outside the current yield surface according to the $\bar{\sigma} - \bar{\varepsilon}$ curve (error due to linearization), the stresses are scaled linearly back to the contour of the yield surface. The new constitutive equations at all integration points are thus found according to Eqs. (4.35) and (4.45). When initial yielding has not occurred or when unloading appears, the constitive equation becomes identical to Hooke's Law. Also, new A- matrices (Eq. (4.48)) for all integration points are computed and stored to be used for the next load step.

The state of stress including principal stresses are printed at all integration points where yielding has occurred and also all elastic points adjacent to the surfaces on the elastic-plastic boundaries. In many cases it is convenient to suppress some of the printing, for instance, printing of stresses may be executed only every third load step.

6.2 NONLINEAR GEOMETRIC EFFECTS

6.2.1 Simply Supported Platestrip Subjected to Uniform Pressure

To check the accuracy of the theory derived here, some comparisons will be made with other solution methods. The first case to be considered is cylindrical bending of a uniformly loaded, simply

supported plate strip. A closed form solution to this problem was given by Timoshenko [45]. Numerical values according to his solution were obtained utilizing the computer and the "successive substitution" iteration technique*.

The same geometry and material properties as used by Murray [19, 20] were chosen. Due to the inplane restraining of the sides and the relatively small thickness, this system is extremely nonlinear. Half the plate was divided into 2 and into 4 elements, see Figure 6.1. The load was applied in 5 steps only from 0 to 5000 psi, using a load increment factor of 1.25 (see Section 5.1.2). Newton iteration was performed at each load level.

The transversal load versus the midspan deflection is shown in Fig. 6.1, whereas the curves for the membrane and bending stresses are given in Fig. 6.2. It is interesting to note that the results continue to improve the further beyond the linear range the load is applied. For instance, the midpoint deflection values are 5.0 and 1.3 percent off in the linear range for 2 and 4 elements, respectively, while the errors are only 3.0 and 0.3 percent for 5000 psi. It is also remarkable that even 2 elements yield quite good results.

6.2.2 Simply Supported Square Plate Subjected to Uniform Pressure

The next example to be considered is a simply supported square plate subjected to uniform transversal load. The edges are restrained against movement perpendicular to the boundary, thereby

---

* Eq. (8), page 8 in Reference [45] was solved using successive substitutions.

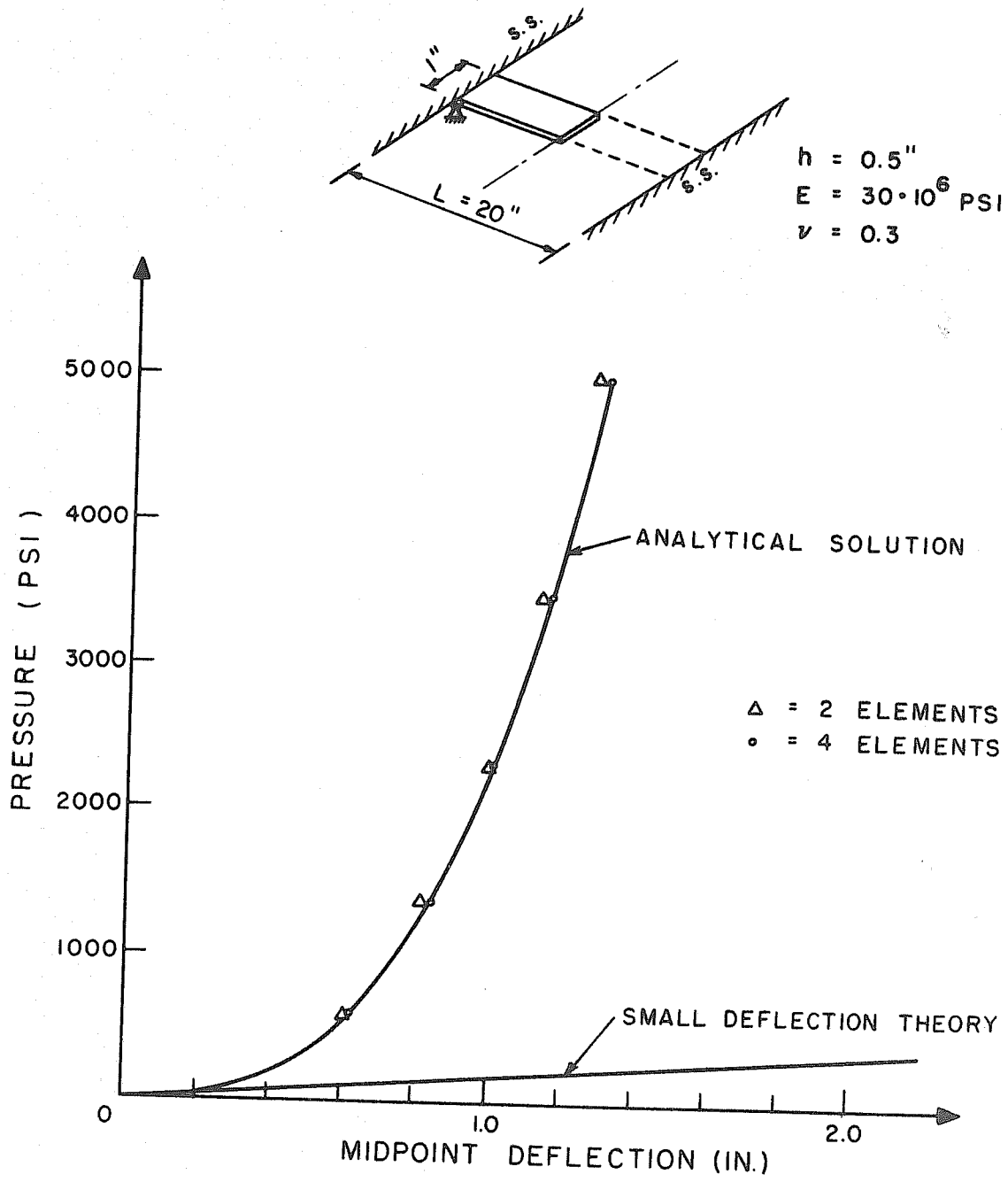

FIG. 6.1 MIDPOINT DEFLECTION OF PLATESTRIP

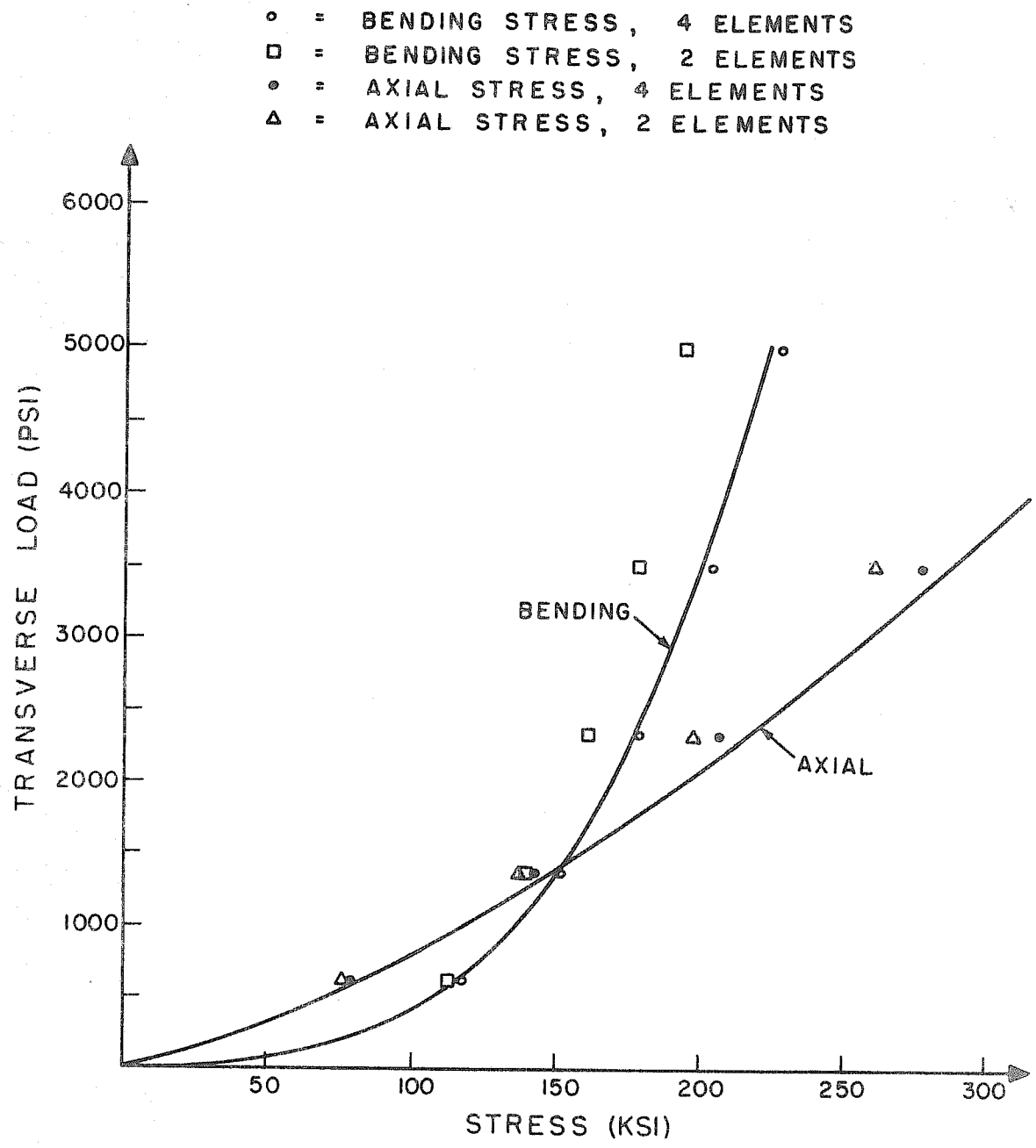

FIG. 6.2 AXIAL AND BENDING STRESSES FOR PLATESTRIP

allowing buildup of membrane forces. This case has previously been studied by Levy [7], who used the von Karman large deflection differential equations for plates and trigonometric series expansions.

The plate is assumed to be 16 by 16 inches and 0.1 inches thick. Youngs modulus is 30×10^6 psi and, as chosen by Levy, Poisson's ratio is 0.316 ($=\sqrt{0.1}$). The normal pressure is applied in 6 steps from 0 to 15 psi, the two first load increments being 1.5 psi and the rest 3.0 psi. A Newton-iteration is performed at each load level. Because of symmetry properties, only one quarter of the plate need to be considered, and it is divided into a 4 by 4 finite element mesh.

The results are compared against those obtained by Levy [7]. Figure 6.3 shows the load plotted against the midpoint deflection while Figures 6.4 and 6.5 show membrane and bending stresses, respectively. The discrepancy between the deflection values are very small, in fact less than 1 percent. However, the bending stresses of Fig. 6.5 are nearly 10 percent lower than Levy's results. Here, it should be noted that Levy's solution cannot be considered as being "exact" since only 6 nonzero terms of the trigonometric expansion were considered by him. Even though his deflection values allegedly are within 1 percent of the true solution, the error of the bending stresses, being functions of the second derivatives of the deflection, may probably amount to several percent. Further, almost identical bending stresses to those obtained here were reported by Murray [19, 20] who used a quite different finite element approach.

This case was also tested using a 2 by 2 finite element mesh. The deflection values were still less than 5 percent off while the computed bending moment were substantially too low.

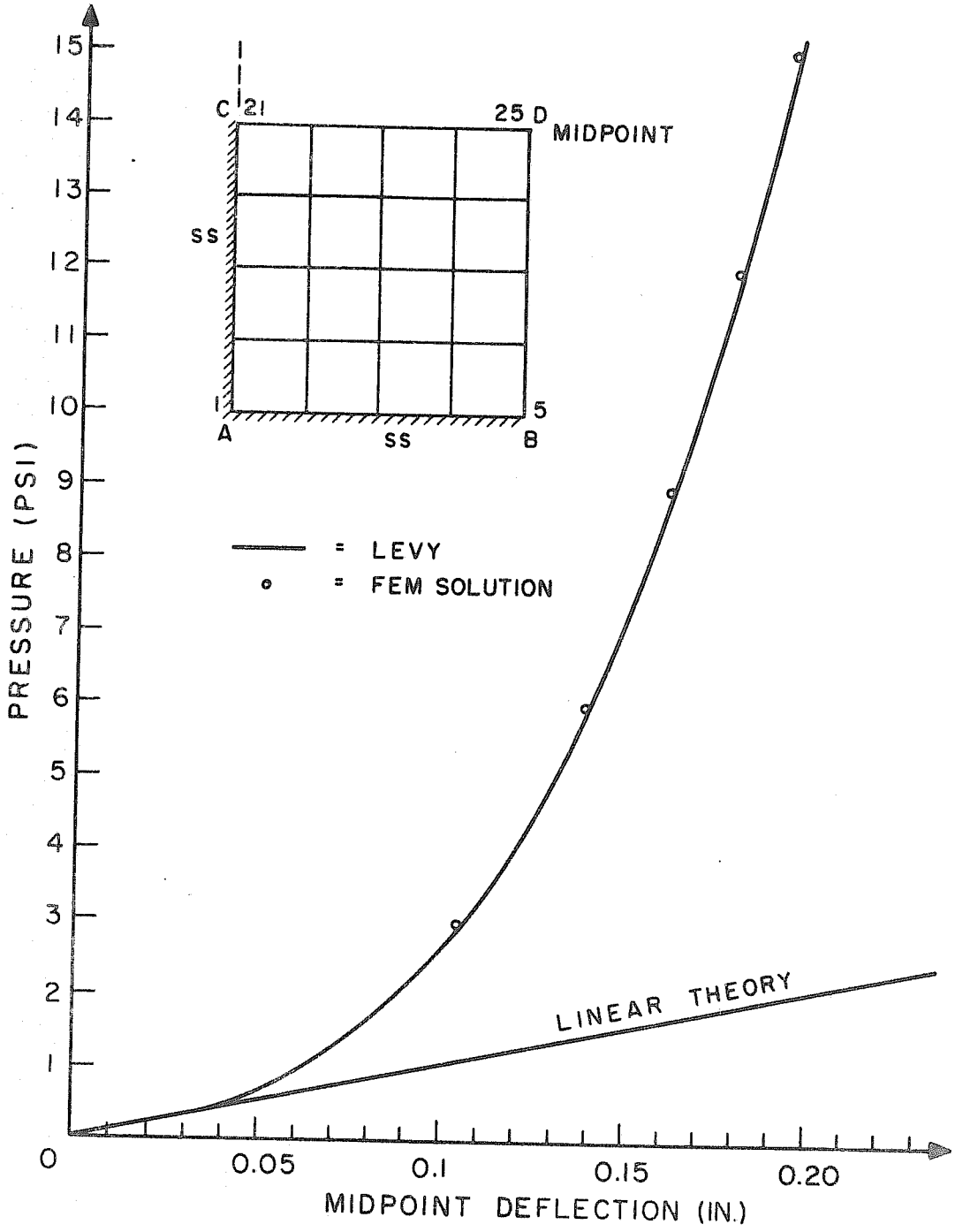

FIG. 6.3 LOAD-DEFLECTION CURVE FOR SQUARE PLATE

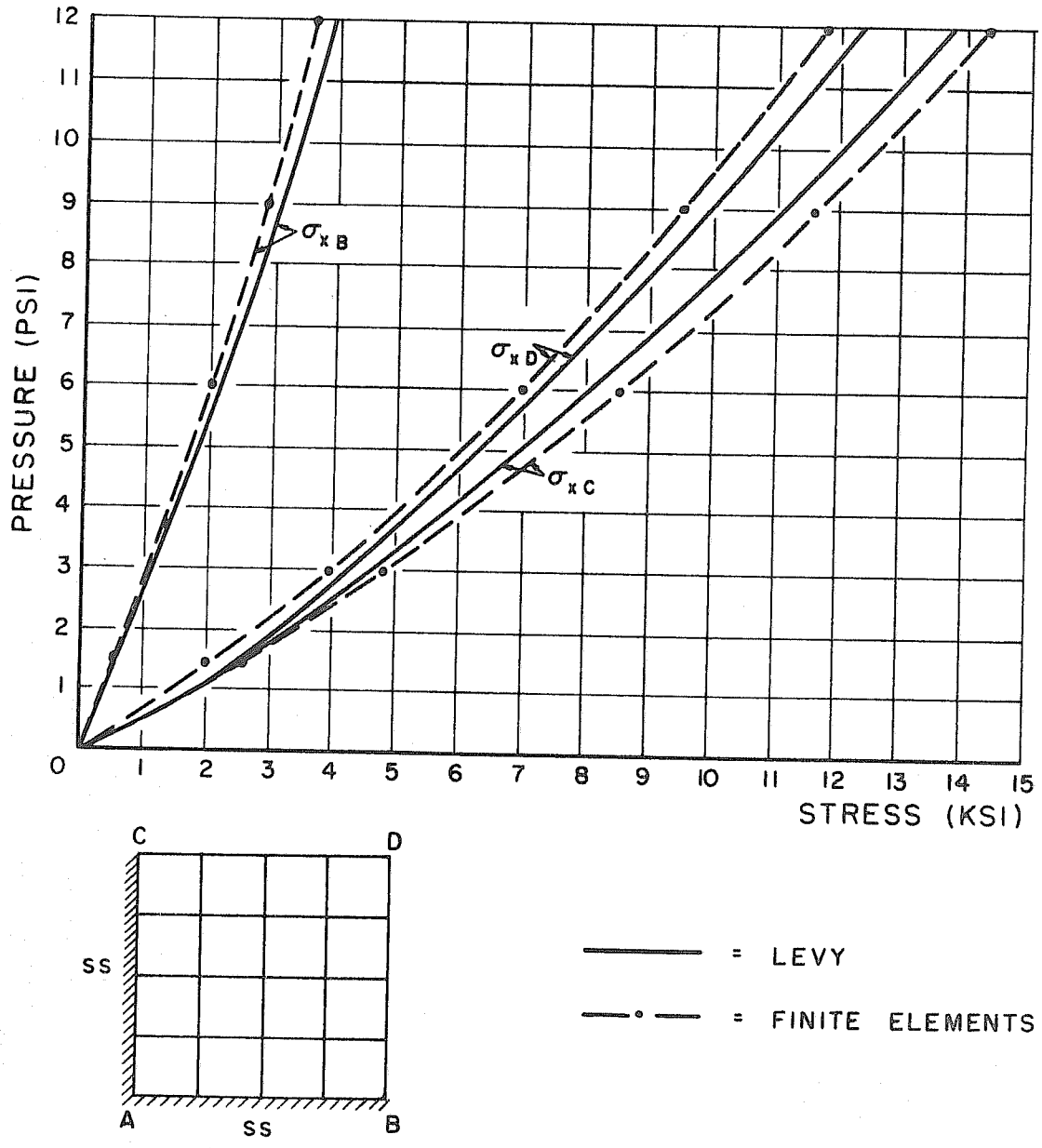

FIG. 6.4 MEMBRANE STRESSES FOR SQUARE PLATE

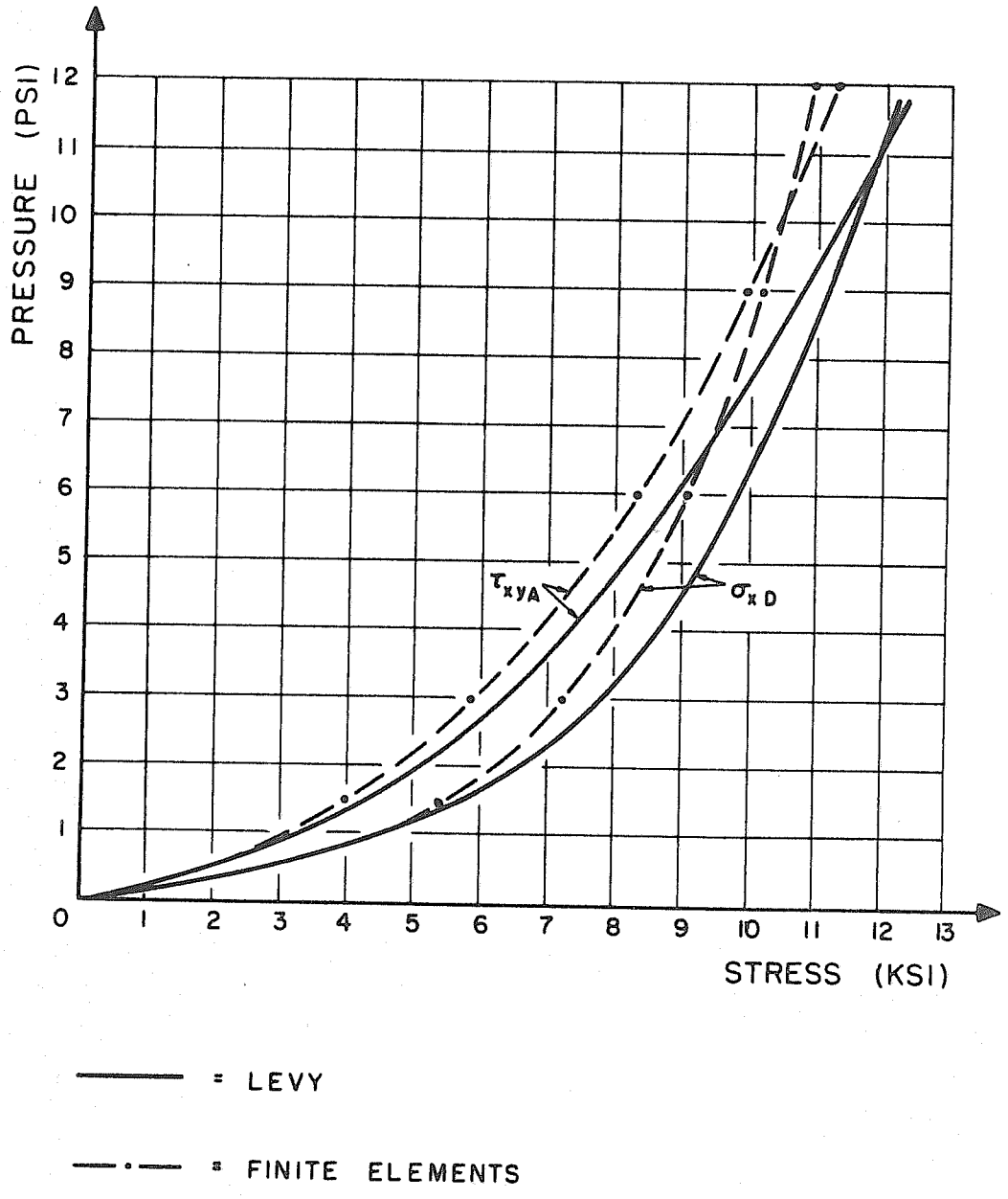

FIG. 6.5 SURFACE STRESSES DUE TO BENDING FOR SQUARE PLATE

Several interesting points are revealed by the numerical results. For instance, the deflected shape changes during load application, it becomes relatively more flat in the central region of the plate for higher load levels. This again implies that the maximum bending moments move away from the midpoint of the plate during increasing pressure. At a pressure of 15 psi the maximum M_x-moment is located at the midpoint between C and D, as shown in Fig. 6.3. As seen from Fig. 6.4, the maximum membrane stresses occur at point B and C, and not at the midpoint D. For p = 15 psi, the maximum principal surface stresses (= 28.4 ksi) appear at midpoints between C and D, and between B and D.

6.2.3 Postbuckling Behavior of Uniaxially Compressed Plate

A simply supported square plate which is uniformly compressed in one direction will now be considered, see Fig. 6.6. The geometric and elastic properties are chosen to be the same as those of the preceding example. The critical stress for linearized buckling of a square plate is [107]

$$\sigma_{x\,cr} = \frac{4\pi^2 D}{a^2 h} \tag{6.1}$$

Substitution of numerical values yields $\sigma_{x\,cr} = 4.28$ ksi.

The main attention will here be concentrated on the post-buckling behavior of the plate since such plates have considerable stiffness and carrying capacity after the so-called "critical load" has been reached. Also this case has been studied by Levy [7] who used the von Karman differential equations for plates and trigonometric series expansions. Before him, several investigators studied post-buckling of plates by more approximate methods [5, 108].

The plate is here analyzed by dividing one quarter of the plate into a 3 by 3 finite element mesh. The compression is imposed by displacing side ACA' (Fig. 6.6) as a straight line. Side AB is allowed to move freely in the plane of the plate.

Fig. 6.8 shows the midpoint deflection as a function of the average compression stress. The average stress was computed by averaging the integrated resulting stresses. A sharp transition of behavior is observed at the "critical" load. The result obtained by Levy [7] is also shown in the figure. The discrepancy between the two curves in the post-buckling zone is due to the different boundary conditions along AB. The finite element computation allows this side to warp freely, whereas the Levy solution forces it to remain a straight line, thereby causing a stiffer system. The finite element solution is again very close to the results reported by Murray [19, 20] who used the same type of boundary conditions as employed here. As pointed out in [19], if inplane displacements normal to boundary AB are restrained, the "buckling load" will be greatly reduced due to the Poisson's ratio effect, whereas the system will become stiffer further out in the post-buckling domain.

Fig. 6.9 demonstrates how the membrane stress-distribution is altered after the "critical" stress has been exceeded. The carrying capacity near the axis CB is strongly reduced whereas the boundary region near AB takes a much larger fraction of the load. Finally, Fig. 6.7 shows the midpoint deflection against the edge compression, assuming that axis BD does not displace in the x-direction. This diagram can easily be combined with Fig. 6.8, yielding the relationship between the average stress and the edge compression.

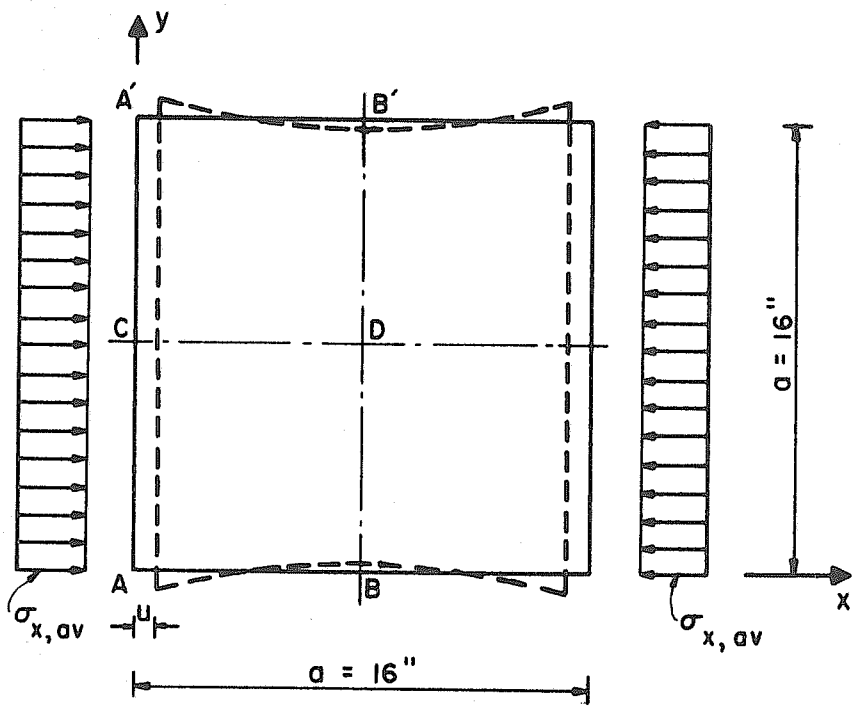

FIG. 6.6 COMPRESSION OF SQUARE PLATE

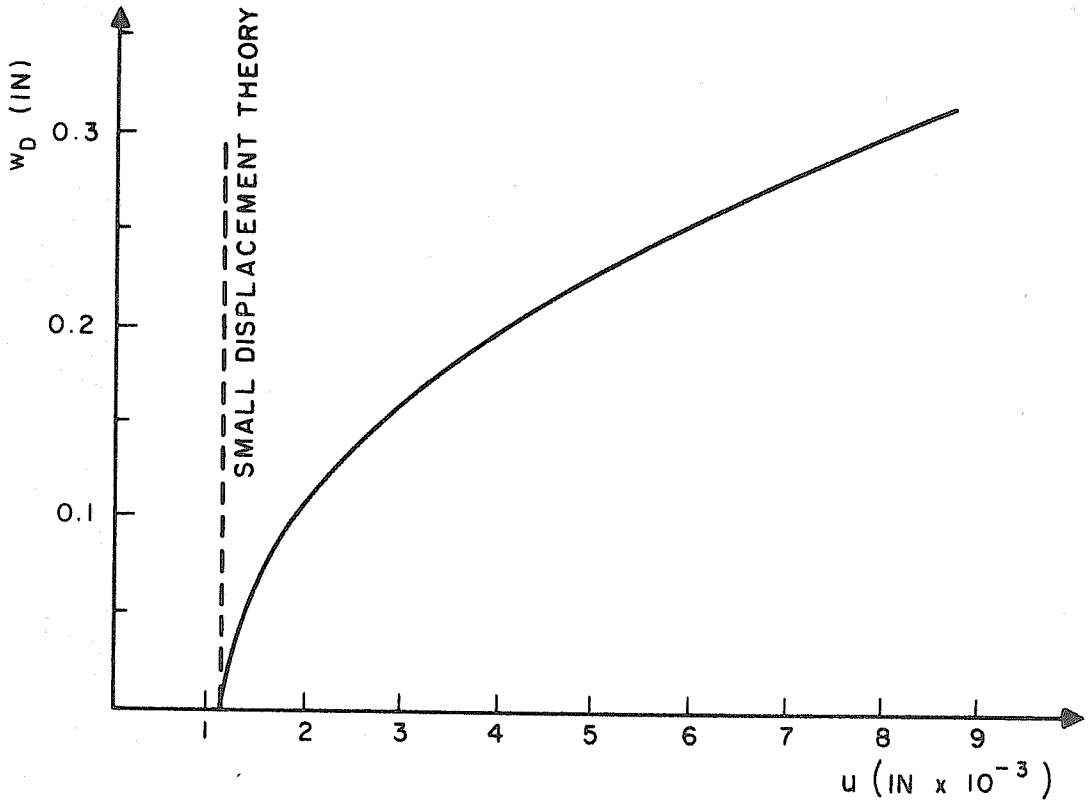

FIG. 6.7 MIDPOINT DEFLECTION VS EDGE DISPLACEMENT

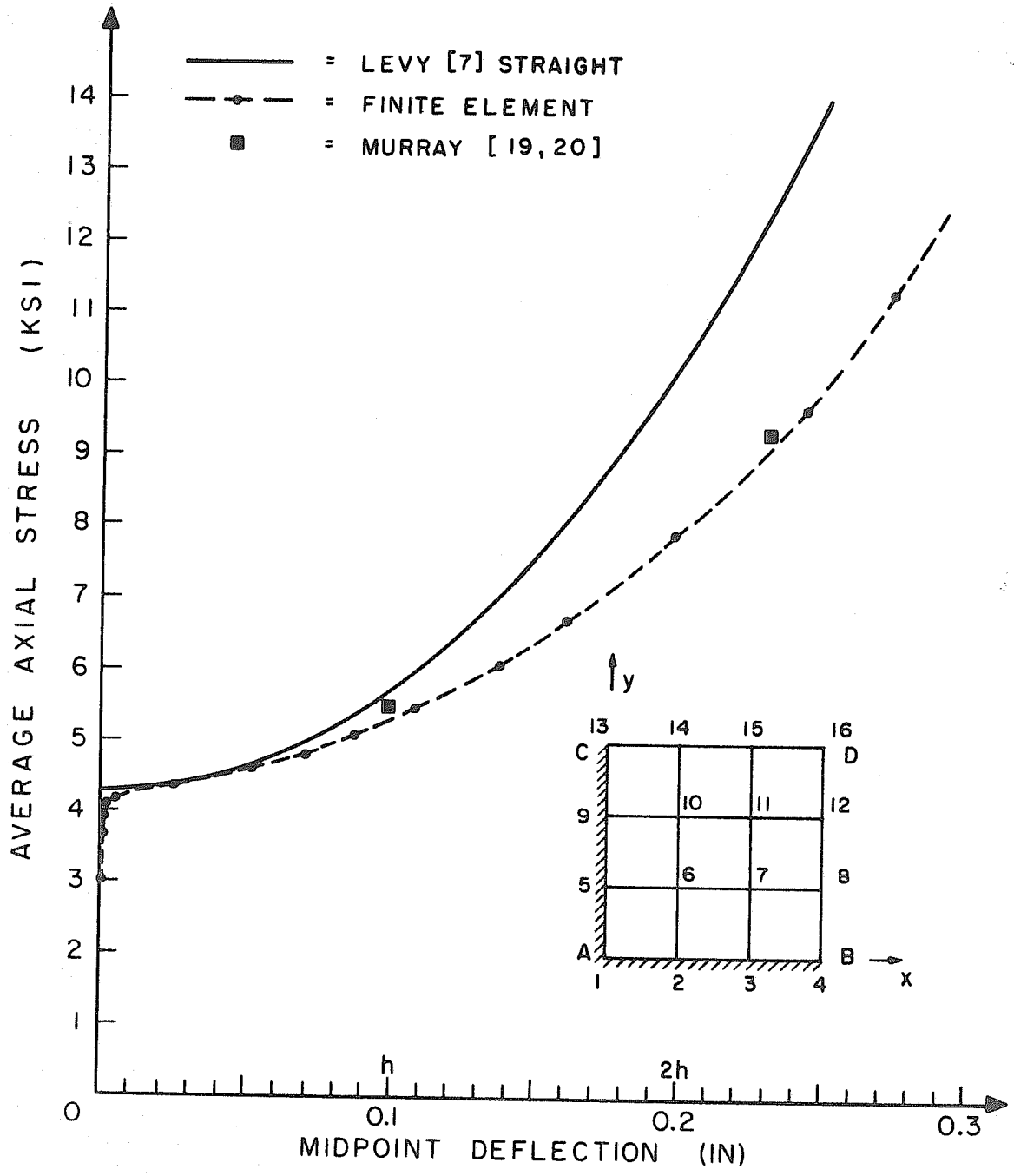

FIG. 6.8 MIDPOINT DEFLECTION

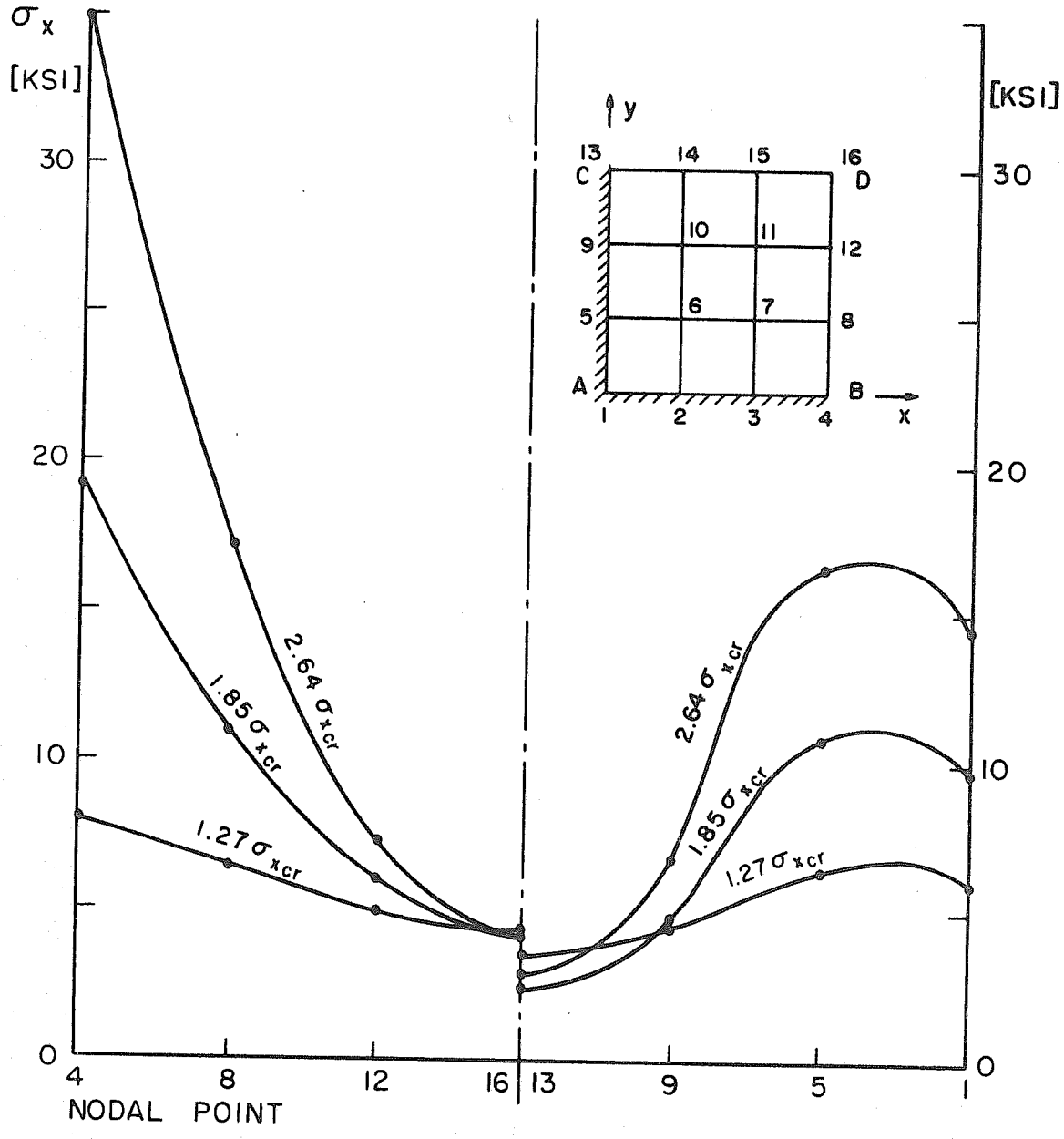

FIG. 6.9 DISTRIBUTION IN PLATE AFTER BUCKLING
($\sigma_{x,\,AVERAGE} = 1.27\,\sigma_{x_{cr}}, 1.85\,\sigma_{x_{cr}}, 2.64\,\sigma_{x_{cr}}$)

It is worth noting that division of the quarter of the plate into only a 2 by 2 mesh yields results within a few percent of what was obtained with the 3 by 3 mesh.

6.2.4 Postbuckling Behavior of Square Plate Subjected to Pure Shear

A simply supported square plate subjected to pure shear will be considered. The critical shear stress for linearized buckling is [107]

$$\tau_{cr} = 9.34 \frac{\pi^2 D}{a^2 h} = 8.44 \frac{E h^2}{a^2}$$

where a is the side length and assuming $\nu = 0.3$. Choosing $E = 6.4 \times 10^4$, $a = 1000$ and $h = 12.5$, the multiplying factor is set equal to unity and hence $\tau_{cr} = 8.44$.

The plate is idealized by a 3 by 3 finite element mesh. The choice of boundary conditions is essential for postbuckling behavior. Fig. 6.10 shows the deflections obtained for pure force (stress) boundary conditions; that is, the consistent nodal point forces along the boundaries are increased proportionally during load application. It is seen from the deflection plots that the initial buckling shape is symmetric about both the compression and the tension diagonal. However, at about two times the critical load, the buckled shape changes quite drastically. The shape no longer remains symmetric about the tension diagonal, whereas symmetry about the compression diagonal is retained.

This behavior can roughly be explained by considering the compression diagonal of the plate as a "beam on elastic foundation" subjected to compression. The elastic support is furnished by second order effects of the tension stresses perpendicular to the compression diagonal. This "foundation" becomes increasingly stiff as the

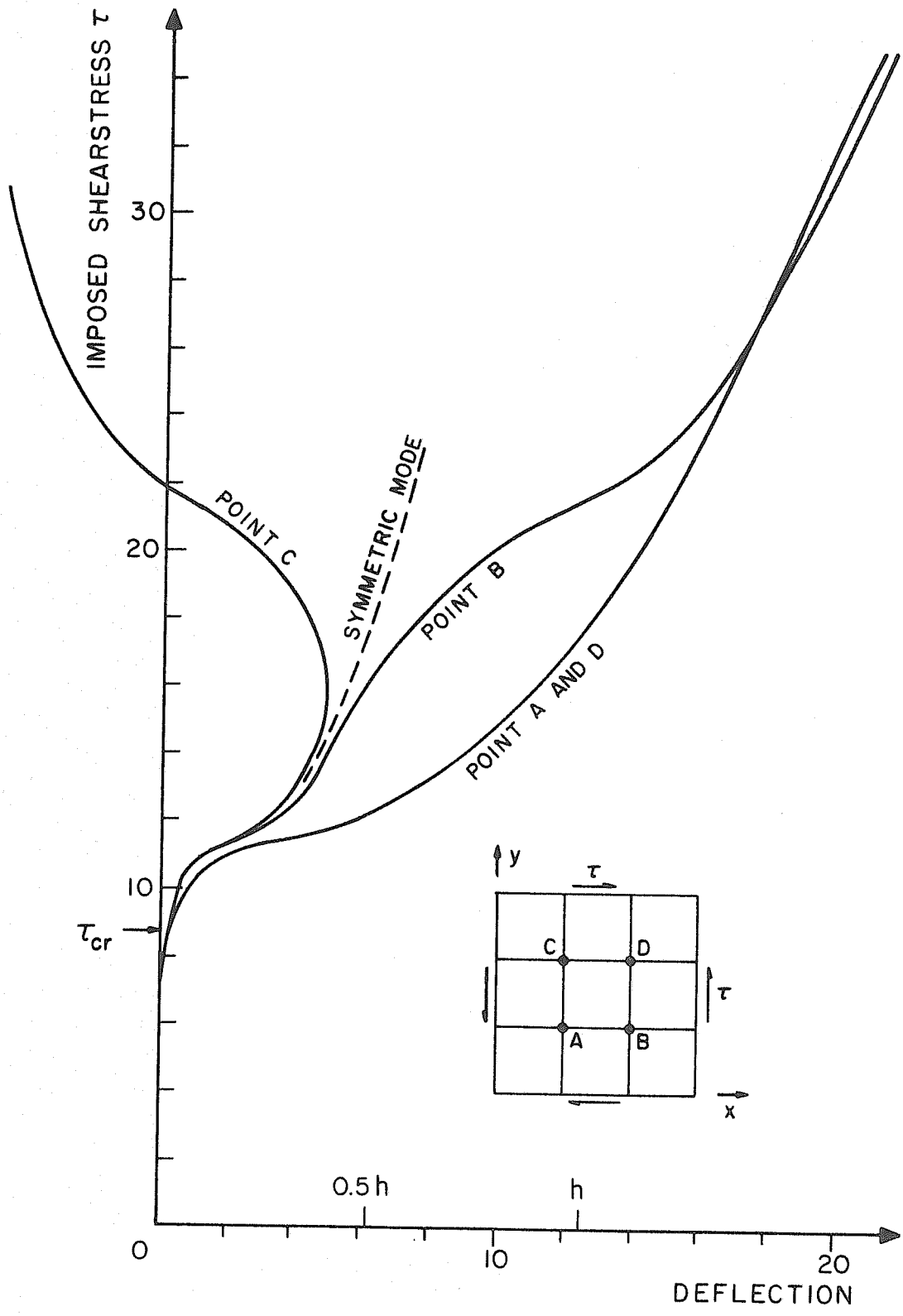

FIG. 6.10 POST-SHEAR BUCKLING OF SQUARE PLATE

deformations increase. It is expected that the plate would exhibit even higher modes when increasing the load further. This kind of post-buckling behavior where wrinkles occur along the compression diagonal has been observed experimentally for very thin plates and the ultimate shear strength of such plates can be estimated using a "diagonal tension" method [107].

The same kind of behavior as shown in Fig. 6.10 was also obtained by imposing pure displacement boundary conditions on the plate so that a rhombic shape of the plate was maintained during deformation. The parallel sides were not allowed to move closer to each other, hence high tension stresses in x and y directions were gradually built up. For these reasons, the deflections obtained were smaller than for the force boundary conditions (roughly 2/3). A 4 by 4 mesh revealed the same general behavior as the 3 by 3 idealization, the results are not shown here because of unfavorable locations of the nodal points with respect to the deflected shape.

6.2.5 Snap-Through of Initially Deformed Plates

The case of initially deformed plates subjected to uniform pressure will now be studied. When the pressure is applied to the convex side of the plate and if it is given a sufficiently large initial deformation, this case constitutes a very interesting problem due to the sudden loss of transversal stiffness of the plate during load application. This type of problem which usually is termed "snap-through", has been extensively studied for the cases of arches and shallow caps [109 -112]. Seemingly, no similar study has previously been performed for general rectangular plates.

A simply supported square plate of the same geometry as previously given in Section 6.2.2, and with edges restrained against inplane movement perpendicular to the plate boundary, will now be studied. As shown in Fig. 6.11, one quarter of the plate is idealized by a 3 by 3 finite element mesh. Both the cases of loading on the convex and on the concave sides as illustrated in Fig. 6.12, will be examined, assuming the initial deflection at the midpoint of the plate to be one and two times the plate thickness. Thus a total of four cases of initial deformation will be considered: $\delta = \pm h$ and $\delta = \pm 2h$. But first the initial shapes are computed as separate problems by giving the displacement δ at the midpoint of the plate and calculating the corresponding elastic shapes. These shapes are later used as input for the initially deformed plates.

The load-deflection curves resulting from the four different cases are plotted in Fig. 6.13. It is seen that even small initial deformations increase the stiffness of the plate substantially when the pressure is applied to the concave side. On the other hand, reduction of the initial stiffness concluding with a sudden "snap" is observed for the $\delta = - h$ and $\delta = - 2h$. In all these cases, the load was applied incrementally with "true" Newton iteration at each load level. For the two cases in which snap occurred, the iteration converged to the second branch of the curve when the pressure was increased above the snap-load. Some difficulties were encountered in obtaining convergence for loads just slightly higher than the snap-load, however, convergence to the second branch was easily obtained after additional load incrementation.

The case in which $\delta = -2h$ was tested for a full load cycle, see Fig. 6.14. The pressure was first increased to + 15 psi, afterwards it was reduced to - 15 psi, thereby obtaining a sort of "hysteresis" loop. The load increments are numbered in the figure thereby demonstrating how the load was applied. A 2 by 2 mesh idealization was utilized for one quarter of the plate, thereby reducing the required computer time. The discrepancy between the results obtained in this manner compared to those obtained with the 3 by 3 mesh were in general very small although the coarser mesh gave a 10 percent higher snap-load.

Figure 6.14 does also furnish a good test of the method. The load-deflection curve for $\delta = +2h$ (pressure on concave side) is also plotted in the same figure. However, it is displaced by $4h$ from the origin corresponding to a complete inversion of the initial shape. The discrepancy between this curve and the second branch of the snap-curve is merely additional flexural bending stiffness associated with the deformation of the initial shape during the snap. The snap-curve does correctly lie above the "displaced" curve. These two curves would in the limit coincide if the thickness of the plate were reduced to zero.

When the ratio δ/a is large, the entire plate should be considered for the snap-through analysis, although the problem seemingly is a doubly symmetric one. This is due to the fact that an unsymmetric buckling configuration gives a lower critical load. This phenomenon is hard to observe experimentally because the snap happens extremely fast and the shape is symmetric both before and after the buckling has occurred. This general unsymmetric case can be handled readily by the

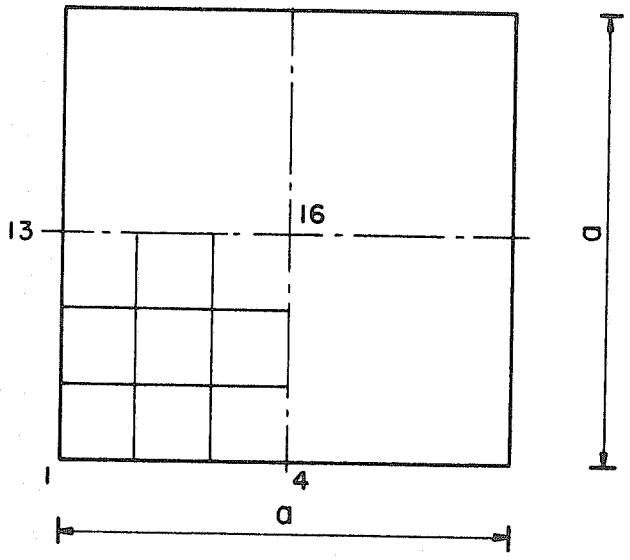

a = 16"
h = 0.1"
E = 30×10^6 psi
ν = 0.316

FIG. 6.11 FINITE ELEMENT IDEALIZATION

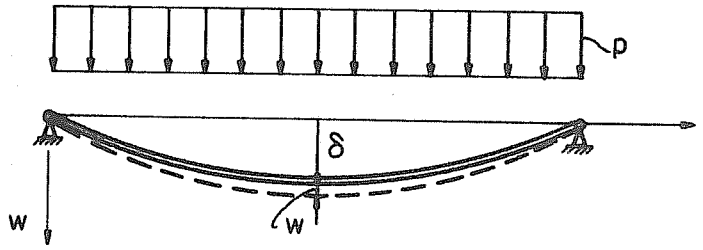

$\delta > 0$

a) PRESSURE ON THE CONCAVE SIDE

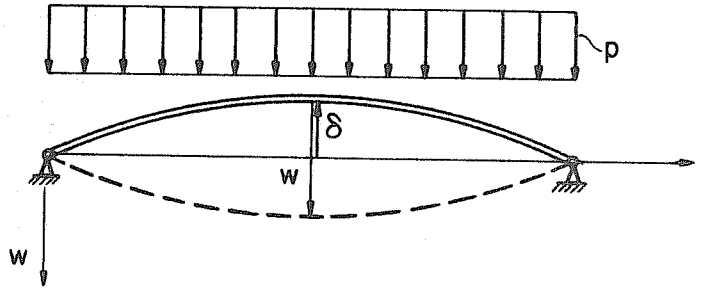

$\delta < 0$

b) PRESSURE ON CONVEX SIDE

FIG. 6.12 LOADING ON INITIALLY DEFORMED PLATE

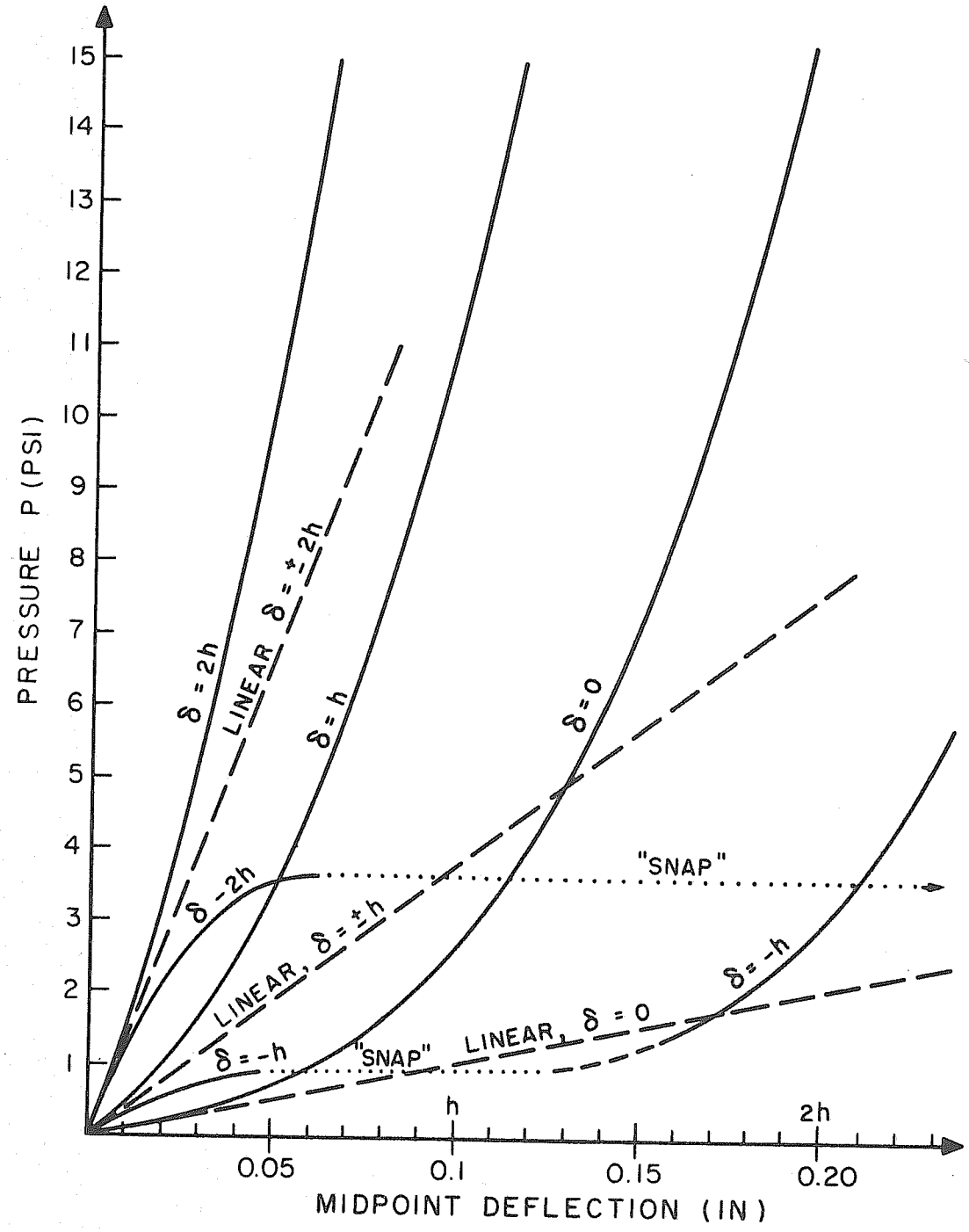

FIG 6.13 LOAD-DEFLECTION CURVES FOR INITIALLY DEFORMED SQUARE PLATE

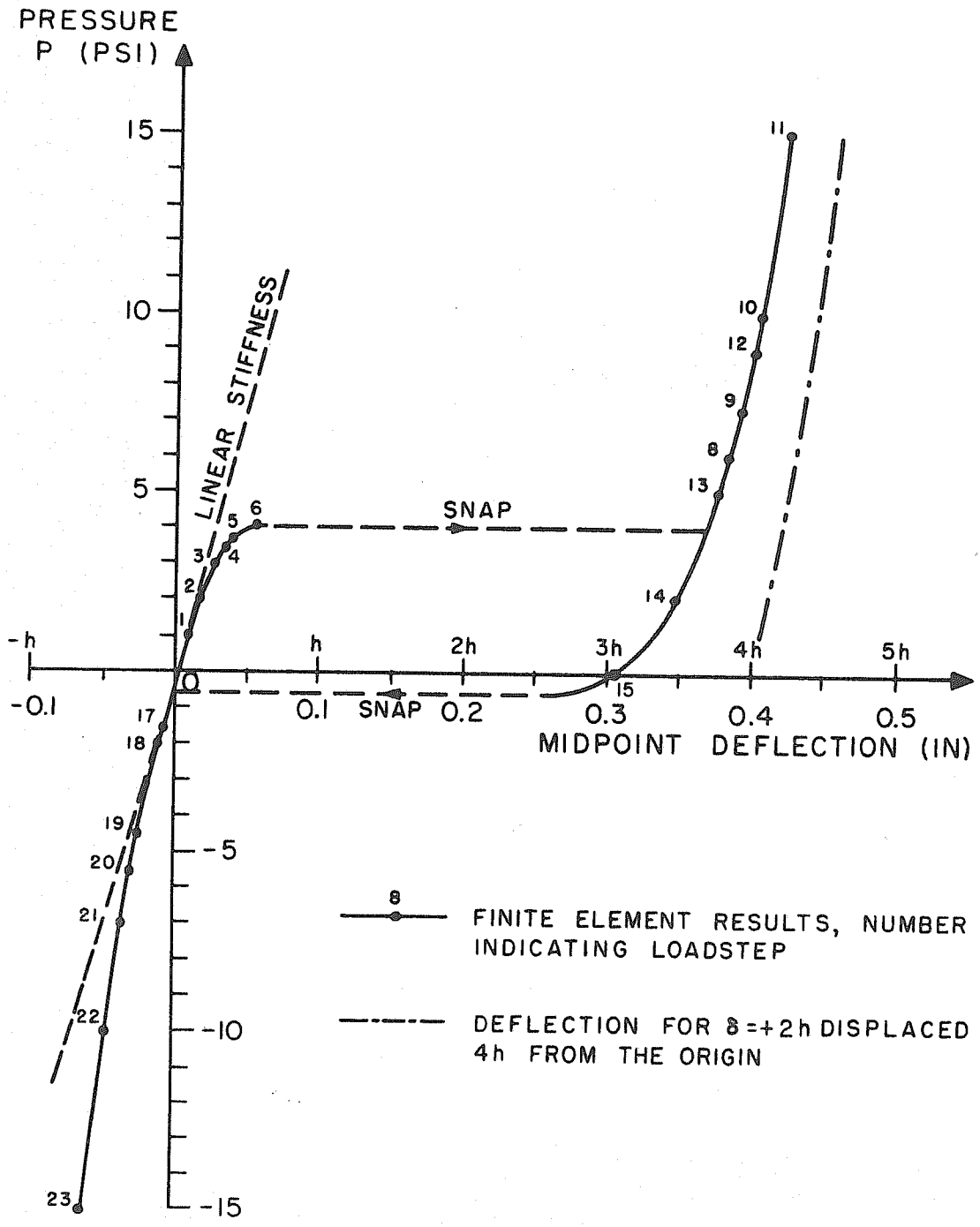

FIG. 6.14 DEFLECTION-CURVE FOR FULL LOADCYCLE, $\delta = -2h$, 2 x 2 MESH

present method; only a small, unsymmetric perturbation in the loading must be added to enable the analysis to achieve the unsymmetric mode.

Initially deformed plates or shallow shells open interesting perspectives for new designs. Such plates have increased stiffness and stress computations reveal that the maximum stresses are substantially reduced due to the altered initial shape. When the loading is applied to the concave side of initially deformed plates, no stability problems are encountered and the plates are greatly improved from a structural point of view. Deformed plates for which snap may occur also have the same favorable characteristics, but a more thorough analysis is required to avoid buckling. A "tool" for such analysis is now available, and the use of shallow rectangular shells should be given serious consideration in many designs for which plane surfaces are not a requirement.

6.3 ELASTIC-PLASTIC PROBLEMS

6.3.1 The Elastic-Plastic Beam

To demonstrate the accuracy and capabilities of the methods described in Chapter 4, a simply supported beam with rectangular cross-section and subjected to a uniform transversal load will be considered. Assuming an elastic-perfectly plastic material and a uniaxial state of stress in the beam, a closed-form solution to this problem was given by Prager and Hodge [23]. Denoting the uniaxial yield stress by σ_{yield} and choosing

$$p_o = 4\sqrt{3}\, k_o b = 4\sigma_{yield}\, b \tag{6.2}$$

as a reference load, a nondimensional loading parameter ρ can be defined by

$$\rho = \frac{P}{P_o}\left(\frac{a}{t}\right)^2 \tag{6.3}$$

where p is the actual load per unit length of the beam. The geometric dimensions of the beam are defined in Fig. 6.15. ρ is chosen such that it is identical to 1 for the ultimate load. The midpoint deflection of the beam will also be described in a nondimensional form making use of the deflection of the initial yielding load

$$W_o^* = \frac{5}{48}\,\frac{P_o a^2}{Ebt} \tag{6.4}$$

The ratio of W_o/W_o^* thus describes the actual midpoint deflection. The load-deflection curve given by Prager and Hodge is shown in Fig. 6.18.

The numerical computations will be based on the plate bending element of Section 4.4.1 and the membrane element of Section 4.4.2. The Poisson's ratio is equal to zero and for simplicity $\sigma_{yield} = 100$.

Plate Bending Elements. The following numerical properties are chosen

$$a = 20, \quad b = 1, \quad t = 1$$

$$E = \frac{5}{3} \cdot 10^4$$

thus leaving $\rho \equiv p$ and $W_o^* = 1$. As shown in Fig. 6.15, half of the beam is divided into 4 equal elements and a 11 point integration scheme through the entire thickness is employed.

Membrane Elements. For this case, a slightly different geometry is chosen

$$a = 10, \quad b = 1, \quad h = 1$$

$$E = \frac{5}{12} \cdot 10^4$$

still yielding $\rho \equiv p$ and $W_o^* = 1$. As shown in Fig. 6.15, 10 equal elements are used to model one quarter of the total beam. It turns out that for this geometry, the decreased stiffness due to the integration scheme using the subtriangle centroids very well balances the overestimated stiffness due to the displacement expansion used for the element.

The results obtained using the two different types of elements are shown in Fig. 6.16. Constant load increments equal to 3 percent of the initial yield load were applied up to the collapse load. The results seem highly satisfactory, the divergence from the true curve is mainly due to the truncation error caused by linearization. As for purely elastic problems, the bending elements are in general more fit for bending type problems like a beam than the membrane elements. However, it is reassuring to observe that the membrane elements are equally accurate in the plastic as in the elastic range.

The locations of the elastic-plastic boundary in the beam for different load levels have also been given in Reference [23]. Comparisons with the numerical results for the bending and the membrane elements show very good correlations in both cases.

Bilinear Material. The plate bending elements were also tested for a bilinear material for which the tangent modulus

$$E_T = 0.25\ E$$

after the initial yield stress has been reached. All other properties were kept the same as for the elastic-perfectly plastic beam. The stress distribution through the thickness of the plate near the midpoint is shown $\rho = 0.667$ and $\rho = 0.984$ in Fig. 6.17. The load-deflection curve for the same beam is plotted in Fig. 6.16 and can be compared with the curve obtained for an elastic-perfectly plastic material.

Combined Bending and Axial Load. Finally, a case of combined bending and axial deformation will be studied, using the element derived in Section 4.4.3. Keeping the same geometry and material properties as for the case of pure bending using plate bending elements, an axial force N where

$$N = \frac{3}{2} \frac{pa^2}{h} = 600\, p$$

is applied to the beam. For this ratio between the transverse and axial load, 50 percent of the maximum stress at the onset of yielding is due to bending, the other 50 percent is due to axial deformation. The transverse and the axial loading are increased proportionally after yielding has occurred, the load steps being 1.5 percent of the initial yield load ($p_o = 0.33$, $N_o = 200$). An analytical calculation reveals that the ultimate capacity of the cross-section is reached for $p = 0.48$ and $N = 288$. The neutral axis is then located at the distance 0.279 from the free surface, see Fig. 6.18.

The computed stresses for $p = 0.333$ and $p = 0.412$ are also plotted in the same figure. It turns out that this case becomes rather unstable for higher loads since small load increments result in large changes in deformation and stress pattern. Indeed, infinite deformations are required to obtain the theoretical collapse stress

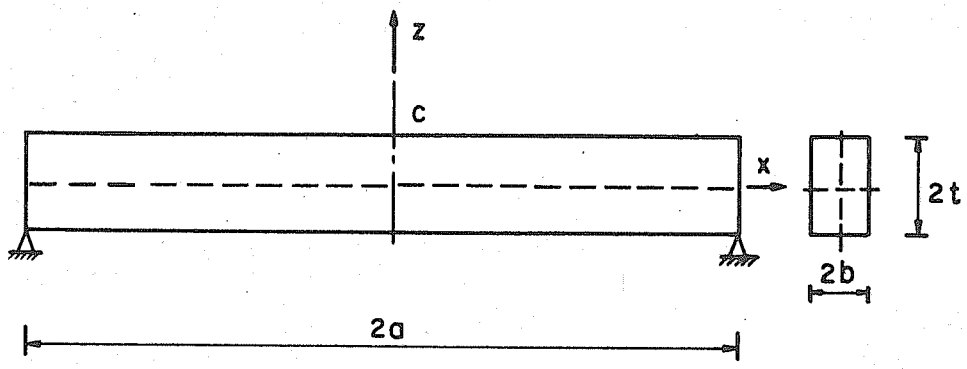

GEOMETRY OF BEAM

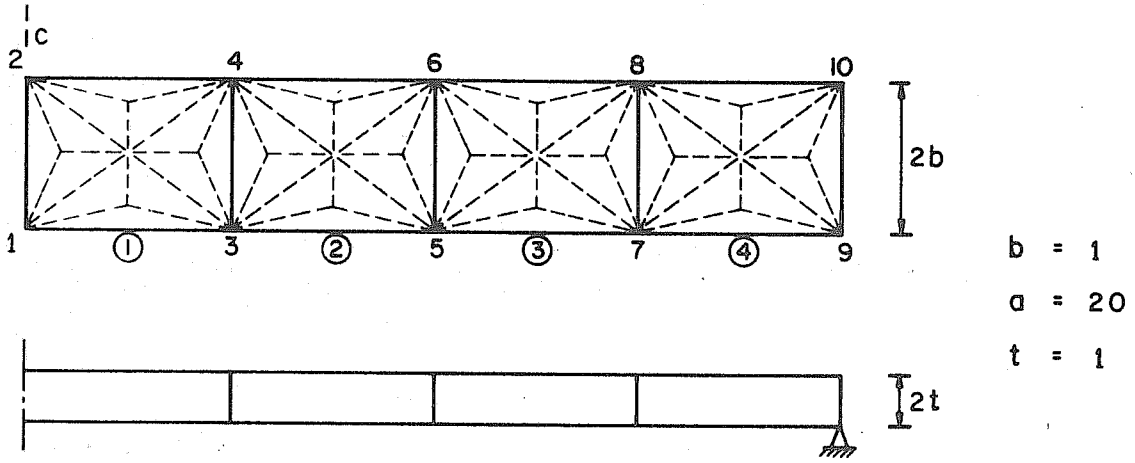

PLATE BENDING ELEMENT IDEALIZATION (1/2 BEAM)

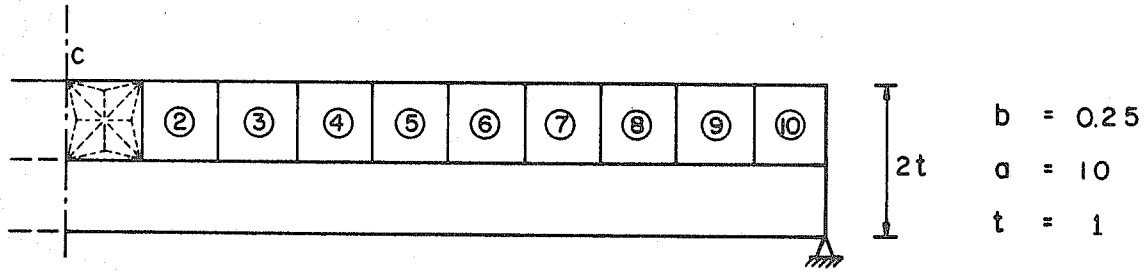

MEMBRANE ELEMENT IDEALIZATION (1/4 BEAM)

FIG. 6.15 FINITE ELEMENT IDEALIZATION FOR ELASTIC PLASTIC BEAM

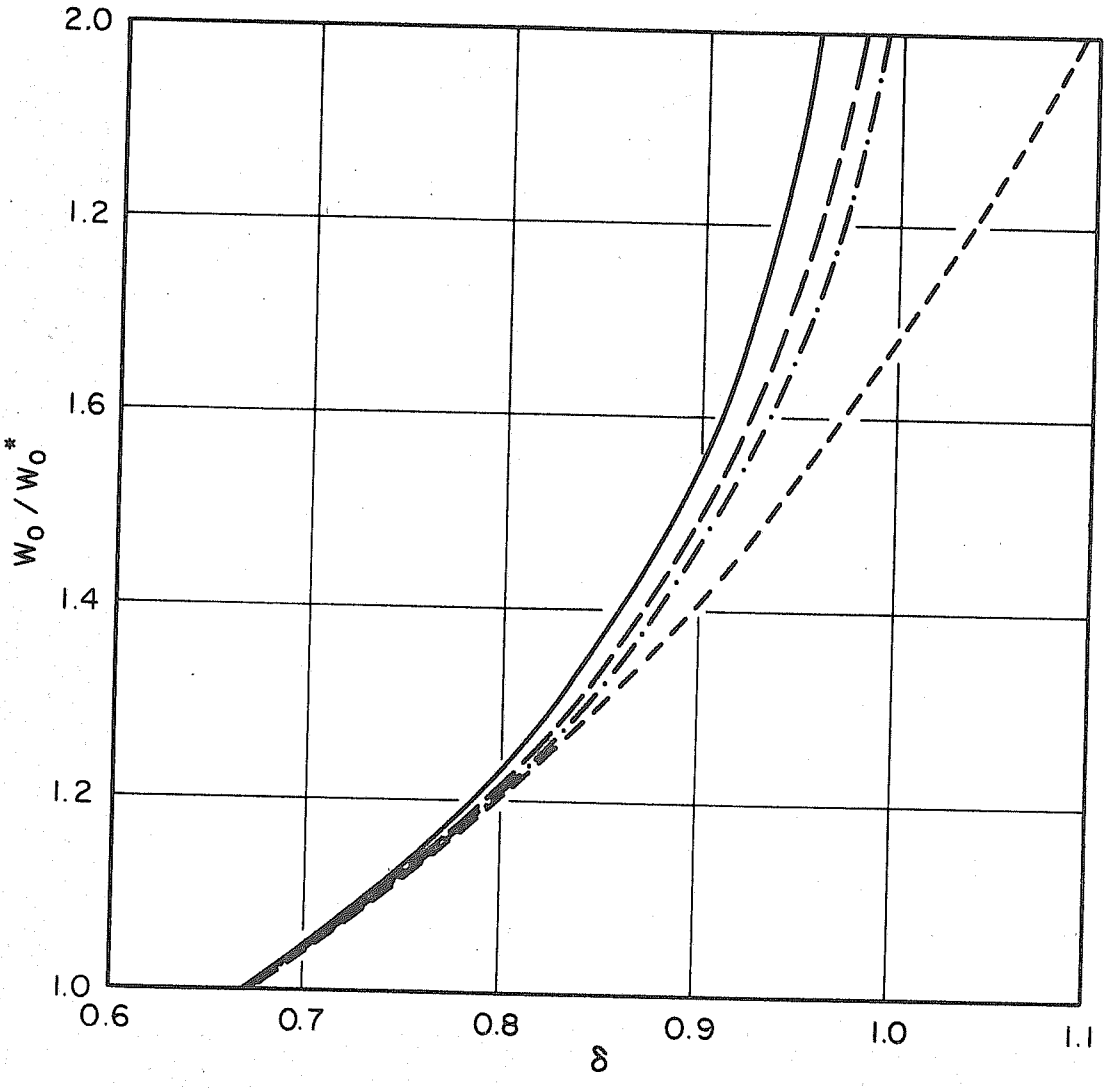

——— = PRAGER AND HODGE

—·—·— = 4 PLATE BENDING ELEMENTS

— — — = 10 MEMBRANE ELEMENTS

— — — — = 4 PLATE BENDING ELEMENTS, E_T = 0.25 E

FIG. 6.16 ELASTIC - PLASTIC BENDING OF BEAM

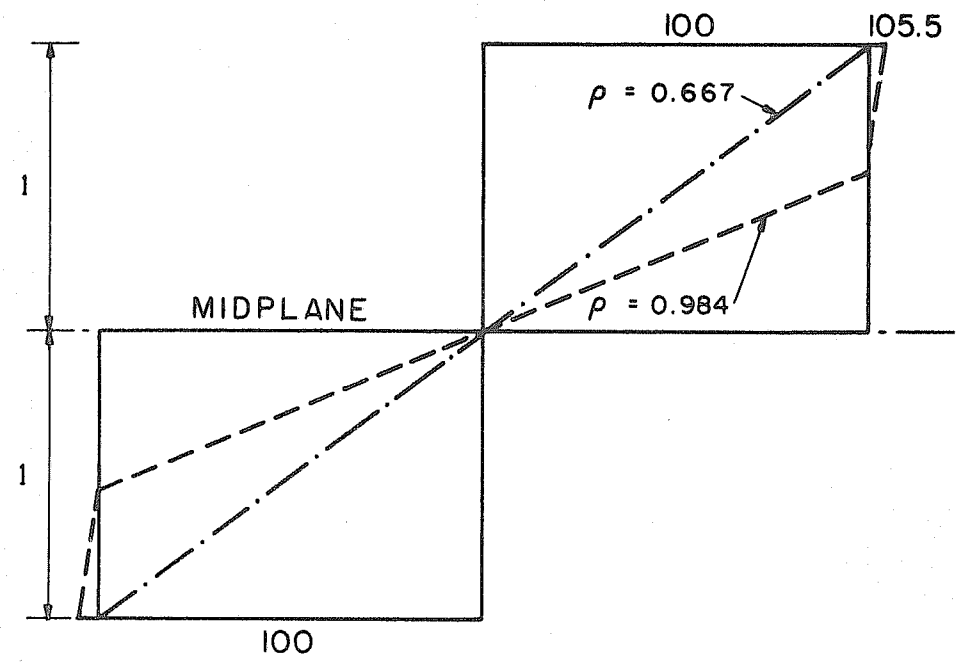

FIG. 6.17 STRESS DISTRIBUTION THROUGH BEAM, PURE BENDING, STRAIN-HARDENING MATERIAL

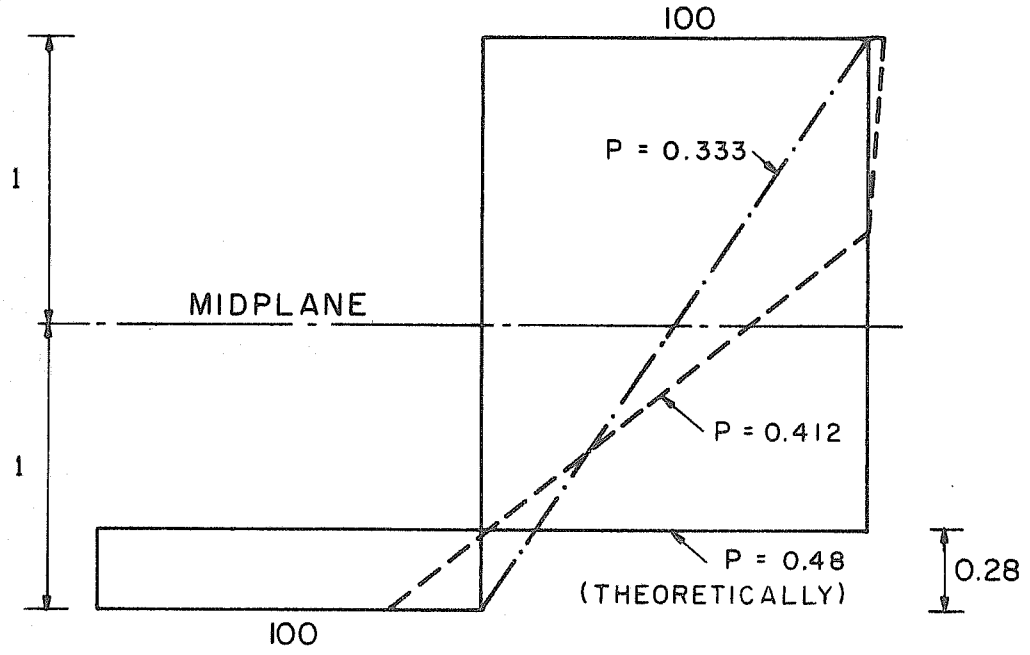

FIG. 6.18 STRESS DISTRIBUTION FOR COMBINED LOADING, $\left(\frac{\sigma_{BEND}}{\sigma_{AXIAL}}\right)_{INITIAL} = 1$

pattern shown in the figure. For these reasons, the numerical procedure become unstable for loads higher than $p = 0.412$ when only one element (with 11 Gaussian integration points) was employed through the entire thickness.

After initial yielding has taken place, σ_y stresses different from zero occur in the beam. This is due to the adopted Kirchhoff assumptions that require the sides of the beam to remain plane whereas deformations in the plastic zone result in a strong Poisson's ratio effect. For these reasons, the σ_x stresses may rise in accordance with the adopted yield criterion to values slightly higher than σ_{yield}.

6.3.2 Elastic-Plastic Behavior of a Simply Supported Square Plate

A simply supported square plate made of an elastic-perfectly plastic material will now be considered. The plate is shown in Fig. 6.19. Using the extremum principles of plasticity, Prager and Hodge [28] presented an upper bound solution to this problem when the plate is subjected to a uniform pressure

$$P_{upper} = 12\, k_o \left(\frac{t}{a}\right)^2 = \frac{12}{\sqrt{3}}\, \sigma_{yield} \left(\frac{t}{a}\right)^2 = 6.93\, \sigma_{yield} \left(\frac{t}{a}\right)^2 \qquad (6.5)$$

An estimate of the ultimate load may also be obtained by a limit analysis approach like the "yield line theory". This approach is based on maximum moment capacity for a fully yielded cross-section in an uniaxial state of stress

$$M_o = \sigma_{yield}\, t^2 \qquad (6.6)$$

Assuming a collapse mechanism along the two crossing diagonals of the plate, a work and energy analysis yields the ultimate load.

$$P_{ult} = \frac{6 M_o}{a^2} = 6 \sigma_{yield} \left(\frac{t}{a}\right)^2 \tag{6.7}$$

Making use of a constant M_o is not a very accurate assumption when the von Mises yield criterion is employed. The true state of stress in the plate is indeed two-dimensional. Thus the actual stress perpendicular to the plastic hinge line may be higher than σ_{yield}. For these reasons, Eq. (6.7) probably represents an underestimation of the true ultimate pressure load.

Also here, the loading can be expressed in a nondimensional fashion

$$\rho = \frac{p a^2}{6 M_o} = \frac{p}{6 \sigma_{yield}} \left(\frac{a}{t}\right)^2 \tag{6.8}$$

thus $\rho = 1$ for the limit load predicted by the yield line approach.

One quarter of the panel is analyzed using 2 by 2 and 4 by 4 finite element meshes. As shown in Fig. 6.19, the geometry and material properties are the same as used in Reference [30] for a similar problem. Here, an 11 point integration scheme through the thickness of the plate is employed, and the load increments are 3 percent of the initial yield load. Denoting the midpoint deflection at the onset of yielding by W_o^*, the resulting load-deflection curves are given in Fig. 6.19. As expected, the ultimate loading obtained by the finite element solutions lie between the values predicted by the yield line theory and Prager and Hodge's upper bound solution.

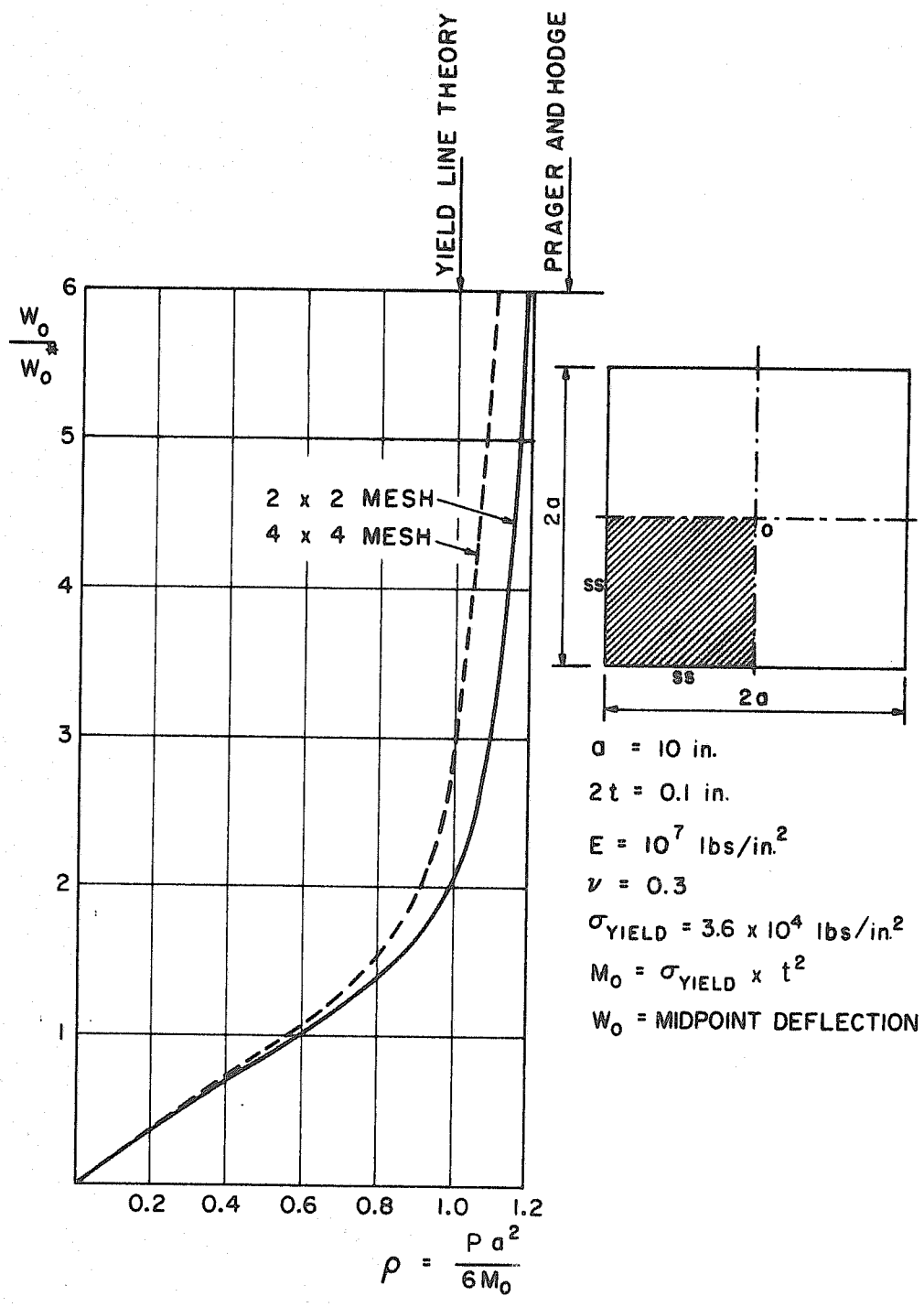

FIG. 6.19 LOAD DEFLECTION CURVE FOR SIMPLY SUPPORTED SQUARE PLATE

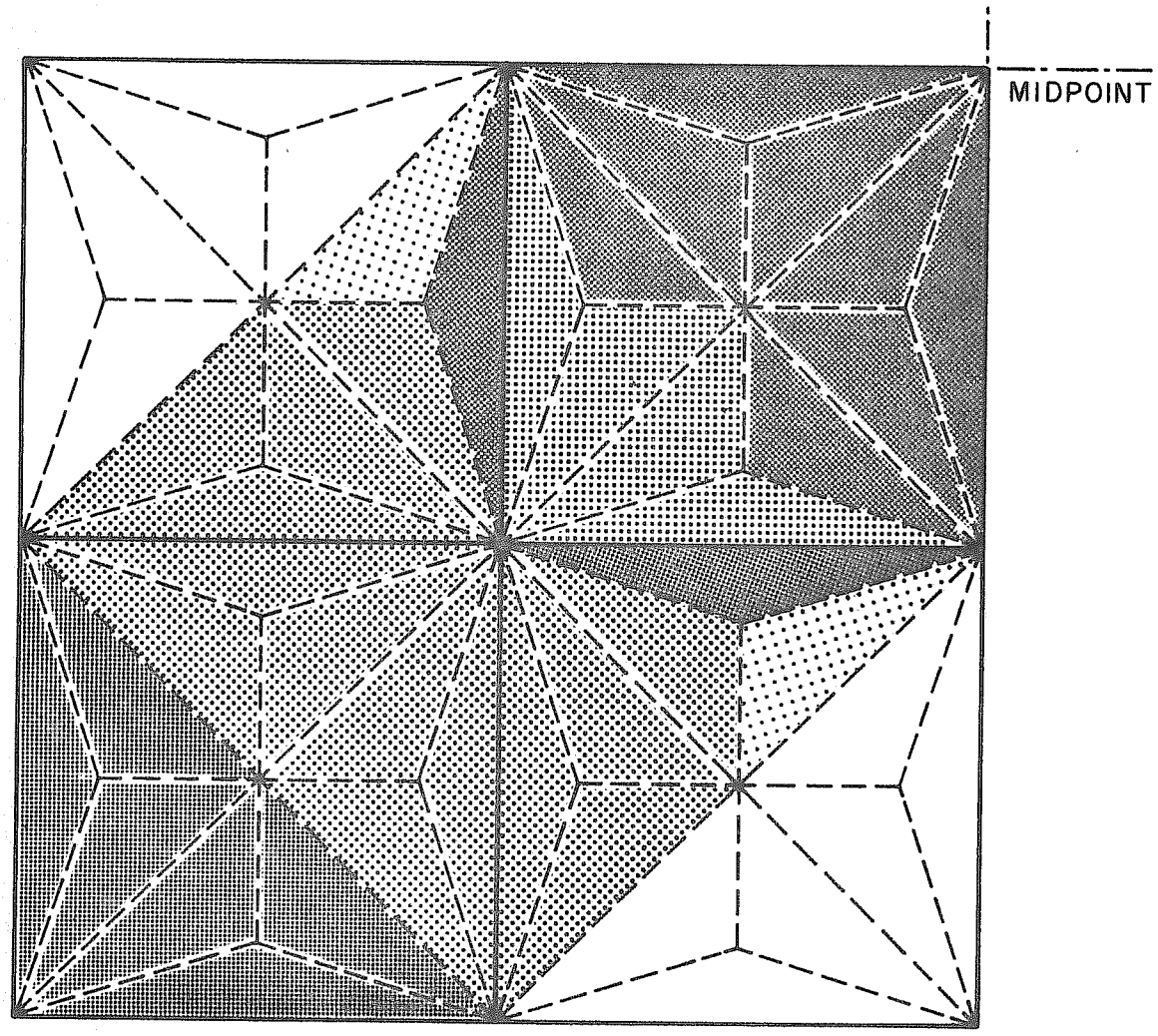

YIELD ZONES FOR ONE QUARTER OF THE PLATE

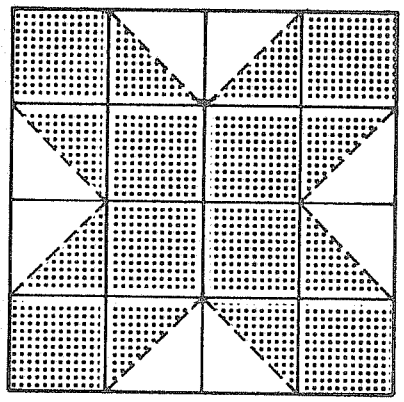

YIELDED AREAS FOR TOTAL PLATE

YIELDED AT 8 INT. POINTS

YIELDED AT 6 INT. POINTS

YIELDED AT 4 INT. POINTS

UNYIELDED

FIG. 6.20 EXTENSION OF YIELD ZONES FOR ρ = 1.06 2 x 2 MESH

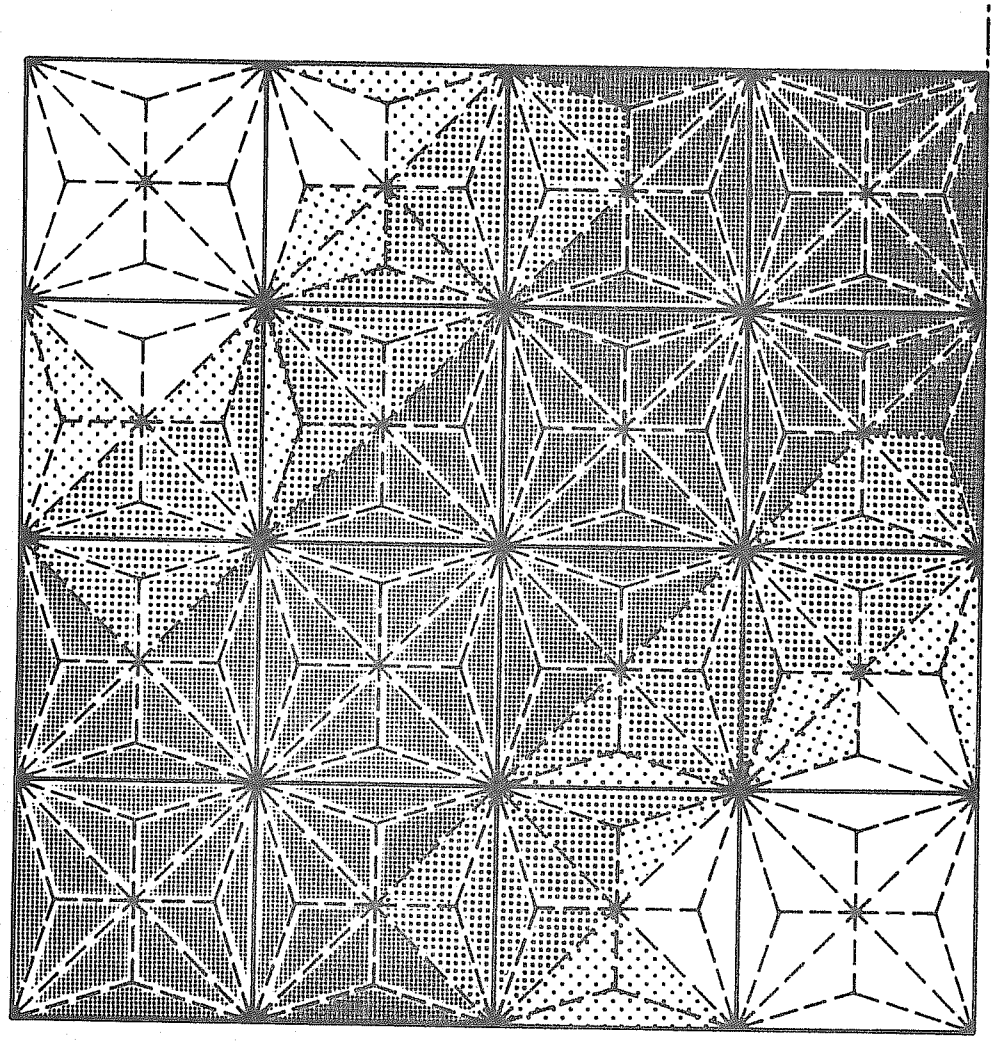

FIG. 6.21 EXTENSION OF YIELD ZONES FOR $\rho = 0.99$
4 by 4 MESH

Moreover, the curve obtained using the 4 by 4 mesh is almost identical to the one given by Armen et. al. [30] who used a 6 by 6 idealization for a quite different type of finite element.

The extensions of the plastic zones for pressures close to the ultimate loading are demonstrated in Fig. 6.20 and Fig. 6.21. The number of yielded points through the entire plate thickness is indicated by using three different forms of shading. Yielding always starts from the surfaces and is symmetric about the plate's midplane. The development of plastic bands that run diagonally is evident. In Fig. 6.21 in particular, it is interesting to observe a rather sharp yield line extending from the corner to the midpoint of the plate. The amount of yielding through the thickness gradually decreases in moving away from the diagonal.

6.3.3 Trapezoidal Plate Under Uniform Pressure

The final example of inelastic material behavior is a plate of trapezoidal shape shown in Fig. 6.22. The plate which is clamped on three sides while the fourth side is free, is subjected to a uniform pressure. The plate is assumed to be made of an elastic-perfectly plastic material. Geometric and material properties are given in Fig. 6.24. Due to symmetry about the B-D axis, only half the plate need be considered during the analysis.

An estimate of the ultimate load the plate can carry is made using the yield line theory. The assumed collapse mechanism is shown in Fig. 6.23, the distance x being a variable denoting the location of yield line C-E. After an expression for p is obtained by means of work considerations, x may be found by minimizing p with respect to x. When $a = b$,

$$x = 0.555\ a$$

and the ultimate pressure is

$$P_{ult} = 5.46 \frac{M_o}{a^2} = 5.46 \frac{\sigma_{yield}\ h^2}{4\ a^2} = 0.213$$

Since the yield line theory has limited validity for metallic materials, the value above only represents a rough estimate of the ultimate load. The collapse mechanism shown in Fig. 6.23 is not the only one possible. However, introduction of more complicated patterns are not expected to change the resulting p_{ult} very much.

Half the plate is analyzed using a 4 by 4 quadrilateral element mesh shown in Fig. 6.24. The element mesh is chosen to be more refined close to the clamped boundaries. The pressure versus the deflection at point B is plotted in Fig. 6.15. The collapse load seems to be somewhat higher than the prediction by the limit load analysis. The load was applied in steps equivalent to 10 percent of the initial yield pressure, thus a total of 25 load increments produced the curve in Fig. 6.25. 11 integration points were utilized through the total thickness of the plate.

The extent of the yielded zones for three different pressure levels are illustrated in Figs. 6.27, 6.28 and 6.29. The formation of of plastic hinges along the clamped boundaries are evident. Any development of a sharp yield line corresponding to line C-E in Fig. 6.23 is not evident; however, an increased yielding activity about this line is apparent. Another interesting feature is the change of the deflected shape during loading in the plastic domain. This is demonstrated in Fig. 6.26 by plotting the deflected shapes along the

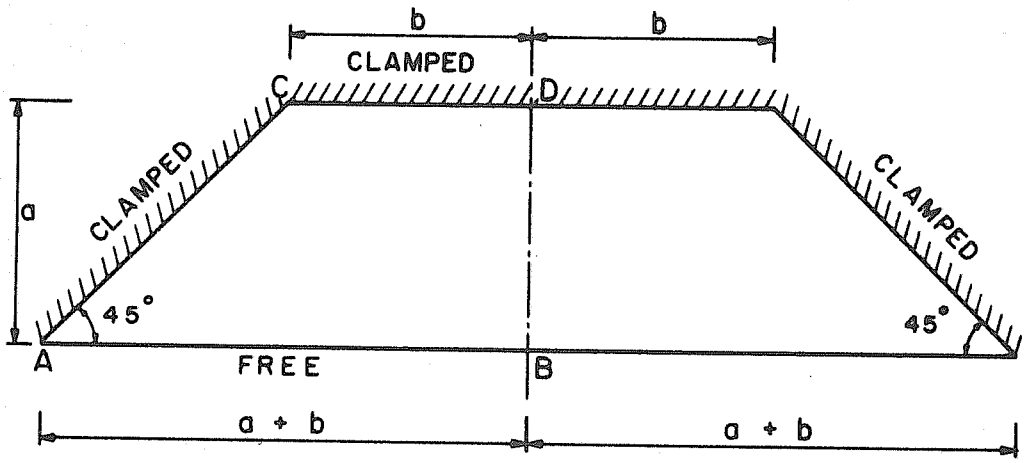

FIG. 6.22 TRAPEZOIDAL PLATE

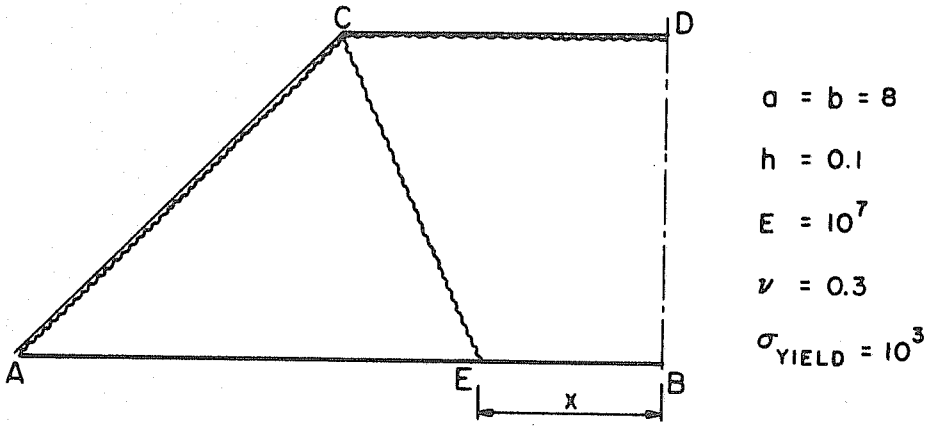

FIG. 6.23 ASSUMED YIELD LINE MECHANISM

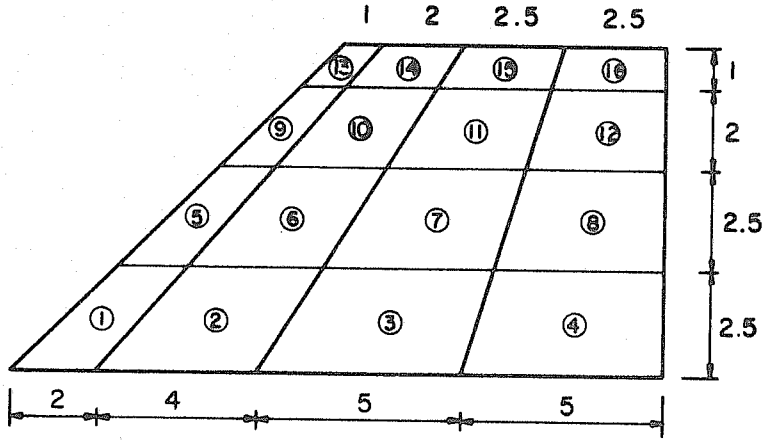

FIG. 6.24 FINITE ELEMENT IDEALIZATION

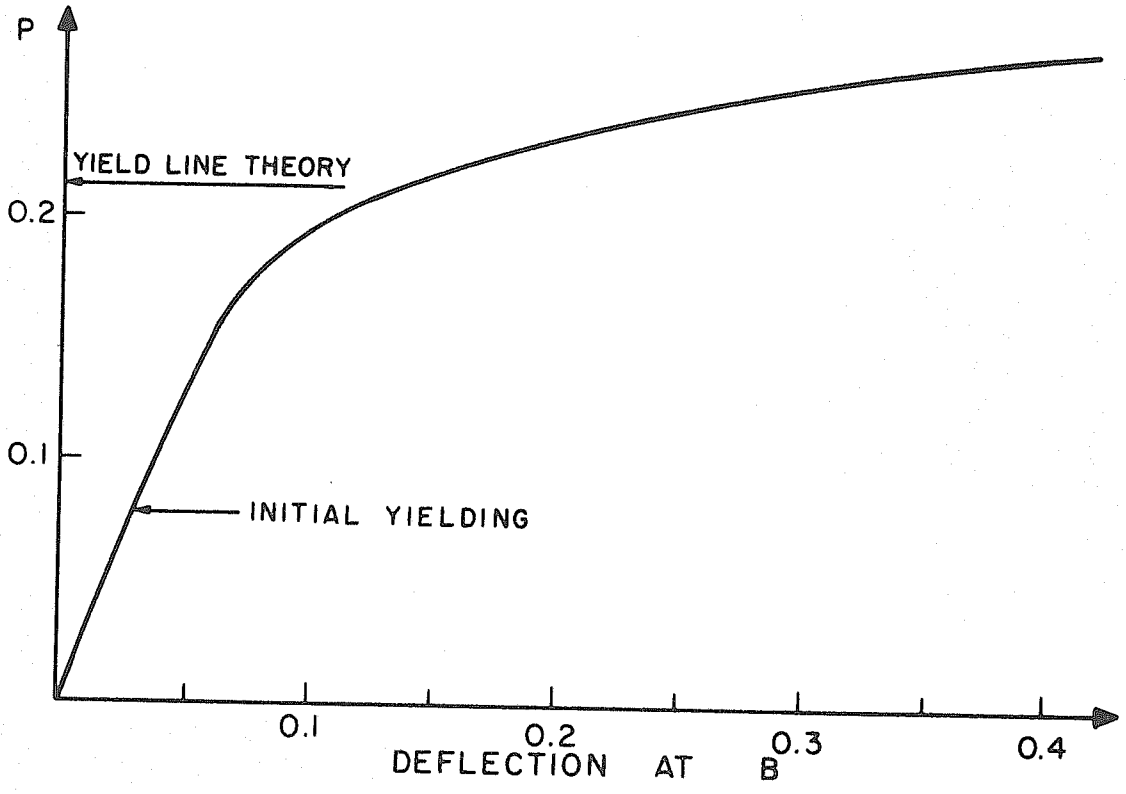

FIG. 6.25 LOAD-DEFLECTION CURVE FOR TRAPEZOIDAL PLATE

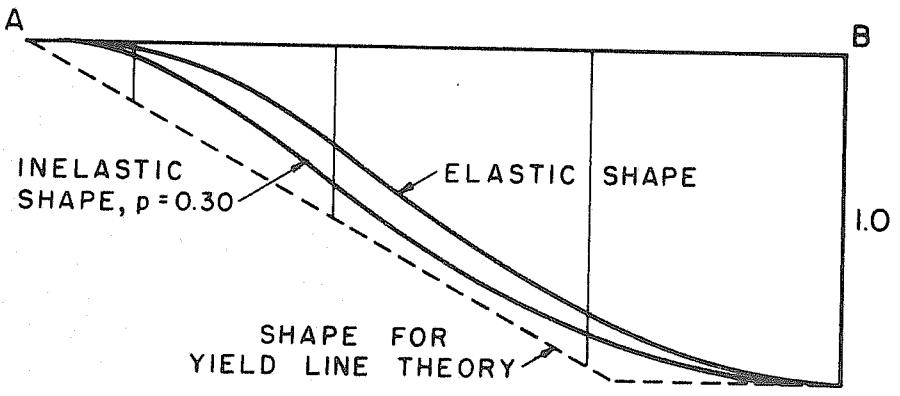

FIG. 6.26 CHANGES IN DEFLECTED SHAPE ALONG LINE A-B

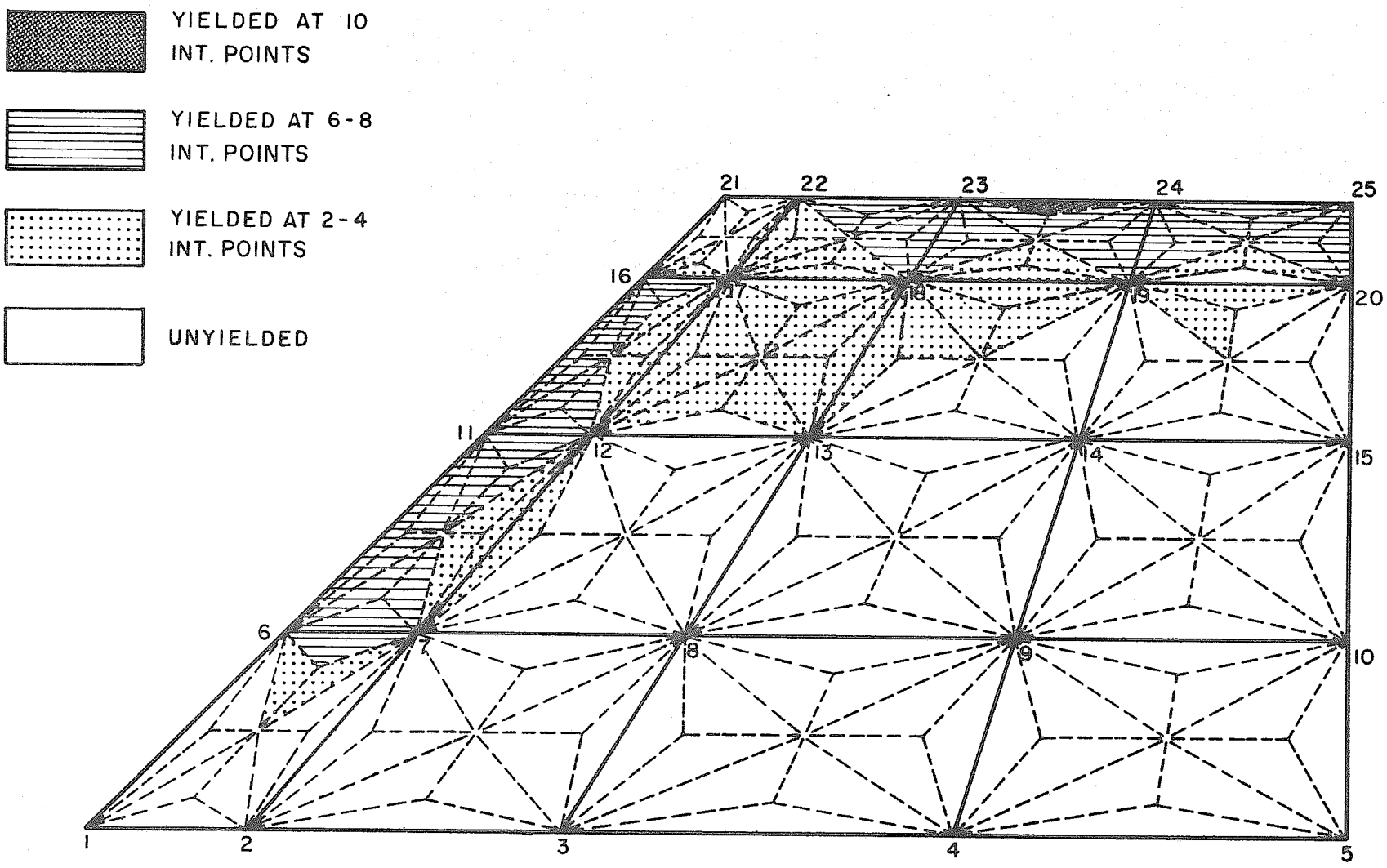

FIG. 6.27 EXTENSION OF YIELD ZONES FOR p = 0.173 (PSI)

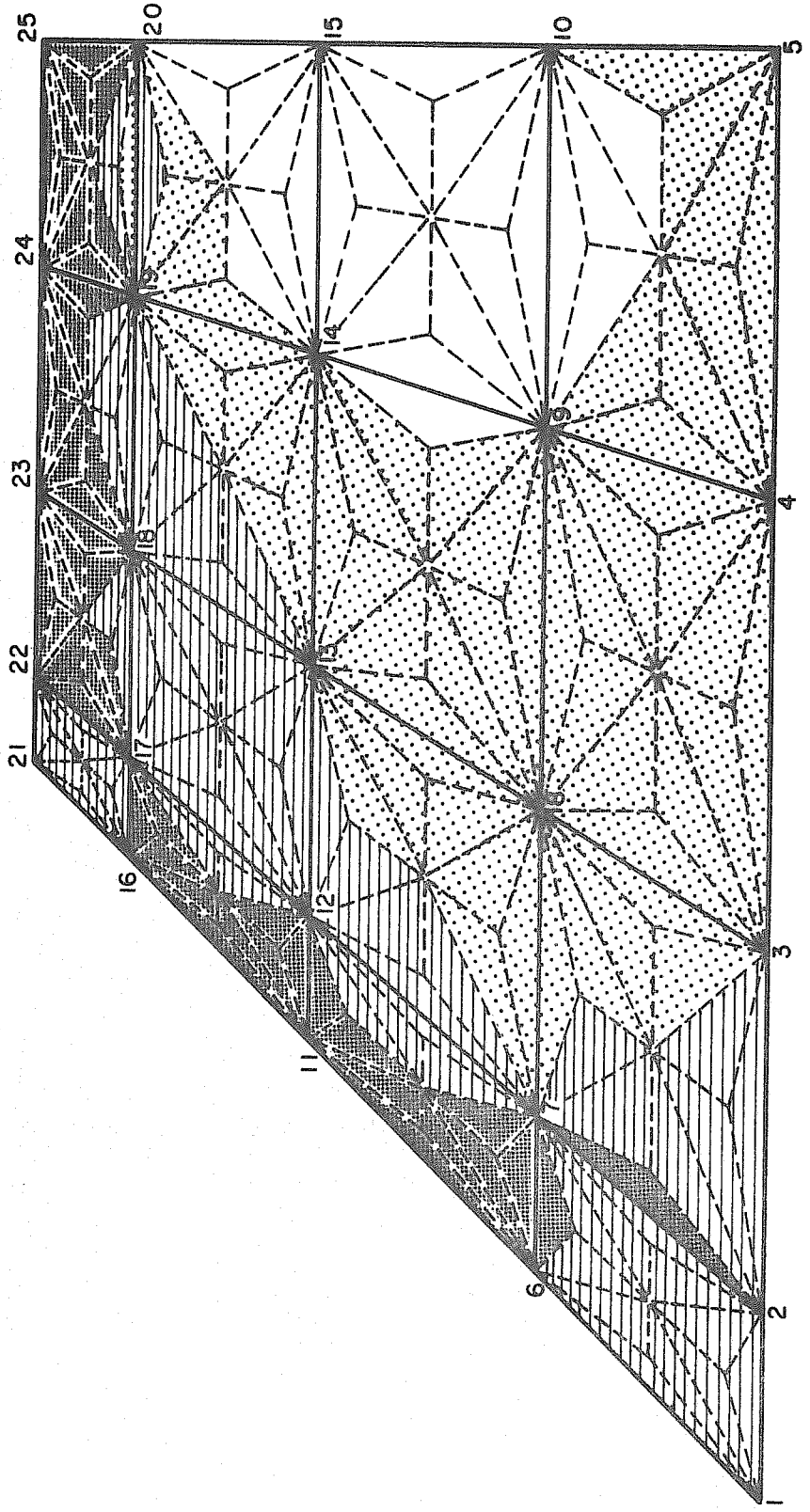

FIG. 6.28 EXTENSION OF YIELD ZONES FOR p = 0.221 (PSI)

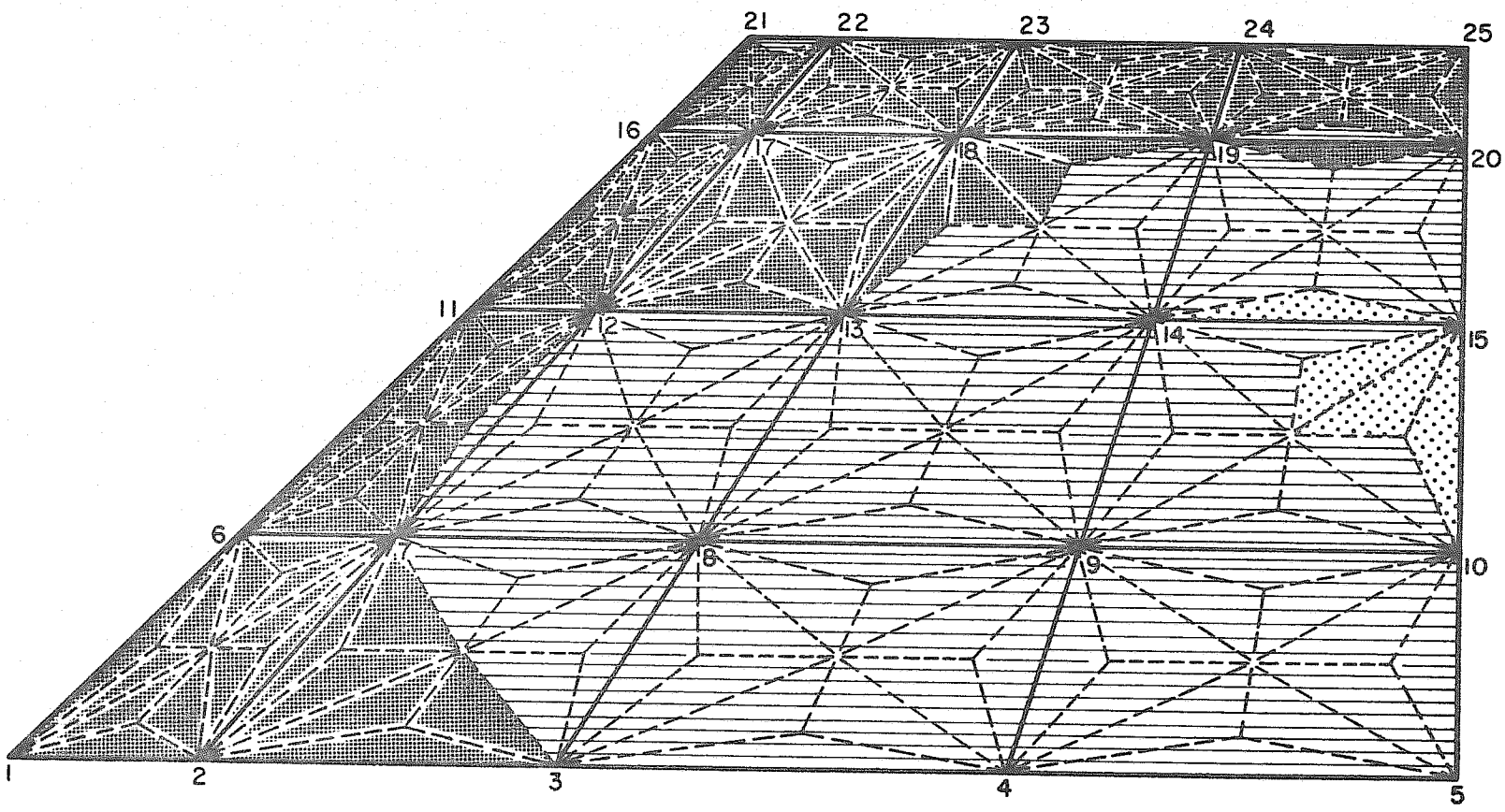

FIG. 6.29 EXTENSION OF YIELD ZONES FOR p = 0.268 (PSI)

free edge A-B during elastic and inelastic loading. It is evident that the shape becomes increasingly like the one assumed for the yield line theory in the inelastic loading range.

6.4 COMPUTER TIME REQUIREMENTS

All computations in the preceding were performed with a CDC 6400 computer (65 K memory). Some characteristic computer times per element for the nonlinear analysis are:

Operation		Time CP sec's
Plane element	Basic matrices	0.034
	Tangent stiffness	0.044
	Unbalanced forces	0.048
	Tangent stiffness plus unbalanced forces	0.057
Shallow shell element	Basic matrices	0.060
	Tangent stiffness	0.072
	Unbalanced forces	0.077
	Tangent stiffness plus unbalanced forces	0.089
Incremental stiffness for inelastic plate bending element, 11 integration points through thickness		0.170 - 0.330
Incremental stiffness for inelastic membrane element		0.125 - 0.160
Incremental stiffness for combined bending and membrane action, 11 integration points through thickness		0.540 - 0.690

The nonlinear large deflection stiffnesses were computed using a 2 by 2 Gaussian quadrature. These times do not include assemblage of the system stiffness matrix or printing of stresses for the inelastic elements. "Basic matrices" indicates formulation time of matrices from which the tangent stiffness and the unbalanced forces are obtained by direct linear combination, see Sections 2.4.4. and 2.4.5. Since the formulation time of the incremental stiffness for the inelastic elements is dependent on the number of integration points where yielding has occurred, the time is indicated by its lower and upper limits.

Some typical computer time requirements for some of the previous examples are:

Example	No. of elements	No. of load increments	Total No. of iterations	CP time in secs.
Platestrip Sec. 6.2.1	4	5	41	20
Square plate Sec. 6.2.2	16	6	20	75
Snap-through Sec. 6.2.5	4	23	88	72
Inelastic beam, bending element Sec. 6.3.1	4	19	0	24
Inelastic beam membrane element Sec. 6.3.1	10	19	0	35
Trapezoidal plate Sec. 6.3.3	16	29	0	171

For the inelastic examples, a considerable amount of peripheral processor time was spent in addition to the central processor time. However, the total storage requirement for the inelastic program is moderate (50, 000 octal) and cost of "PP"-time is therefore small.

The computer time requirements indicated here for large deflection and inelastic analysis of plates clearly demonstrates that such calculations are highly feasible from an economic standpoint.

7. SUMMARY AND SUGGESTIONS FOR FURTHER DEVELOPMENT

Efficient procedures for solving nonlinear plate problems have been developed in the present investigation. Assuming a Ritz-type method of approach, a set of equilibrium and a set of incremental equations have been derived for large deflections of initially deformed plates (shallow shells). These equations are well suited for numerical computations using modern electronic computers.

Based on these equations, a nonlinear, doubly curved, quadrilateral finite element accounting for both flexural and membrane behavior has been developed. This element has proven to be computationally highly efficient and accurate. Using this element a great variety of different problems can be analyzed, such as large deflection plate problems, post buckling problems, problems of combined inplane and transversal loading, snap-through problems and many others.

A general quadrilateral finite element accounting for inelastic material behavior has also been developed. The derivation of this element is based on the flow theory of plasticity, the von Mises yield criterion and isotropic hardening of the material. Both membrane and flexural behaviors are accounted for. This element is capable of inelastic analysis of plates of general shapes and under general loading conditions. Using an incremental technique, the complete deformation and stress patterns throughout the load application are obtained. This analysis also reveals the ultimate load and the corresponding collapse mechanism.

Several numerical techniques for solving nonlinear structural problems have been tested and discussed. It was concluded that for

large deflection problems of plates, a combination of load-incrementation and Newton-Raphson iteration is generally the best approach. The problems of convergence and accuracy have also been studied.

Two computer programs were developed in connection with this investigation, one for handling large deflections of initially deformed plates and one for treating inelastic behavior of plates. Computer time comparisons with other numerical methods previously reported in the literature reveal that the methods developed here undoubtedly are among the most efficient yet available. In several cases the present methods proved to be more than one order faster than similar methods reported previously.

One obvious extension of the present work is to combine the two existing computer programs into one which accounts for both geometric and material effects. The effort required for this extension is merely a matter of programming since the theoretical derivations for such an operation is readily available in the present report.

A logical extension of the present line of research would be to include the effect of discrete, eccentric stiffeners on the plate. Stiffened plates constitute a frequently occurring type of structure. The interaction between the stiffeners and the main plate is believed to be essential for the postbuckling behavior and the ultimate strength of the structure. The stiffeners could probably be accounted for using the same nonlinear element as was developed for the plate itself. The inclusion of discrete stiffeners would then essentially be a matter of combining and assembling these elements in a global, 3-dimensional coordinate system. However, a major problem would be the complexity and the proportions of the stiffened plate problem itself requiring many

finite elements for the modeling. This is particularly true for an extensive nonlinear analysis.

Another natural extension would be to use the presently developed finite elements for the analysis of general shell structures. Since the large deflection quadrilateral is doubly curved, it could be used for arbitrarily shaped, thin shells. Using a Lagrangian description, the deformation of each element would have to be referred to a local coordinate system lying in an "average" plane of the reference configuration of the element concerned. All stiffnesses would have to be transformed to a global, Cartesian reference system before assemblage. Whether such an approach, which in fact only would require a simple extension of the present plate program, would be sufficient for highly nonlinear systems, remains to be tested. In the case of really large shell deformations, an updating of the local coordinate systems throughout deformation might become necessary.

Although much research already has been done in the field of nonlinear finite elment analysis, some basic foundations of the method still remain to be clarified. In particular, the mathematical foundations for applying Ritz-type solution techniques to nonlinear problems ought to be further investigated. Hopefully, this will result in formal proofs of convergence as presently available for linear finite element analysis.

8. REFERENCES

1. von Karman, T., "Encyclopädie der mathematischen Wissenschaften", Vol. 15/4, pp. 349, 1910.

2. Föppl, A., "Vorlesungen über technische Mechanik", Vol. 5, pp. 132, Leipzig, 1907.

3. Timoshenko, S.P. and Gere, J.M., Theory of Elastic Stability, McGraw-Hill Book Company, New York 1961 (second edition).

4. Marguerre, K. and Trefftz, E., Über die Tragfähigkeit eines Längsbelasteten Plattenstreifens nach Überschreiten den Beullast, Zeitschrift fur angewandte Mathematik und Mechanik, Vol. 17, pp. 85, 1937.

5. Marguerre, K., Die mitteragende Breite der gedrückten Platte, Luftfahrt-Forschung, Vol. 14, pp. 121, 1937.

6. Way, S., Uniformly Loaded, Clamped Plates with Large Deflection, Proc. 5th Intern. Congr. Appl. Mechanics, Cambridge, Mass. 1938.

7. Levy, S., Bending of Rectangular Plates with Large Deflections, NACA Technical Note No. 846, 1942.

8. Levy, S., Square Plates with Clamped Edges under Normal Pressure Producing Large Deflections, NACA Technical Note No. 847, 1942.

9. Wang, Chi-Teh, Nonlinear Large-Deflection Boundary value Problems of Rectangular Plates, NACA Technical Note No. 1425.

10. Coan, J.M., Large-Deflection Theory for Plates with Small Initial Curvature Loaded in Edge Compression. Journal of Applied Mechanics, Vol. 18, Trans. ASME, Vol. 73, 1951, pp. 143-151.

11. Turner, J.L., Clough, R.W., Martin, H.C., and Topp, L.J., Stiffness and Deflection Analysis of Complex Structures, J. Aero. Science, Vol. 23, No. 9, Sept. 1956, pp. 805-825.

12. Turner, M.J., Dill, E.H., Martin, H.C. and Melosh, R.J., Large Deflection Analysis of Complex Structures Subjected to Heating and External Loads, J. Aero-Space Science, Vol. 27, pp. 97-106, Feb. 1960.

13. Argyris, J.H., Kelsey, S. and Kamel, H., Matrix Methods Structural Analysis, Agardograph 72 (editor: de Veubeke, F.), Pergamon Press, pp. 105-120, 1964.

14. Martin, H.C., Derivation of Stiffness Matrices for the Analysis of Large Deflection and Stability Problems, Proc. 1st Conf. on Matrix Methods in Struct. Mech., AFFDL-TR-66-80, pp. 697-715, 1966.

15. Felippa, C.A., Refined Finite Element Analysis of Linear and Nonlinear Two-Dimensional Structures, Ph.D. Dissertation, Univ. of Calif., Berkeley, first part published as SESM Report 66-22, 1966.

16. Wissmann, J.M., Nonlinear Structural Analysis; Tensor Formulation, Proc. 1st Conf. on Matrix Methods in Struct. Mech., AFFDL-TR-66-80, pp. 679-696, 1966.

17. Gallagher, R.H., Gellatly, R.A., Padlog, J., and Mallett, R.H., Discrete Element Procedure for Thin-Shell Instability Analysis, AIAA Journal, Vol. 5, No. 1, pp. 138-144, 1967.

18. Oden, J.T., Numerical Formulation of Nonlinear Elasticity Problems, Journal of the Structural Division, ASCE, Vol. 93, No. ST3, pp. 235-255, 1967.

19. Murray, D.W., Large Deflection Analysis of Plates, Ph.D. Dissertation, Univ. of Calif., Berkeley, Report No. SESM 67-44, 1967.

20. Murray, D.W. and Wilson, E.L., Finite Element Large Deflection Analysis of Plates, Journal of the Structural Division, ASCE, Vol. 95, No. EM1, pp. 143-165, 1969.

21. Murray, D.W. and Wilson, E.L., Finite Element Postbuckling Analysis of Thin Elastic Plates, AIAA Journal, Vol. 7, No. 10, 1969.

22. Brebbia, C., and Connor, J., Geometrically Nonlinear Finite-Element Analysis, Journal of the Engineering Mechanics Division, ASCE, Vol. 95, No. EM2, pp. 463-483, 1969.

23. Prager, W. and Hodge, P.G., Theory of Perfectly Plastic Solids, Dover Publications, New York, 1951.

24. Padlog, J., Huff, R.D., and Holloway, G.F., The Unelastic Behavior of Structures Subjected to Cyclic, Thermal and Mechanical Stressing Conditions, Bell Aerosystems Co., Report WPADD TR 60-271, 1960.

25. Argyris, J.H., Kelsey, S., and Kamel, W.H., Matrix Methods of Structural Analysis. A Precis of Recent Developments. Proc. 14th Meeting of Structures and Materials Panel, AGARD, 1963.

26. Marcal, P.V., and King, I.P., Elastic-Plastic Analysis of Two-Dimensional Stress Systems by the Finite Element Method. Int. J. Mech. Sci., Vol. 9, No. 3, pp. 143-145, 1967.

27. Khojasteh-Bakht, M., Analysis of Elastic-Plastic Shells of Revolution under Axisymmetric Loading by the Finite Element Method, Ph.D. Dissertation, Univ. of Calif., Berkeley, Report No. SESM 67-8, 1967.

28. Yaghmai, S., Incremental Analysis of Large Deformations in Mechanics of Solids with Applications to Axisymmetric Shells of Revolution. Ph.D. Dissertation, Univ. of Calif. Berkeley, Report No. SESM 68-17, 1968.

29. Marcal, P.V., Finite Element Analysis of Combined Problems of Nonlinear Material and Geometric Behavior, Brown University, Providence, R.I., Technical Report No. N00014-0007/1, 1969.

30. Armen, H., Pifko, A., and Levine, H.S., Finite Element Method for the Plastic Bending Analysis of Structures, Proc. 2nd. Conf. on Matrix Methods in Struct. Mechanics, AFFDL-TR-68-150, 1968.

31. Marcal, P.V., Comperative Study of Numerical Methods of Elastic-Plastic Analysis, AIAA Journal, Vol. 6, No. 1, pp. 157-158, 1967.

32. Green, A.E. and Zerna, W., Theoretical Elasticity, Oxford University Press, 1954.

33. Green, A.E. and Adkins, J.E., Large Elastic Deformations and Non-linear Continuum Mechanics, Oxford University Press, 1960.

34. Truesdell, C., and Toupin R., Classical Field Theories, Handbuch der Physik (editor: Flügge, S.), Vol. III/1, 1960.

35. Truesdell, C. and Noll, W., The Nonlinear Field Theories of Mechanics, Handbuch der Physik, Vol. III/3 (editor: Flügge, S.), 1965.

36. Fung, V.C., Foundations of Solid Mechanics, Prentice-Hall, 1965.

37. Malvern, L.E., Introduction to the Mechanics of a Continuous Medium, Prentice-Hall 1969.

38. Washizu, K., Variational Methods in Elasticity and Plasticity, Pergamon Press, 1968.

39. Hellinger, E., Der allgemeine Ansatz der Mechanik der Kontinua, Encyclopädie der Mathematischen Wissenschaften, Vol. 4, Part 4, pp. 90-95, 1914.

40. Reissner, E., On a Variational Theorem in Elasticity, Journal of Mathematics and Physics, Vol. 29, No. 2, pp. 90-95, 1950.

41. Trefftz, E., Über die Ableitung der Stabilitäts - Kriterien des elastischen Gleichgewichtes aus der Elastizitäts theorie endlicher Deformationen, Proc. of the 3rd Int. Congr. for Appl. Mech., pp. 44-50, Stockholm 1930.

42. Cauchy, A.L., Sur L'Equilibrie et le Mouvement Interior de Corps Consideres Comme des Masses Continues, Ex. de Math. 4, Oeuvres (2) pp. 342-349, 1829.

43. Truesdell, C., The Mechanical Foundations of Elasticity and Fluid Dynamics, Intern. Science Review Series, Vol. 8, Part 1, pp. 99-103, Gordon and Breach, 1966.

44. Love, A.E.H., A Treatise on the Mathematical Theory of Elasticity, Dover Publications, New York, 1944 (4th ed. 1927).

45. Timoshenko, S.P. and Woinowsky-Krieger, S., Theory of Plates and Shells, McGraw-Hill Book Company, New York, 1959.

46. Novozhilov, V.V., Theory of Elasticity, Pergamon Press, New York, 1961.

47. Marguerre, K., Zur Theorie der gekrümmten Platte grosser Formändrung, Proc. of the 5th International Congress for Applied Mechanics, pp. 93-101, 1938.

48. Flügge, W. and Conrad, D.A., Singular Solutions in the Theory of Shallow Shells, Technical Report No. 101, Division of Engineering Mechanics, Stanford University, 1956.

49. Reissner, E., On Some Aspects of the Theory of Thin Elastic Shells, Journal of the Boston Society of Civil Engineers, pp. 100-133, 1955.

50. Vlasov, V.S.,Allgemeine Schalentheorie und ihre Anwendung in der Technik, Akademie-Verlag, Berlin, 1958.

51. Mikhlin, S.G., Variational Methods in Mathematical Physics, Macmillan Co., 1964 (translantion of the 1957 Russian edition).

52. Mikhlin, S.G., The Problem of the Minimum of a Quadratic Functional, Holden-Day Inc., 1965 (translation of the 1952 Russian edition).

53. Novozhilov, V.V., Foundations of the Nonlinear Theory of Elasticity, Graylock Press, Rochester, N.Y. 1953.

54. Boley, B.A. and Weiner, J.H., Theory of Thermal Stresses, John Wiley, 1960.

55. Langhaar, H.L., Energy Methods in Applied Mechanics, Wiley, New York, 1962.

56. Varga, R.S., Matrix Iterative Analysis, Prentice-Hall Inc., New Jersey, 1962.

57. Forsythe, G.E. and Wasow, W.R., Finite Difference Methods for Partial Differential Equations, John Wiley and Sons, Inc., New York, 1960.

58. Greenspan, D., On Approximating Extremals of Functionals-I. The Method and Examples for Boundary Value Problems, Bull. Int. Comp. Centre, Vol. 4, University of Rome, pp. 99-120, 1965.

59. Greenspan, D., On Approximating Extremals of Functionals-II. Theory and Generalizations Related to Boundary Value Problems for Nonlinear Differential Equations, Int. J. Engrg. Sci., Vol. 5, pp. 571-588, 1967.

60. Bushnell, D. and Almroth, B.O., Finite-Difference Energy Method for Nonlinear Shell Analysis, Proc. LMSC/AFFDL Shell Conference, Palo Alto, Calif., Aug. 10-14, 1970.

61. Jensen, P.S., Finite Difference Techniques for Variable Grids, Proc. LMSC/AFFDL Shell Conference, Palo Alto, Calif., Aug. 10-14, 1970.

62. Zienkiewicz, O.C., The Finite Element Method in Structural and Continuum Mechanics, McGraw-Hill Publ. Company, 1967.

63. Przemeniecki, J.S., Theory of Matrix Structural Analysis, McGraw-Hill Book Co., 1967.

64. Holand, I., and Bell, K., Finite Element Methods in Stress Analysis, Tapir, The Technical Univ. of Norway, 1969.

65. Melosh, R.J., Basis for Derivation of Matrices for the Direct Stiffness Method, AIAA Journal, Vol. 1, pp. 1631-1637, 1963.

66. de Arantes e Oliveira, E.R., Mathematical Foundations of the Finite Element Method, Lab. Nacional de Engenharia Civil, Lisbon, 1967.

67. Felippa, C.A. and Clough, R.W., The Finite Element Method in Solid Mechanics, AMS Symposium on the Numerical Solution of Field Problems in Continuum Mechanics, Durham, N.C., 1968.

68. Clough, R.W. and Tocher, J.L., Finite Element Stiffness Matrices for the Analysis of Plate Bending Proc. 1st Conf. on Matrix Methods in Struct. Mech., AFFDL-TR-66-89, pp. 515-546, 1965.

69. Clough, R.W. and Felippa, C.A., A Refined Quadrilateral Element for Analysis of Plate Bending, Proc. 2nd Conf. on Matrix Methods in Struct. Mech., AFFDL-TR-68-150, pp. 399-440, 1968.

70. Willam, K., Finite Element Analysis of Cellular Structures, Ph.D. Dissertation, Univ. of Calif., Berkeley, 1969.

71. Bergan, P.G., Clough, R.W. and Mojtahedi, S., Analysis of Stiffened Plates Using the Finite Element Method, Report No. UCSESM 70-1, Univ. of Calif., Berkeley, 1970.

72. Doherty, W.P., Wilson, E.L. and Taylor, R.L.,Stress Analysis of Axisymmetric Solids Utilizing Higher-Order Quadrilateral Elements, Report No. 69-3, Str. Eng. Lab., Univ. of Calif., Berkeley, 1969.

73. Wilson, E.L., SAP. A General Structural Analysis Program, Structural Engineering Laboratory, Univ. of Calif., Berkeley, Sept. 1970.

74. Marcal, P.V., The Effect of Initial Displacements on Problems of Large Deflection and Instability. Brown University, Div. of Eng., ARPA-E54, presented Proc. ASCE, Joint Speciality Conf., Optimization and Nonlinear Problems, April 1968.

75. Bogner, F.K., Fox, R.L., and Schmidt, L.A., The Generation of Interelement, Compatible Stiffness and Mass Matrices by the Use of Interpolation Formulas, Proc. 1st Conf. on Matrix Methods in Struct. Mech., AFFDL-TR-66-80, pp. 397-444, 1965.

76. Melosh, R.J., Basis of Derivation of Matrices for Direct Stiffness Method, Journal AIAA, Vol. 1, pp. 1631-1637, 1963.

77. Argyris, J.H., Continua and Discontinua, Proc. 1st Conf. on Matrix Methods in Struct. Mech., AFFDL-TR-66-80, pp. 11-190.

78. Hill, R., The Mathematical Theory of Plasticity, Oxford University Press, 1950.

79. Naghdi, P.M., Stress-Strain Relations in Plasticity and Thermoplasticity. Plasticity. Proceedings of the Second Symposium on Naval Structural Mechanics. (editors: Lee, E.H. and Symonds, P.S.) Pergamon Press 1960.

80. Hencky, H., Zur Theorie plastischer Deformationen und der hierdurch in Material hervorgerufen Nebenspannungen, Z. angew. Math. Mech. Vol. 4, pp. 323-334, 1924.

81. Prandtl, L., Proc. 1st Int. Cong. App. Mech., Delft, pp. 43, 1924.

82. Reuss A., Zeits. ang. Math. Mech., Vol. 10, pp. 266, 1930.

83. Prager, W., The Theory of Plasticity: A Survey of Recent Achievements, (James Clayton Lecture) Proc. Instn. Mech. Engrs., Vol. 169, pp. 41-57, 1955.

84. Ilyushin, A.A., Some Problems in the Theory of Plastic Deformations, (in Russian) Prikl. Mat. Mekh. Vol. 7, pp. 245-272, 1943, Eng. Trans., BMB-12, Grad. Div. Appl. Math., Brown Univ., 1946.

85. Pope, G., A Discrete Element Method for Analysis of Plane Elastic-Plastic Stress Problems, Royal Aeronautical Establishment, TR 65028, 1965.

86. Marcal, P.V., Finite Element Analysis with Material Nonlinearities--Theory and Practice, Proc. Japan-U.S. Seminar on Matrix Methods of Structural Analysis and Design, Tokyo, 1969.

87. Koiter, W.T., General Theorems for Elastic-Plastic Solids, Progress in Solid Mechanics, Vol. 1, (editors: Sneddon, I.N. and Hill, R.) North-Holland Publishing Company, Amsterdam, 1960.

88. Green, A.E. and Naghdi, P.M., A General Theory of Elastic Plastic Continuum, Arch. Rat. Mech. Anal. 18, Vol. 4, pp. 250-281, 1965.

89. Lee, E.H. and Lin, D.T., Finite Strain Elastic Plastic Theory with Application to Plane Wave Analysis, J. Appl. Phys., 38, 1, pp. 19-27, 1967.

90. Lee, E.H., Elastic-Plastic Deformation at Finite Strains, Journ. Appl. Mech., Vol. 36, 1-6, 1969.

91. Tseng, W., A General Constitutive Theory for Elastic-Plastic Crystalline Solids, Ph.D. Dissertation, Univ. of Calif., Berkeley, to be finished April 1971.

92. Drucker, D.C., A More Fundamental Approach for Plastic Stress-Strain Relations, Proc. 1st U.S. Natl. Congr. Appl. Mech. (Chicago, 1951), pp. 487-491, New York, 1952.

93. Bland, D.R., The Two Measures of Work-Hardening, Proc. 9th Intern. Congr. Appl. Mech. (Brussels, 1956), Vol. 8, pp. 45-50, 1957.

94. Batdorf, S.B. and Budiansky, B., A Mathematical Theory of Plasticity Based on the Concept of Slip, NACA Tech. Note 1871, 1949.

95. Phillips, A. and Gray, G.A., Experimental Investigations of Corners in the Yield Surface, ASME, Journ. Bas. Eng., June 1961.

96. Yamada, Y., Kawai, T. and Yoshimum, N., Analysis of the Elastic-Plastic Problems by the Matrix Displacement Method. Proc. 2nd Conf. on Matrix Methods in Struct. Mech., AFFDL-TR-68-150, pp. 1271-1299, 1968.

97. Yamada, Y., Recent Japanese Developments in Matrix Displacement Method for Elastic-Plastic Problems, Proc. Japan-U.S. Seminar on Matrix Methods of Structural Analysis and Design, Tokyo, 1969.

98. Popov, E.P., Khojasteh-Bakht, M. and Yaghmai, S., Bending of Circular Plates of Hardening Material, Int. J. Solids Structures, Vol. 3, pp. 975-988, 1967.

99. Fletcher, R. and Powell, M.J.D., A Rapidly Convergent Descent Method for Minimization, Computer Journal, Vol. 6, No. 163, 1963.

100. Bogner, F.K., et.al., Development and Evaluation of Energy Search Methods of Nonlinear Structural Analysis, AFFDL-TR-65-113, Wright-Patterson AFB, Ohio, 1965.

101. Mallett, R.H. and Schmidt, L.A., Nonlinear Structural Analysis by Energy Search, Journ. of the Str. Div., ASCE, Vol. 93, No. ST3, pp. 221-234, June 1967.

102. Schmidt, L.A., Bogner, F.K. and Fox, R.L., Finite Deflection Structural Analysis Using Plate and Shell Discrete Elements, AIAA Journal, Vol. 6, No. 5, May 1968.

103. Isaacson, E. and Keller, H.B., Analysis of Numerical Methods, John Wiley and Sons, 1966.

104. Henrici, P., Discrete Variable Methods in Ordinary Differential Equations, John Wiley and Sons, 1961.

105. Hildebrand, F.B., Introduction to Numerical Analysis, McGraw-Hill, 1956.

106. Yeh, Chang-Hua, Large Deflection Dynamic Analysis of Thin Shells Using the Finite Element Method, Ph.D. Dissertation, Univ. of Calif. Berkeley, Report No. UCSESM 70-18, 1970.

107. Timoshenko, S.P. and Gere, J.M., Theory of Elastic Stability, McGraw-Hill, 1961.

108. von Karman, T., Sechler, E.E., and Donnell, L.H., The Strength of Thin Plates in Compression. ASME Trans., APM-54-5, Vol. 54, No. 2, pp. 53-57, 1932.

109. Schreyer, H. and Masur, E., Buckling of Shallow Arches, Journ. of the Eng. Mech. Div., ASCE, No. EM4, Aug. 1966.

110. Huddleston, J.V., Finite Deflection and Snap Through of High Circular Arches, Journ. of App. Mech., Dec. 1968.

111. Weinitschke, H.J., On the Nonlinear Theory of Shallow Spherical Shells, J. Soc. Indust. App. Math., Vol. 6, No. 3, pp. 209-232, Sept. 1958.

112. Weinitschke, H.J., On Asymmetric Buckling of Shallow Spherical Shells, J. Math. and Phys. Vol. 44, No. 2, pp. 141-163, June 1965.

APPENDIX A
DISPLACEMENT FUNCTIONS FOR THE LCCT12 ELEMENT

The compatible displacement functions for subtriangle 3 of Fig. 3.2 is given by

$$w^{(3)} = \langle \hat{\varphi}^{(3)} \rangle \{\hat{w}_i\} \tag{A.1}$$

where

$$\langle \hat{\varphi}^{(3)} \rangle = \langle \hat{\varphi}^{(3)}_{w1}, \hat{\varphi}^{(3)}_{\theta_{x1}}, \hat{\varphi}^{(3)}_{\theta_{y1}}, \hat{\varphi}^{(3)}_{w2}, \hat{\varphi}^{(3)}_{\theta_{x2}}, \hat{\varphi}^{(3)}_{\theta_{y2}}, \hat{\varphi}^{(3)}_{w3}, \hat{\varphi}^{(3)}_{\theta_{x3}}, \hat{\varphi}^{(3)}_{\theta_{y3}}, \hat{\varphi}^{(3)}_{\theta_4}, \hat{\varphi}^{(3)}_{\theta_5}, \hat{\varphi}^{(3)}_{\theta_6} \rangle \tag{A.2}$$

and

$$\{\hat{w}_i\}^T = \langle w_1, \theta_{x1}, \theta_{y1}, w_2, \theta_{x2}, \theta_{y2}, w_3, \theta_{x3}, \theta_{y3}, \theta_4, \theta_5, \theta_6 \rangle$$

The individual terms of the interpolation polynomial given in terms of the geometry and rational coordinates of the entire triangular element are [69]*

$$\hat{\varphi}^{(3)}_{w1} = \zeta_1^2(3-2\zeta_1) + 6\mu_3\zeta_1\zeta_2\zeta_3 + \zeta_3^2[3(\lambda_2-\mu_3)\zeta_1 + (2\mu_2-\lambda_2)\zeta_3 - 3\mu_3\zeta_2]$$

$$\hat{\varphi}^{(3)}_{\theta_x 1} = \zeta_1^2(b_2\zeta_3 - b_3\zeta_2) + (b_1 - b_3\mu_3)\zeta_1\zeta_2\zeta_3$$
$$+ \frac{1}{6}\zeta_3^2[3(b_2\lambda_2 + b_3\mu_3 - 2b_1)\zeta_1 + 3(b_3\mu_3 - b_1)\zeta_2 + (3b_1 - b_2\lambda_2 - 2b_3\mu_3)\zeta_3]$$

$$\hat{\varphi}^{(3)}_{w2} = \zeta_2^2(3-2\zeta_2) + 6\lambda_3\zeta_1\zeta_2\zeta_3 + \zeta_3^2[3(\mu_1-\lambda_3)\zeta_2 + (2\lambda_3-\mu_1)\zeta_3 - 3\lambda_3\zeta_1]$$

$$\hat{\varphi}^{(3)}_{\theta_x 2} = \zeta_2^2(b_3\zeta_1 - b_1\zeta_2) + (b_3\lambda_3 - b_2)\zeta_1\zeta_2\zeta_3 \tag{A.3}$$
$$+ \frac{1}{6}\zeta_3^2[3(2b_2 - b_3\lambda_3 - b_1\mu_1)\zeta_2 + 3(b_2 - b_3\lambda_3)\zeta_1 + (-3b_2 + b_1\mu_1 + 2b_3\lambda_3)\zeta_3]$$

---

* These are the same terms as given in Reference [69], except for a sign error that was detected in that publication

$$\hat{\varphi}^{(3)}_{w3} = \zeta_3^2[3(1+\mu_2)\zeta_1 + 3(1+\lambda_1)\zeta_2 + (1-\mu_2-\lambda_1)\zeta_3]$$

$$\hat{\varphi}^{(3)}_{\theta x3} = \frac{1}{6}\zeta_3^2[3(3b_1+b_2+b_1\lambda_1)\zeta_2 + (b_2\mu_2 - b_1\lambda_1)\zeta_3 - 3(b_1+3b_2+b_2\mu_2)\zeta_1]$$

$$\hat{\varphi}^{(3)}_{\theta 4} = \frac{4A}{3L_3}[6\zeta_1\zeta_2\zeta_3 + \zeta_3^2(5\zeta_3 - 3)]$$

$$\hat{\varphi}^{(3)}_{\theta 5} = \frac{4A}{3L_1}[\zeta_3^2(3\zeta_2 - \zeta_3)]$$

$$\hat{\varphi}^{(3)}_{\theta 6} = \frac{4A}{3L_2}[\zeta_3^2(3\zeta_1 - \zeta_3)]$$

For $\hat{\varphi}^{(3)}_{\theta y i}$ $(i = 1,2,3)$ change all b's in $\hat{\varphi}^{(3)}_{\theta x i}$ to a's.
The expressions of (A.3) apply to subtriangle 3 where $\zeta_1 \geq \zeta_3$, $\zeta_2 \geq \zeta_3$. Similar functions are obtained for the subtriangles 1 and 2 by permuting cyclically all superscripts and subscripts like 1-2-3 to 2-3-1 and 4-5-6 to 5-6-4.

The natural coordinates are defined by

$$\zeta_i = \frac{A_i}{A} \qquad (A.4)$$

that is the natural coordinates of a point P in the triangle is defined as the ratios of the areas A_i of the subtriangles subtended by that point to the total area of the triangle. The differences between the corner coordinates defines the following quantities

$$a_i = x_k - x_j \quad ; \quad b_i = y_j - y_k \qquad (A.5)$$

where i, j, and k are cyclic permuntations of 1, 2 and 3 (when i=1, then j=2 and k=3). Finally

$$L_i^2 = a_i^2 + b_i^2 \tag{A.6}$$

$$\mu_i = - \frac{a_i a_j + b_i b_j}{L_i^2} \tag{A.7}$$

and

$$\lambda_i = 1 - \mu_i \tag{A.8}$$

APPENDIX B

DISPLACEMENT FUNCTIONS FOR THE MEMBRANE ELEMENT

The inplane displacements for the quadrilateral are given by

$$u = \langle \phi_v \rangle \begin{Bmatrix} u_1 \\ u_2 \\ u_3 \\ u_4 \\ u_5 \end{Bmatrix} \qquad v = \langle \phi_v \rangle \begin{Bmatrix} v_1 \\ v_2 \\ v_3 \\ v_4 \\ v_5 \end{Bmatrix} \tag{B.1}$$

where u_i and v_i are the nodal point displacements. Using the natural coordinate system as shown in Fig. 3.3, the interpolation polynomials become

$$\langle \phi_v \rangle^T = \frac{1}{4} \begin{Bmatrix} (1-\xi) & (1-\eta) \\ (1+\xi) & (1-\eta) \\ (1+\xi) & (1+\eta) \\ (1-\xi) & (1+\eta) \\ 4\,(1-\xi^2) & (1-\eta^2) \end{Bmatrix} \tag{B.2}$$

Note that the corner points have coordinate values of ± 1 in the natural system. The transformation from a natural coordinate system to a Cartesian one is a simple bilinear form, see Reference [62].

APPENDIX C

REFORMULATION OF ONE OF THE NONLINEAR STIFFNESS TERMS

One of the nonlinear stiffness terms of the equilibrium equation given by Eq. (2.87) will now be further studied. Multiplying this matrix (Eq. (2.91)) by the inplane displacement vector the following set of forces is obtained

$$\{R_1\} = \int_A [B_{w2}]^T [W_i]^T [P_3]\, dA\, \{v_i\} \tag{C.1}$$

Use of Eq. (2.69) yields

$$\{R_1\} = \int_A [B_{w2}]^T [W_i]^T [B_{w1}]^T [D_{11}] [B_v]\, dA\, \{v_i\}$$

$$= \int_A [B_{w2}]^T [W_i]^T [B_{w1}]^T \{N_o\}\, dA \tag{C.2}$$

where $\{N_o\}$ is a set of membrane forces, corresponding to the mid-plane stresses.

Now, using Eqs. (2.55), (2.62) and (2.64)

$$\{R_1\} = \int_A \underbrace{\left[\frac{\partial \varphi_w^T}{\partial x} \;\middle|\; \frac{\partial \varphi_w^T}{\partial y}\right]}_{n \times 2} \underbrace{\left[\begin{array}{c|c} w_i^T & 0 \\ \hline 0 & w_i^T \end{array}\right]}_{2 \times 2n} \underbrace{\left[\begin{array}{c|c|c} \frac{\partial \varphi_w^T}{\partial x} & 0 & \frac{\partial \varphi_w^T}{\partial y} \\ \hline 0 & \frac{\partial \varphi_w^T}{\partial y} & \frac{\partial \varphi_w^T}{\partial x} \end{array}\right]}_{2n \times 3} \underbrace{\{N_o\}}_{3 \times 1} dA$$

$$= \int_A \Big[\Big\langle \frac{\partial \varphi_w}{\partial x} \Big\rangle^T \Big\langle \frac{\partial \varphi_w}{\partial x} \Big\rangle \{w_i\} \;\Big|\; \Big\langle \frac{\partial \varphi_w}{\partial y} \Big\rangle^T \Big\langle \frac{\partial \varphi_w}{\partial y} \Big\rangle \{w_i\} \;\Big|\; \text{(cont.)}$$

$$\Big(\Big\langle \frac{\partial \varphi_w^T}{\partial x} \Big\rangle \Big\langle \frac{\partial \varphi_w}{\partial y} \Big\rangle + \Big\langle \frac{\partial \varphi_w}{\partial y} \Big\rangle^T \Big\langle \frac{\partial \varphi_w}{\partial x} \Big\rangle \Big) \{w_i\} \Big] \{N_o\} dA$$

$$= \int_A \begin{bmatrix} \frac{\partial \varphi_w}{\partial x} \\ \frac{\partial \varphi_w}{\partial y} \end{bmatrix}^T \begin{bmatrix} N_{ox} & N_{oxy} \\ N_{oxy} & N_{oy} \end{bmatrix} \begin{bmatrix} \frac{\partial \varphi_w}{\partial x} \\ \frac{\partial \varphi_w}{\partial y} \end{bmatrix} dA\, \{w_i\} \tag{C.3}$$

The matrix defined by the last integral is the geometric stiffness for plates as given by Martin [14].

APPENDIX D

SIMPLIFIED DISPLACEMENT FUNCTIONS FOR COMPUTATION OF NONLINEAR STIFFNESS TERMS

In a non-dimensional ξ-η coordinate system for a rectangle, the Hermitian interpolation polynomials yield

$$w = \langle \varphi_w \rangle \{w_i\} \tag{D.1}$$

where

$$\{w_i\}^T = \langle w_1, \theta_{x1}, \theta_{y1}, w_2, \theta_{x2}, \theta_{y2}, w_3, \theta_{x3}, \theta_{y3}, w_4, \theta_{x4}, \theta_{y4} \rangle \tag{D.2}$$

and

$$\langle \varphi_w \rangle^T = \begin{Bmatrix} (2-3\xi+\xi^3)(2-3\eta+\eta^3) \\ b(2-3\xi+\xi^3)(1-\eta-\eta^2+\eta^3) \\ -a(1-\xi-\xi^2+\xi^3)(2-3\eta+\eta^3) \\ (2+3\xi-\xi^3)(2-3\eta+\eta^3) \\ b(2+3\xi-\xi^3)(1-\eta-\eta^2+\eta^3) \\ -a(-1-\xi+\xi^2+\xi^3)(2-3\eta+\eta^3) \\ (2+3\xi-\xi^3)(2+3\eta-\eta^3) \\ b(2+3\xi-\xi^3)(-1-\eta+\eta^2+\eta^3) \\ -a(-1-\xi+\xi^2+\xi^3)(2+3\eta-\eta^3) \\ (2-3\xi+\xi^3)(2+3\eta-\eta^3) \\ b(2-3\xi+\xi^3)(-1-\eta+\eta^2+\eta^3) \\ -a(1-\xi-\xi^2+\xi^3)(2+3\eta-\eta^3) \end{Bmatrix} \tag{D.3}$$

The local nodal point numbering is that of Fig. 3.3. a and b are half the side-lengths.

DISTRIBUTION LIST

40 Commander
Naval Ship Research and
Development Center
Washington, D. C. 20034
Attn: Code L41 (39)
Code 513 (1)

5 Commander
Naval Ship Systems Command
Department of the Navy
Washington, D. C. 20360
Attn: SHIPS 2052 (2)
SHIPS 031
SHIPS 03423
SHIPS 034

9 Commander
Naval Ship Engineering Center
Department of the Navy
Center Building, Prince Georges Center
Hyattsville, Maryland 20782
Attn: SEC 6101
SEC 6110
SEC 6113
SEC 6114
SEC 6120
SEC 6128 (2)
SEC 6129
SEC 6131

20 Director
Defense Documentation Center
5010 Duke Street
Alexandria, Virginia 22314

2 Chief of Naval Material
Department of the Navy
Washington, D. C. 20360
Attn: MAT 031
MAT 26

2 Chief of Naval Research
Department of the Navy
Washington, D. C. 20360
Attn: ONR 439
ONR 463

2 Chief of Naval Operations
Department of the Navy
Washington, D. C. 20350
Attn: OP 366
OP 07T

1 Commanding Officer and Director
Naval Applied Science Laboratory
Flushing & Washington Avenues
Brooklyn, New York 11251

1 Director (2027)
Naval Research Laboratory
Washington, D. C. 20390

1 U. S. Naval Postgraduate School
Monterey, California 93940
Attn: Library

1 Commander
Boston Naval Shipyard
Boston, Massachusetts 02129
Attn: Technical Library

1 Commander
Charleston Naval Shipyard
Naval Base
Charleston, South Carolina 29408
Attn: Technical Library

1 Commander
Long Beach Naval Shipyard
Long Beach, California 90802
Attn: Technical Library

1 Commander
Norfolk Naval Shipyard
Portsmouth, Virginia 23709
Attn: Technical Library

1 Commander
Pearl Harbor Naval Shipyard
Box 400, Fleet Post Office
San Francisco, California 96610
Attn: Code 246-P

1 Supervisor of Shipbuilding, Conversion and Repair, USN
4th Naval District
2430 Broadway
Camden, New Jersey 08104

1 Supervisor of Shipbuilding, Conversion and Repair, USN
General Dynamics Corporation
Electric Boat Division
Groton, Connecticut 06340

1 Supervisor of Shipbuilding, Conversion and Repair, USN
Newport News Shipbuilding and Drydock Company
Newport News, Virginia 23607

1 Supervisor of Shipbuilding, Conversion and Repair, USN
Ingalls Shipbuilding Corporation
Pascagoula, Mississippi 39567

1 Commanding Officer
Naval Civil Engineering Laboratory
Port Hueneme, California 93041

1 Commanding Officer
Navy Underwater Sound Laboratory
Fort Trumbull
New London, Conn. 06320

1 Commander
Naval Electronics Laboraotry Center
San Diego, California 92152

1 Commander
Naval Weapons Center
China Lake, California 93555

1 U. S. Dpeartment of Commerce
Maritime Administration
Washington D. C. 20235

1 Commandant
U. S. Coast Guard Headquarters
1300 E. Street N. W.
Testing & Development Division
Washington D. C. 20591

1 Wright Patterson Air Force Base
Chief Applied Mechanics Group
Ohio, 45433

1 Wright Patterson Air Force Base
Structures Division
ATTENTION: F. J. Janik, Jr.
Ohio, 45433

1 Commander
Philadelphia Naval Shipyard
Philadelphis, Penna 19112
Attn: Code 240

1 Commander
Portsmouth Naval Shipyard
Portsmouth, N. H. 03801
Attn: Technical Library

1 Commander
Puget Sound Naval Shipyard
Bremerton, Washington 98314
Attn: Engineering Library

1 Commander
San Francisco Bay Naval Shipyard
Vallejo, California 94952
Attn: Technical Library

Security Classification

DOCUMENT CONTROL DATA - R & D

(Security classification of title, body of abstract and indexing annotation must be entered when the overall report is classified)

1. ORIGINATING ACTIVITY (Corporate author)	2a. REPORT SECURITY CLASSIFICATION
Division of Structural Engineering and Structural Mechanics, University of California, Berkeley	Unclassified
	2b. GROUP

3. REPORT TITLE

Non-linear Analysis of Plates Considering Geometric and Material Effects

4. DESCRIPTIVE NOTES (Type of report and inclusive dates)

Technical Report

5. AUTHOR(S) (First name, middle initial, last name)

Pal G. Bergan

6. REPORT DATE	7a. TOTAL NO. OF PAGES	7b. NO. OF REFS
April 1971	168	112

8a. CONTRACT OR GRANT NO.	9a. ORIGINATOR'S REPORT NUMBER(S)
N00014-69-A-0020-1045	UCSESM 71-7
b. PROJECT NO. SF 013 0301	
c.	9b. OTHER REPORT NO(S) (Any other numbers that may be assigned this report)
d.	

10. DISTRIBUTION STATEMENT

This document has been approved for public release and sale, its distribution is unlimited.

11. SUPPLEMENTARY NOTES	12. SPONSORING MILITARY ACTIVITY
---	Naval Ship Research and Development Center Dept. of Navy, Washington, D.C. 20007

13. ABSTRACT

The purpose of this investigation is to study nonlinear behavior of plates considering both geometric and physical nonlinearities. Large deflections are accounted for using the von Karman strain expressions for plates and initial deformations are considered using the Marquerre shallow shell theory. Establishing the variational principles, the equilibrium and incremental equations for general Rayleigh-Ritz type solution methods are derived. The finite element method is adopted for the numerical solution of the problem. A doubly curved quadrilateral element including nonlinear geometric effects is derived. Special simplifications are made resulting in a highly efficient technique. Inelastic material behavior is accounted for using the flow theory of plasticity. In particular, the Prandtl-Reuss flow rule and isotropic hardening are utilized. Inelastic, quadrilateral finite elements allowing for both membrane and flexural behavior are developed. The tangent stiffness approach is adopted forming the incremental stiffnesses by numerical integration over the volume of the elements. Different general numerical techniques for solving nonlinear structural problems are considered. The problems of convergence and accuracy of iteration methods are also discussed. A wide range of numerical examples are presented, such as large deflections of different plates, post buckling behavior of plates, snap-through problems and inelastic behavior of various plates.

DD FORM 1 NOV 65 1473 (PAGE 1)

S/N 0101-807-6801

Security Classification

14. KEY WORDS	LINK A		LINK B		LINK C	
	ROLE	WT	ROLE	WT	ROLE	WT
Finite Element Analysis						
Membrane Elements						
Bending Elements						
Non-linear Displacements						
Non-linear Material Properties						
Plastic flow theory						
Prandtl-Reuss flow rule						
Doubly curved quadrilateral elements						
Shall shells						
Snap-through analysis						
Post-buckling plate behavior						